Processing and Analysis of Lidar Derived Point Cloud Models of Low-Rise Large-Volume Steel Frame Buildings Damaged in Hurricane Michael

Kristinn Mar Bjarnason

A thesis

submitted in partial fulfillment of the

requirements for the degree of

Master of Science in Civil Engineering

University of Washington

2020

Committee:

Jeffrey W. Berman

Michael Motley

Program Authorized to Offer Degree:

Civil and Environmental Engineering

University of Washington

Abstract

Processing and Analysis of Lidar Derived Point Cloud Models of Low-Rise Large-Volume Steel Frame Buildings Damaged in Hurricane Michael

Kristinn Mar Bjarnason

Chair of the Supervisory Committee:
Jeffrey W. Berman
Civil and Environmental Engineering

Hurricane Michael made landfall in Panama City on the Florida Panhandle on October 10, 2018 as a Category 5 hurricane and caused substantial damage. Low-rise large-volume steel frame buildings (LRLVBs) suffered in particular, and many of them demonstrated similar failure patterns where a short side of the building collapsed, either partially or fully. Following the hurricane, a response team including staff from the NSF RAPID Facility, a natural hazard reconnaissance facility headquartered at the University of Washington, was sent to Panama City where the damage was documented. This was done using lidar scanners, photographs from both handheld cameras and drones, and various other equipment.

The use of lidar in reconnaissance to document structural damage following the occurrence of natural hazards is particularly compelling as it can speed data collection relative to physically measuring elements while providing for rich 3D data sets.

The accuracy and viability of lidar for use in building reconnaissance was examined in this thesis with a focus on techniques requiring limited computing power. The results show that large scale measurements such as the dimensions of the building, column spacing, etc. can be obtained within the margin of error for construction tolerances allowed in AISC steel building construction specifications. It is found that measurements of structural cross-sections are possible from the obtained data but require specific scanner locations and more rigorous post-processing of the data. The results of the work are recommendations for terrestrial lidar reconnaissance specifically related to steel buildings.

TABLE OF CONTENTS

LIST OF FIGURES

LIST OF TABLES

ACKNOWLEDGEMENTS

I would like to thank everyone at the RAPID Facility for providing the resources needed to conduct this research, along with their help, whenever needed, and for being excellent company in the lab.

I would also like to thank my friends and family for providing support, along with numerous distractions to delay this work. In particular, I would like to thank my girlfriend, Jessica Matyas, for her support throughout this process, and her English expertise she so selflessly provided.

Lastly, I want to thank my desk neighbors at More Hall 109C for their company, lively conversations about soccer around the world, and passive-aggressive “good mornings” when I showed up in the afternoon.

Chapter 1. INTRODUCTION

1.1 BACKGROUND

Point clouds are sets of data points in space and can be constructed from photographs, or in the case of this study, from lidar scanning. Lidar is a portmanteau of light and radar, and functions much in the same way as radar, but instead of using radio waves it uses lasers. These types of scans have mostly been used in large scale survey applications such as landslides, forests or mining. Recently, higher density point clouds and improved point accuracy has become available through better equipment, software and processing tools, raising the possibility of using these large-scale techniques on more intricate objects such as structural elements within buildings.

In the 3D point cloud models derived from lidar data; it is important to note that anything that is not visible from the scanner setup location will not be visible in the final model. Figure 1.1 demonstrates this by showing the view from a single scan location where a wide flange column looks to be complete, but when viewed on the cross-sectional level it becomes clear that everything that is not visible is in fact not part of the model. This shows the importance of choosing the scan locations carefully to capture every side of the items of interest.

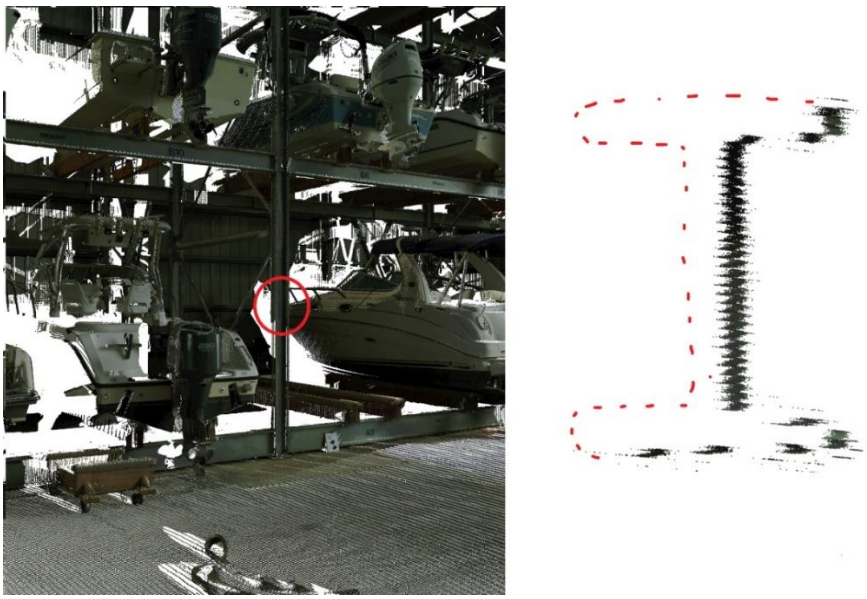

Figure 1.1. An outside view of a wide flange column along with the cross-sectional view.

The use of lidar in reconnaissance to document structural damage following the occurrence of natural hazards is particularly compelling as it can speed data collection relative to physically measuring elements while providing for rich 3D data sets. The speed of data collection allows the researchers to gather vast amounts of data in the geographical zone of interest to compare the damage of multiple buildings, which can help to establish patterns of damage. In addition to easing the analytical process, it also serves as a highly effective visualization tool as the structures are virtually rebuilt as point clouds and can be observed from whichever angle is desired, whereas photographs and video recordings are much more limited. This eliminates the need for a highly detailed plan on what to measure and record since those decisions can all be made in the processing phase following the site visit, which is essential in reconnaissance missions since natural disasters do not allow for a window of planning before striking.

Hurricane Michael made landfall on the Florida Panhandle on October 10, 2018, and with that became the first Category 5 hurricane on the Saffir Simpson Hurricane Wind Scale to strike the contiguous United States since Hurricane Andrew in 1992. It was the first Category 5 hurricane to hit the Florida Panhandle since measurements started and the fourth strongest in terms of wind speed to make landfall in the contiguous United States. The maximum wind speed recorded was 139 mph (62.1 m/s) at Tyndall Air Force Base, where four of the eleven buildings examined here were located, before the sensors failed, so it was possibly even higher (Beven et al., 2019). It caused an estimated $25.1 billion (NCEI, 2019) in damages, and between $4.7 (Wilson, 2019). and $6 billion (Philipps, 2018b) of those were to the Tyndall Air Force Base, mainly the 17 Lockheed Martin F-22 Raptor stealth tactical fighter aircrafts left at the base before Michael made landfall (Philipps, 2018a), but the military budgeting is not the subject of this thesis.

Low-rise large-volume steel frame buildings (LRLVBs) suffered from significant damages in Panama City, Florida, and many them demonstrated similar failure patterns where the windward facing side collapsed, either partially or fully. When Hurricane Michael made landfall, the buildings examined here were subjected to winds from the northeast (Beven et al., 2019), which coincides with the damage recorded on the short sides of the LRLVBs facing north, northeast or east. While the research conducted here does not focus particularly on the specifics of the structural

failure or what forces were at play, it can provide valuable information to research focused in that direction.

Following the hurricane, a response team from NHERI RAPID, a natural hazard reconnaissance facility headquartered at the University of Washington, was sent to Panama City where the damage was documented. This was done using lidar scanners, photographs from both handheld cameras and drones, and various other equipment. During the mission, over twelve buildings were documented to varying extents, of which eleven will be discussed here. The team consisted of members from the University of Washington led by Jeffrey Berman, Auburn University led by David Roueche, and RAPID led by Jake Dafni.

1.2 RESEARCH OBJECTIVE

The research objective of the experiments conducted here in this thesis are as follows:

- Examine the viability of lidar derived point clouds as an analytical tool for structural damage in a post-disaster setting, in this case, with a focus on low-rise large-volume steel frame buildings (LRLVBs).
- Compare different lidar scanning methods with regards to scan type, location of scans, scan density, scan distribution, etc.
- Determine the accuracy and viability of measurements of different scales within the point clouds that can be split into two general groups.
    - Envelope information such as length, width and height of buildings along with column spacing, purlin spacing and slopes over longer distances.
    - Detailed information, mainly on the cross-sectional level for the steel elements analyzed here.
- Explain and demonstrate methods that are easily accessible to other researchers that have minimal experience with point clouds in accordance with the philosophy of NSF sponsored NHERI RAPID facility.
- Provide point cloud models of varying scales and sizes for the DesignSafe-CI Data Depot for further natural hazard research.

- Suggest improvements that may be made to future reconnaissance missions in post-disaster zones to improve various aspects of the resulting point cloud models.

1.3 Document Overview

This thesis contains five chapters in addition to this introduction, each serving a purpose to address the research objectives stated.

Chapter 2 focuses on the background of the research conducted here by summarizing relevant past research on structural applications of point clouds, giving a synopsis of the Lidar technology used and providing a brief description of the NHERI RAPID facility that accommodated the research.

Chapter 3 serves as a description of the experimental setup used here, though not very methodical or scientifically rigorous due to the nature of post-disaster reconnaissance. It gives an overview of resources used and the limitations that they might have.

Chapter 4 explains and demonstrates the registration process of each of the eleven buildings and goes into detail on the quality of data gathered. Topics such as point cloud cleaning, ease of the registration process and problems that arose, both expected and unexpected.

Chapter 5 focuses on the analysis of the data gathered. This means the measuring process, both the large scale and the detailed measurements, error factors and how they can be minimized, and the viability of the analysis with point clouds of different qualities.

Chapter 6 is a summary of the research conducted along with conclusions and recommendations for future work regarding post-disaster data collection and analysis.

Chapter 2. PROJECT BACKGROUND

2.1 INTRODUCTION

This chapter provides context for the research conducted here as well as providing background information on lidar technology and the facility where the processing was carried out. Section 2.2 briefly discusses the essential background information on lidar technology a reader must have in order to understand the content of this thesis. Section 2.3 discusses the role of the NSF supported NHERI RAPID Facility that provided the resources required to conduct this research as well as explaining how other researchers can utilize those same resources for their work. Section 2.4 reviews past research on lidar applications in structural engineering and indicates the relevance of this study within the context of the prior work.

2.2 LIDAR OVERVIEW

The oldest record of a lidar-like system comes from the Hughes Aircraft Company in 1961 (New Radar System, 1961). This is shortly after the invention of the actual laser, but ideas on the utilization of such technology can be dated back to the 1930s (Synge, 1930). The invention of the lidar system was developed through various avenues, most prominently through rangefinders and altimeters, especially in military applications.

Lidar works by emitting a laser light to surrounding surfaces and, using a sensor, measures the reflection of those surfaces. It then processes those reflections with regards to the difference in laser return times and preset wavelengths to compute the 3D position of each point that the laser reaches. That information can then be used to build a fully three-dimensional model. Modern scanners also take photographs while scanning and proceed to automatically match those photographs with laser scans from the same angles to color the points. This allows the point cloud to not only display geometric shapes, but also the textures based on color and color gradient.

A lidar scanner consists of a few vital components, with other additional ones being optional and not required to produce a 3D model. Those vital components are a laser, scanner and optics,

photodetector and receiver electronics, and sensors. Most modern lidar scanners also incorporate position and navigation systems such as GPS and an inertial measurement unit.

Lidar scanners can be split into two distinct types: airborne or terrestrial. Airborne lidar can be mounted on an airplane, or more commonly in recent years, unmanned aerial vehicles, or drones. They can also be fitted into satellites e.g. for atmospheric research. Terrestrial scanners can either be mobile or stationary, where the mobile ones are commonly mounted on moving vehicles to survey paths such as streets, power lines, bridges or trees. Stationary scanners, like the ones used here, are mobile to a certain level as they are commonly mounted on tripods and can be moved around between scans.

Lidar scanners have been used for a variety of projects through the years and continue to be integrated into various fields. Examples of these are: agriculture where lidar scans can be used to produce yield maps, detect insect activity and classify species; archeology so that sites can be preserved in different stages of excavation; autonomous vehicles where object detection plays a vital role; biology and forestry where biomass and tree canopy cover can be detected over large areas; geology where ground motion can be measured over long periods of time; atmospheric science where clouds, aerosols and other particles can be scanned; and mining to observe and measure the removal of ore from mines.

2.3 RAPID FACILITY

The NHERI Natural Hazards Reconnaissance Facility, more commonly referred to as the RAPID Facility was developed in 2016 and 2017 and opened for use by the natural hazards community in 2018 and is headquartered at the University of Washington. It is a collaboration project between the University of Washington, Oregon State University, Virginia Tech and the University of Florida, and is supported with grants from the National Science Foundation.

The RAPID facility specializes in natural hazard and disaster research using the latest available technology which researchers from around the country, and in some cases internationally, can access.
Their objective, as stated on their website, are as follows:

- Acquiring, maintaining, and operating state-of-the-art data collection equipment,
- Developing and supporting mobile applications for interdisciplinary field reconnaissance,
- Providing advisory services and basic equipment logistics support for research investigations,
- Facilitating the systematic archiving, processing and visualization of acquired data in DesignSafe-CI,
- Training a broad user base through workshops and other activities, and
- Engaging the public by facilitating citizen science initiatives, as well as through community outreach and education.

Practically all the resources used in this research project were supplied by the RAPID Facility and a team from there carried out the field work required in acquiring the data. The resources provided include processing computers, office space, information whenever it was requested, and all the software licenses required.

2.4 SUMMARY OF PAST RESEARCH

As previously stated, lidar technology has been used in one form or another for decades, but with the rapid advancement of technology and processing power of computers, the research conducted on this subject becomes, for the most part, obsolete rather quickly. For this reason, it is unnecessary to extensively review literature published prior to the mid-2000s. The focus of this review is on lidar applications in structural engineering.

Early research of the applications of lidar often focused on the identification of structures using point clouds. In a study conducted by Vosselman et al. in 2003, both airborne and terrestrial laser scanners were used to capture large point clouds of different objects and structures. This study completed an overview of different methods for extracting data about surfaces using point clouds. These methods include the extraction of smooth surfaces, iterative extraction of planar surfaces, and the direct extraction of parameterized shapes.

This research provides a baseline for the identification, visualization, and analysis of structures and their components, which is basic and fundamental to the work of this thesis. Vosselman et al. (2003) established example applications of these methods. For the extraction of smooth surfaces,

grouping nearby points that share a certain property allows for the extraction of multiple groups of points that represent the smooth surface. Using both terrestrial and aerial scanning allows for a 3D application of this technique. In using point clouds for the iterative extraction of planar surfaces, polyhedral objects can be identified by implementing variations of the smooth surface technique. Finally, direct extraction of parameterized shapes allows visualization of shapes such as cylinders and spheres. By using these analyses within point clouds, this study was able to model a city center, recognize a bridge surrounded by vegetation, and separate the segmentation of a tree, all of which are similar to the objective of this research, though simplified and with lesser computing capacity.

The basic dimensions of buildings, hereafter called envelope data, have also been the focal point of previously conducted research. In Zeng et al. (2008), a triangulated irregular network (TIN) model, where continuous surfaces are modelled exclusively with triangular facets, middle step method was developed to reconstruct simple buildings digitally from lidar point clouds. This method uses point clusters to establish building plane boundaries and from there can calculate 3D coordinates for different building corner points. This allows for a visualization of a simple building.

Later, the work of Xiong et al. (2013) explored ways of creating building information models (BIMs) using point clouds extracted by laser scanners, expanding on the ideas from Zeng et al. (2008). In order to do one, an algorithm was developed to be able to convert point cloud data into a building information model, in order to reduce the time and effort previously required to visualize laser scanning data. Using this method, a 3D model of a simple building was extracted. This was done by identifying corner points and the other main visual structural components of a built environment.

Building off these initial studies, the research of Walsh et al. (2013) directly addresses the potential application that point clouds have in post-disaster reconnaissance and their role in being able to model buildings without any existing knowledge of their structural systems. Using lidar 3D point clouds, they captured geometric range data for complex structures and developed a foundational process of extracting the important information from raw point clouds, such as the location,

orientation, and size of different components of a structure. Prior algorithms, such as the ones discussed previously, were used as a basis for identifying planes and corner points. Additional algorithms were then created to allow for the removal of extraneous features and outlying points. This resulted in a method to visualize structures and detect objects with applications in structural engineering, such as structural health monitoring, collapse assessment, and post-hazard assessments. Walsh et al. demonstrated their method on synthetic scenes as well as test specimens and a collapsed bridge and suggested it could be further expanded to determine damage locations within structures.

Lidar point clouds have been particularly useful in measurements that rely on having models of structural elements in their undamaged state, allowing for an understanding of the damage inflicted by disastrous events. Olsen et al. (2009) presents methods of intuitive slicing, which can be automated for rapid analysis and visualization of full-size structures. This is more effective than traditional photographic analysis, as it provides complete 3D views of structures that are consistent and can trace changes in structural integrity that are not visible in photos. They measured volumetric change, deformation, and more thorough lab testing and scans of a concrete beam with promising results.

Olsen et al. (2013) later developed methods that detected change from the original point cloud in situ, which can save vast amounts of time in post-processing. Previously, scan surveys had to be compared and analyzed to detect changes and had to be conducted during post-processing upon return to the office. This limited the effectiveness and efficiency of field investigations, as any questions or inconsistencies raised upon analysis then required a new field investigation to be made. Olsen et al. (2013) developed a methodology to quickly reference scans upon field acquisition. The new algorithm was tested in both lab and field settings and showed great success in rapid and accurate testing, although those tests were on large-scale models such as landslides.

Similar ideas were also used by Watson et al. (2011) in bridge inspections. Lidar scans of a bridge were prepared to create baseline geometric information about the structure, then performed again after nearby construction blasting was completed. The dense point clouds of each scan allowed for

the comparison of critical sections and geometries, in order to detect changes and ensure the safety of the bridge.

This method allows for a full-scale 3D scan of a structure to be kept in a database, then compared to new models via proximity analysis. The potential applications of this within structural engineering are wide, with post-disaster assessment and analysis being a prominent area of interest. This is because this method can both be used to establish effects and damage information of disturbance events, as well as identify the effects on a structure that may be time-consuming or impossible to find using traditional methods, but this was not explicitly explored in this study.
Multiple studies have been conducted in recent years where the spatial recognition of lidar is coupled with image processing-based point clouds such as SfM (Structure from Motion). Valença et al. (2017) developed a novel method called MCrack-TLS, which automatically detects cracks in concrete bridges by visualizing the data gathered by laser scanning. Point clouds are formed and analyzed by algorithms that identify and characterize cracking. This method was tested on a concrete viaduct in Portugal as a case study and showed success in identifying cracks in such concrete structures.

Similarly, Erkal et al. (2017) implemented a strategy of using lidar to visualize the deterioration of structures, with the added element of photos. This is referred to as opening the fourth wall, as it combines traditional visual strategies of crack detection with the geometric data that can be collected via point cloud analysis. In the past, using images with increasing resolution to detect cracks has been researched thoroughly. By adding those processes to lidar scans, textures, colors, and cracking patterns that cannot be identified by lidar alone are able to be analyzed via point clouds and SfM.

Mohammadi et al. (2018) used this mix of photographs and lidar data to analyze structural damage in a post-earthquake setting, much like the reconnaissance work done in this thesis. They used an algorithm to analyze point cloud and photographic data and identify cracking, deterioration, and other damage on structures. This was performed on two case studies, a high-rise condominium and a pagoda-style temple, with good success. This research was very useful in demonstrating the

capabilities of SfM, although the algorithms and methods are not directly applicable here because it relied mostly on color properties, as the structures being analyzed were concrete and masonry.

Hou et al. (2017) concluded that spatial data is much more robust than the image processing techniques described, since environmental factors can obscure the colors and lead to inaccuracies. Four algorithms (two spatially based and two image based) were compared on a variety of structural damages, including corrosion, erosion, aging, water damage, lichen, and physical damage. The spatial algorithms were more effective at gathering damage data on structural elements, due to the fact that moisture and lighting is variable and thus intensity and RGB analyses can be confused with wet or shaded areas. In addition, spatial data can be used to identify geometric anomalies that may not be picked up by image processing.

Another use for this mix of technologies is when terrestrial lidar has to be supplemented with airborne scans. Structure from Motion only requires a camera which are already commonplace in unmanned aerial vehicles (UAVs) and are much cheaper than airborne lidar scanners and with little extra cost, interior scans of buildings can be supplemented with SfM models of the roofing and other inaccessible locations from terrestrial lidar (Wood et al. 2015). This allows for the inherent disadvantage of lidar as a line-of-sight technology to be somewhat negated, by reducing the number of occlusions that may impact readings by a laser scanner. Overall, Wood et al. (2015) found that UAV images are able to supplement lidar point clouds to create holistic scene reconstructions, which can be extremely beneficial in post-disaster reconnaissance, as was done in this thesis.

In the case of this study, it was deemed unnecessary to supplement the lidar scans, since the focus is on steel frames and most of the applications of the color-based detection methods are concrete or masonry focused. Structural damage to steel is much likelier to be in the form of spatial deformation and thus the color becomes irrelevant to the research.

Prior research on purely steel buildings has shown promise and is progressing rapidly with automated methods for measuring deflection of steel beams from point cloud data being developed by Cabaleiro et al. (2015) and the extraction of steel frame connections and their properties by

some of the same authors (Cabaleiro et al. 2014). Those studies focus heavily on thoroughly scanned elements in a controlled setting, whereas the reconnaissance applications discussed here are more limited in their coverage and predictability.

Although all of this research shows great promise and demonstrates the capabilities of algorithms to identify and extract objects from point clouds, this thesis focuses on the robustness of methods anyone can apply to models with minimal experience and preparation, and to make suggestions as to how a field crew should conduct reconnaissance missions in the future to produce acceptable results.

The nature of reconnaissance lidar scanning is unpredictable since the accessibility, extent of damage and the type of building in question is variable. Identifying general principles that enhance the quality of the data within the buildings examined here (LRLVBs) has not been examined to its full extent and this paper aims to fill in these gaps.

Chapter 3. DESCRIPTION OF SURVEYED LOW-RISE LARGE-VOLUME BUILDINGS

3.1 INTRODUCTION

Following Hurricane Michael, a team of researchers from the University of Washington (including staff from the NHERI RAPID Facility) and Auburn University traveled to Panama City, FL, with support from a grant from the National Science Foundation to survey damage to LRLVBs. Prior reconnaissance missions to the affected area identified LRLVBs as having a high rate of failure resulting in potentially severe economic losses. The team deployed with several lidar scanners and UAVs from the RAPID Facility as well as camera and surveying equipment. In total, data at more than twelve individual LRLVBs buildings was collected during the one-week duration in the field. Due to conditions in the field, data could not be identically collected at each site. For example, in some cases the team had access to the interior of the buildings and in other cases they did not. Further, because this was a post-disaster mission and the condition of each building was relatively unknown except for a few exterior photos there was very little time to prepare data collection strategies in advance. While this complicates processing and analysis of the collected lidar and comparison of data quality between sites, it also offers opportunities to study the impact on resulting point cloud quality of tradeoffs that are often made in the field between amount of data collected and the time on site.

In this Chapter, the locations and alignment of the buildings are mapped and compared to the dominant wind directions during the hurricane. Descriptions of each building and its hurricane damage are also provided. Then, the data gathering process is discussed, along with descriptions of the instruments used in the field. Finally, the hardware and software used in the data processing are described. This is necessary because the performance of the hardware is directly related to the size of point clouds a user can feasibly manipulate and the software used will be repeatedly referenced in the text.

3.2 GEOGRAPHIC DISTRIBUTION OF BUILDING SITES

Figure 3.1 shows the measured wind speeds where Hurricane Michael made landfall on the Florida Panhandle, with Panama City marked within a rectangle. Figure 3.2 shows a map that was constructed to display the alignment of the buildings, with exaggerated dimensions and red color to denote which side suffered damage in the hurricane. The buildings at Tyndall Air Force Base are shown in Figure 3.3 and Figure 3.4, which display maps before and after the hurricane respectively. Note that the Tyndall buildings did not suffer structural collapse, instead they had damage to the roof (Buildings 316, 375 and Hangar 5) and some failure of cladding systems (Building 333 and 375).

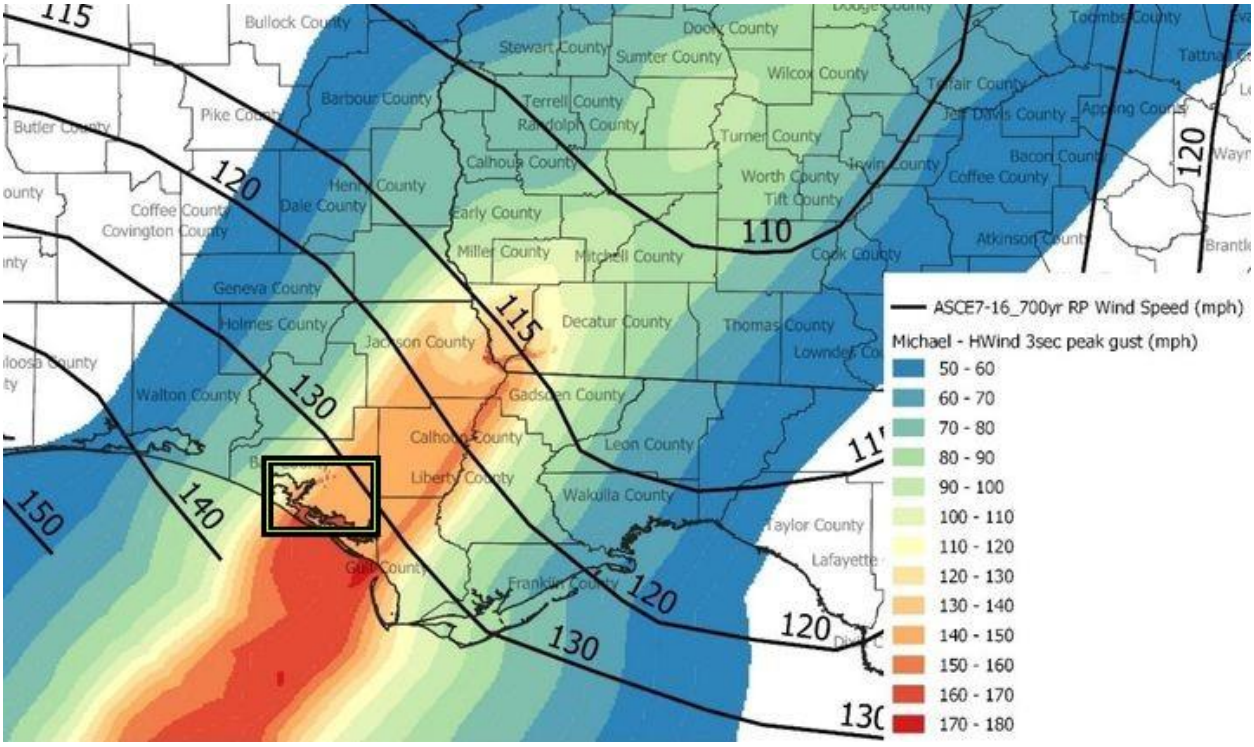

Figure 3.1. RMS HWind 3-second gust footprint for Hurricane Michael overlaid with the design wind speed contours in ASCE 7-16 (Datin et al., 2019).

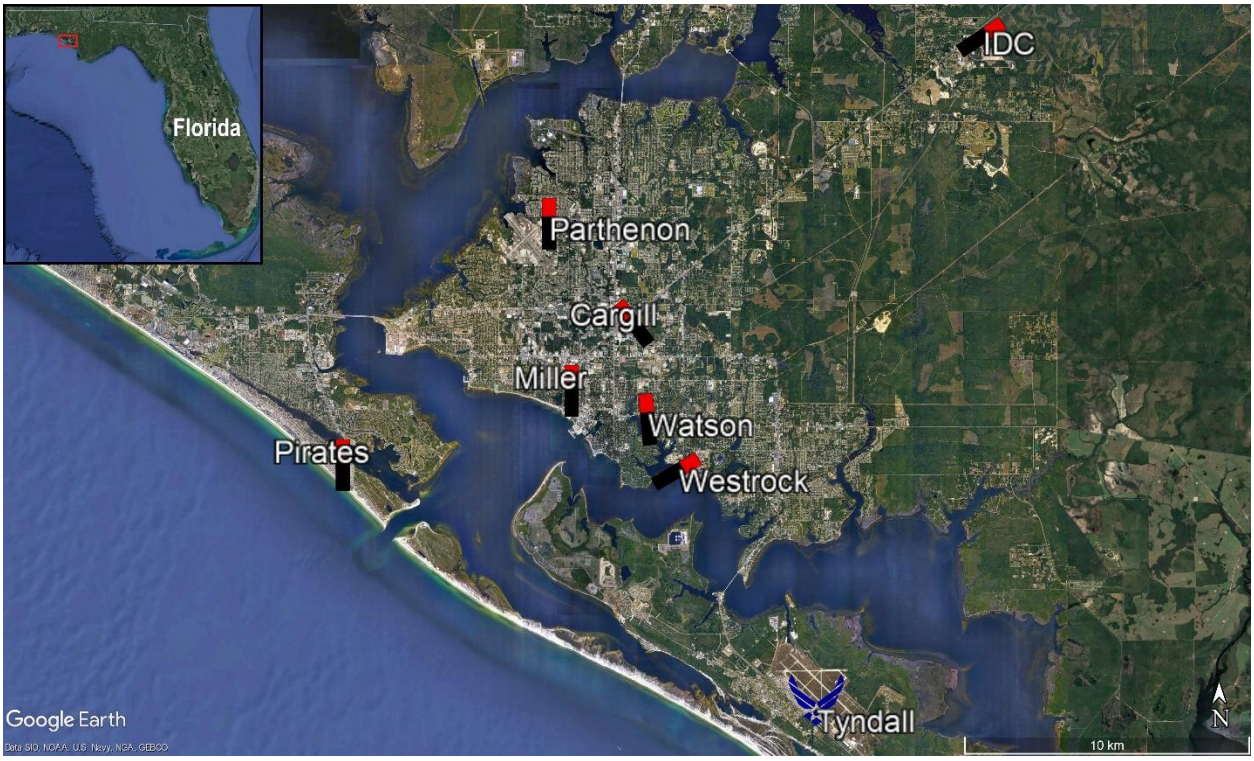

Figure 3.2. Overview map of Panama City, Florida. (Google, 2015)

Due to the proximity of the buildings at Tyndall Air Force base to each other, aerial photographs were used to show the alignment. Figure 3.3 shows the area before Hurricane Michael and Figure 3.4 shows the extents of the damage directly following the hurricane.

Figure 3.3. A closer look at Tyndall Air Force Base in 2015 (Google, 2015)

Figure 3.4. A closer look at Tyndall Air Force Base on October 12, 2018 (Google, 2018)

3.3 BUILDING AND DAMAGE DESCRIPTIONS

3.3.1 *Westrock East Terminal*

The Westrock East Terminal building is a typical steel framed LRLVB, but there are some nuances to it. The site was designed to have to an additional building that interconnected with the damaged building but it was not yet constructed. Additionally, there were three attached smaller buildings which are shown in the drawings in Appendix A, where building A was the only one scanned after it was severely damaged in the hurricane.

For the purpose of this thesis, building A is the main focus, and can be described as a single open space with no division into rooms. The roof is spanned laterally with non-prismatic, wide flange beams that are supported on both longitudinal sides with columns and in a centrally offset row towards the south side of the building as can be seen in Figure 3.6. The ridge of the roof is centrally offset too, and the slope of the roof is the same on both sides, so the difference is made up with different roof heights on either side which can be seen in Figure 3.5.

Longitudinally, the roof is spanned by truss girders with smaller beams acting as purlins and joists. Cross bracing is found between some columns on the edges of the building. The building parts not scanned here are building B, which is an overhang over train tracks on the north side of the building, building C, which is a hut attached to the east side, and building D, another hut that is on the south side.

The building suffered a complete collapse of the first bay (between column lines 20 and 21) on the northeastern side and some damages to the second and third bay (between column lines 18 and 20) as is demonstrated in Figure 3.7 and Figure 3.8. The purlins in the first bay show large deflections indicative of buckling and the failure of multiple connections, while the second and third bay mostly demonstrate surface damage to cladding along with comparatively minor deflections of the purlins.

A more comprehensive overview of the building dimensions and the numbering conventions in the local coordinate system can be seen in Appendix A.

Figure 3.5. A view of the intact face of Westrock East Terminal demonstrating the off-center roof pitch.

Figure 3.6. A view from inside Westrock East Terminal showing the framing and columns.

Figure 3.7. A view of the damaged face of Westrock East Terminal.

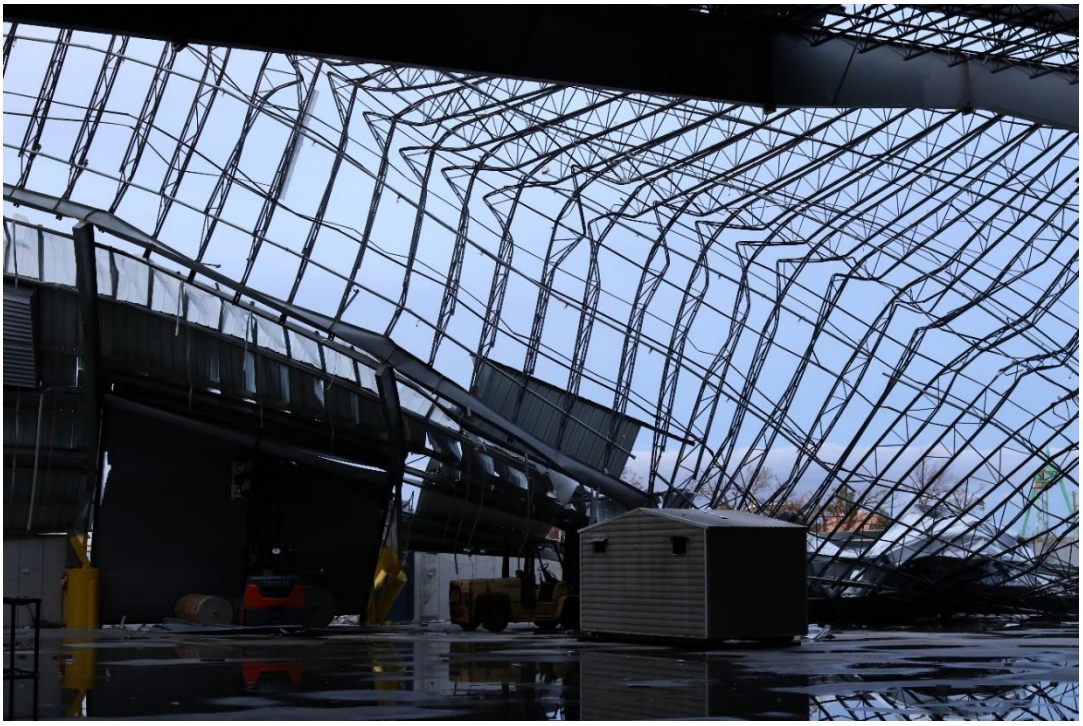

Figure 3.8. A photograph showing the buckled roof trusses in Westrock East Terminal.

3.3.2 *Watson Landings Marina*

Watson Landings Marina is a relatively symmetric steel frame LRLVB that is used as a marine storage building. It consists of a single open space with four story boat racks, seen in Figure 3.10, along both longitudinal walls that are an integral part of the structural system. The structural system and racks are a proprietary design from Roof & Rack Products, Inc. so the dimensions gathered from the scans cannot be compared directly to anything found in the drawing set. All that is known is that they consist of wide flange beams and columns, with slender cross bracing.
Outside the boat racks the system is relatively straightforward, as there are columns all along the edge, with large non-prismatic beams spanning the lateral direction of the roof and purlins between them as can be seen in Figure 3.9 and Figure 3.10. The ridge of the roof is central and the slope towards the center is equal from both sides.

The first bay of Watson Landings Marina from the north (between column lines 1 and 2) collapsed almost completely as can be seen in Figure 3.11, with both the columns along line 1 and the purlins spanning the first bay showing signs of buckling. A closer view of the buckled purlins in the first bay can be seen in Figure 3.12 along with signs of local buckling in the purlins in the second bay. In addition, it is clear that the connections between the first two bays, especially towards the west side (between column lines F and H) suffered some damages, most likely as a result of the buckling in the first bay.

A more comprehensive overview of the building dimensions and the numbering conventions in the local coordinate system can be seen in Appendix A.

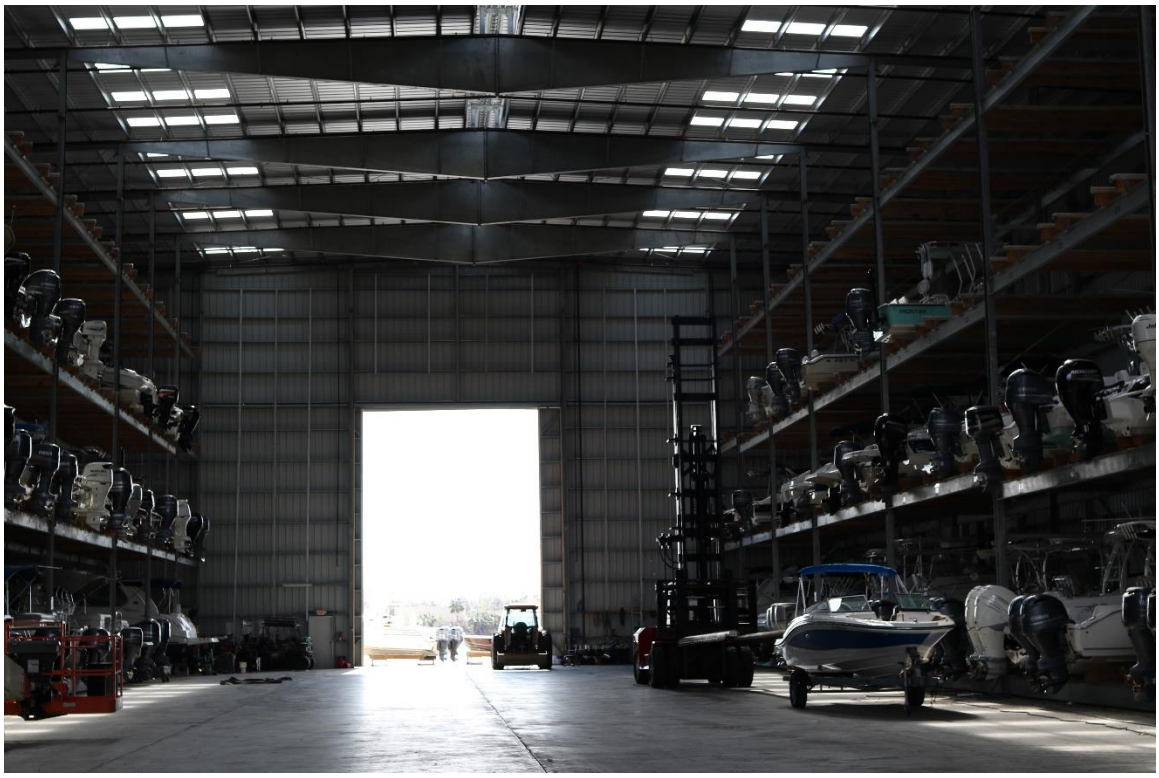

Figure 3.9. A view of the undamaged side of Watson Landings Marina.

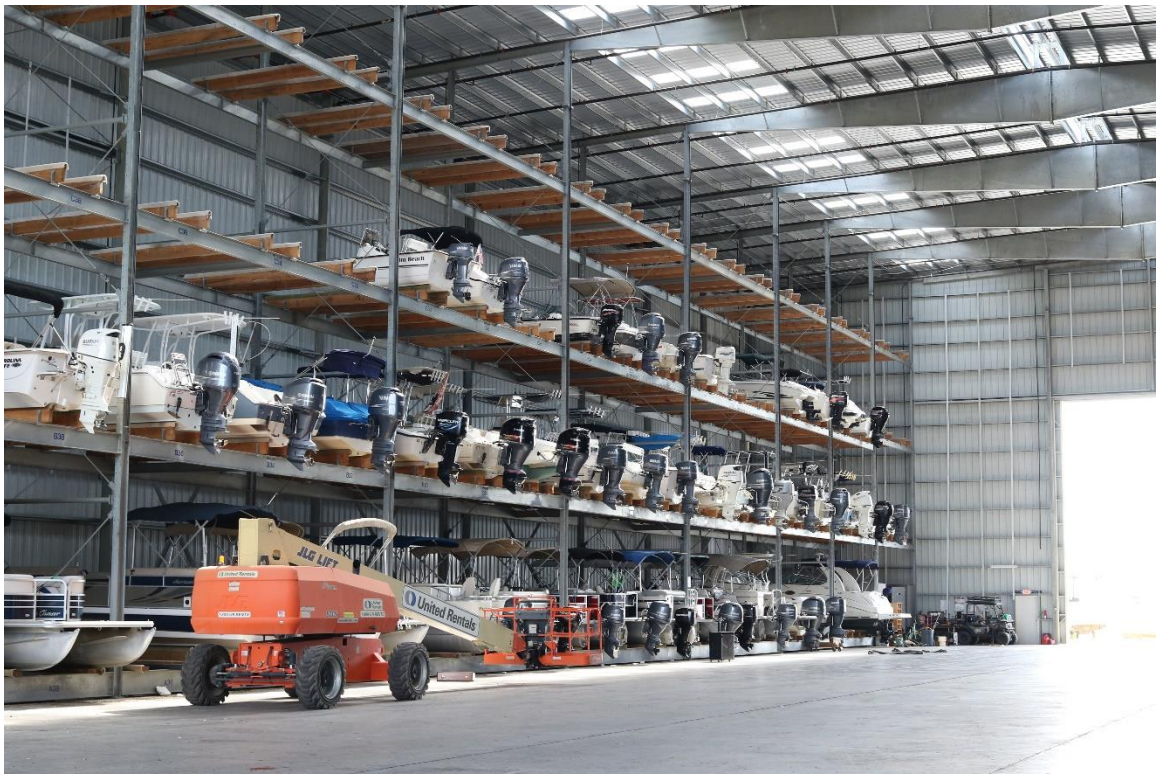

Figure 3.10. A view of the boat racks of Watson Landings Marina.

Figure 3.11. A view of the damaged face of Watson Landings Marina.

Figure 3.12. A view of the buckled purlins of Watson Landings Marina.

3.3.3 *Intermodal Distribution Center*

The Intermodal Distribution Center (IDC) has some major differences from most other buildings here, as its outer walls are concrete tilt-up walls, and not the usual steel columns with cladding, as can be seen on the back side of Figure 3.14. It is like Westrock East Terminal in the way that not the whole building was scanned, so everything but the most recent addition in the north-east end is missing. This most recent addition is shown in Figure 3.13 and is the part of the building right of the taller middle section in the figure, with damages visible on the rightmost edge. All the damage recorded was in that area, so no vital data is missing.

The roof consists of truss girders in both directions and is supported by five rows of columns in addition to columns at the tilt-up walls along the edge. These elements can all be seen in Figure 3.14, which is taken from the westernmost corner of the building towards the southeast facing wall. The scanned area is a single open space with no dividing elements other than the rows of columns.

The Intermodal Distribution Center suffered a complete collapse of the first bay on the northeastern face (between column lines 17 and 18), including the complete detachment of the concrete tilt-up wall without any clear evidence of failure within the wall itself. The absence of a northeastern facing wall is clear in Figure 3.15 and Figure 3.16, and there is also evidence of failures in the connections to the roof trusses, possibly stemming from the large deformations due to buckling of the roof system. The damage extended one bay further into the building around the center, between column lines 16 and 17 in the NW-SW direction and between column lines B and D in the NE-SE direction with further collapse of the roofing system.

A more comprehensive overview of the building dimensions and the numbering conventions in the local coordinate system can be seen in Appendix A.

Figure 3.13. Overview picture of the IDC.

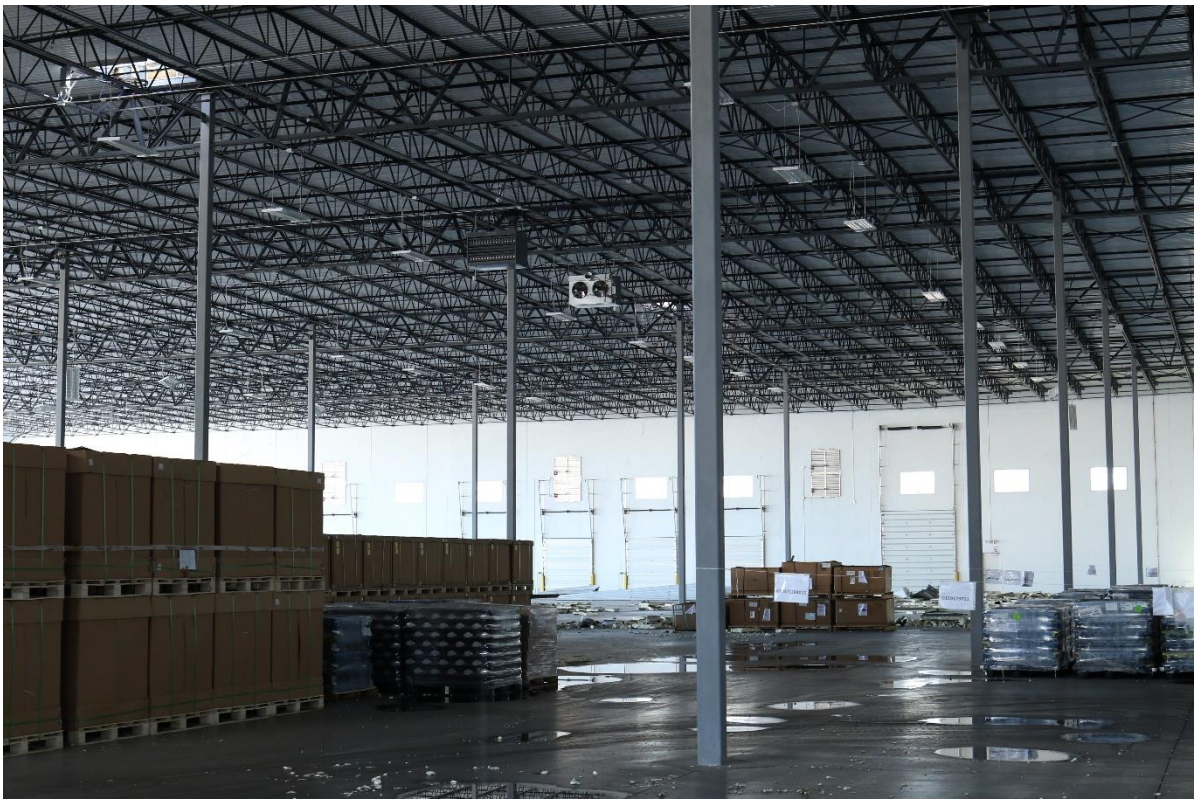

Figure 3.14. Column setup and roof framing from the IDC.

Figure 3.15. The damaged face of the IDC.

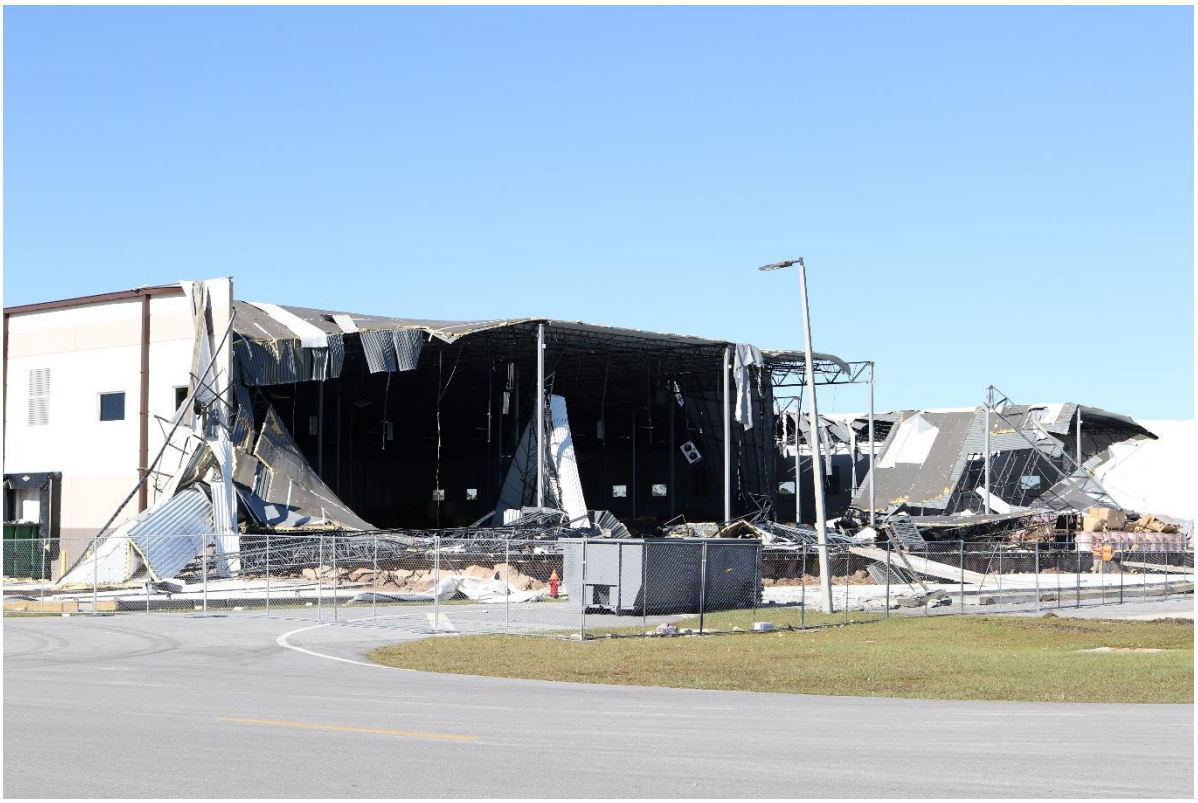

Figure 3.16. The damaged face of the IDC.

3.3.4 *Cargill Distribution Center*

Cargill Distribution Center is another storage facility that falls neatly into the LRLVB category. It is supported by wide flange columns along the edges and beams run laterally towards the ridge of the roof, which is central in this case. A truss girder runs along the whole ridge and supports the beams spanning the roof, along with lifting machinery used within the facility shown in Figure 3.17. The building consists of one open space, divided only by the truss girder in the middle.

The first two bays from the northernmost side collapsed completely, along with the wall on the west side spanning those same bays, while the central truss system and the eastern facing longitudinal wall did not collapse. Roof cladding was torn off one bay further into the building and slight damage to the cladding can be observed further into the building. These damages can be seen in Figure 3.18.

Cargill Distribution Center also suffered from damages in other places than the windward facing side, which was not observed in other buildings in this dataset. The back wall on the southernmost side fell out of the frame and cladding was torn out of the easternmost facing wall around bay 4 from the south as can be seen in Figure 3.19.

It is worth noting that some clean-up work had been done on the collapsed north side without any documentation, so the damage could have been exaggerated by that work.

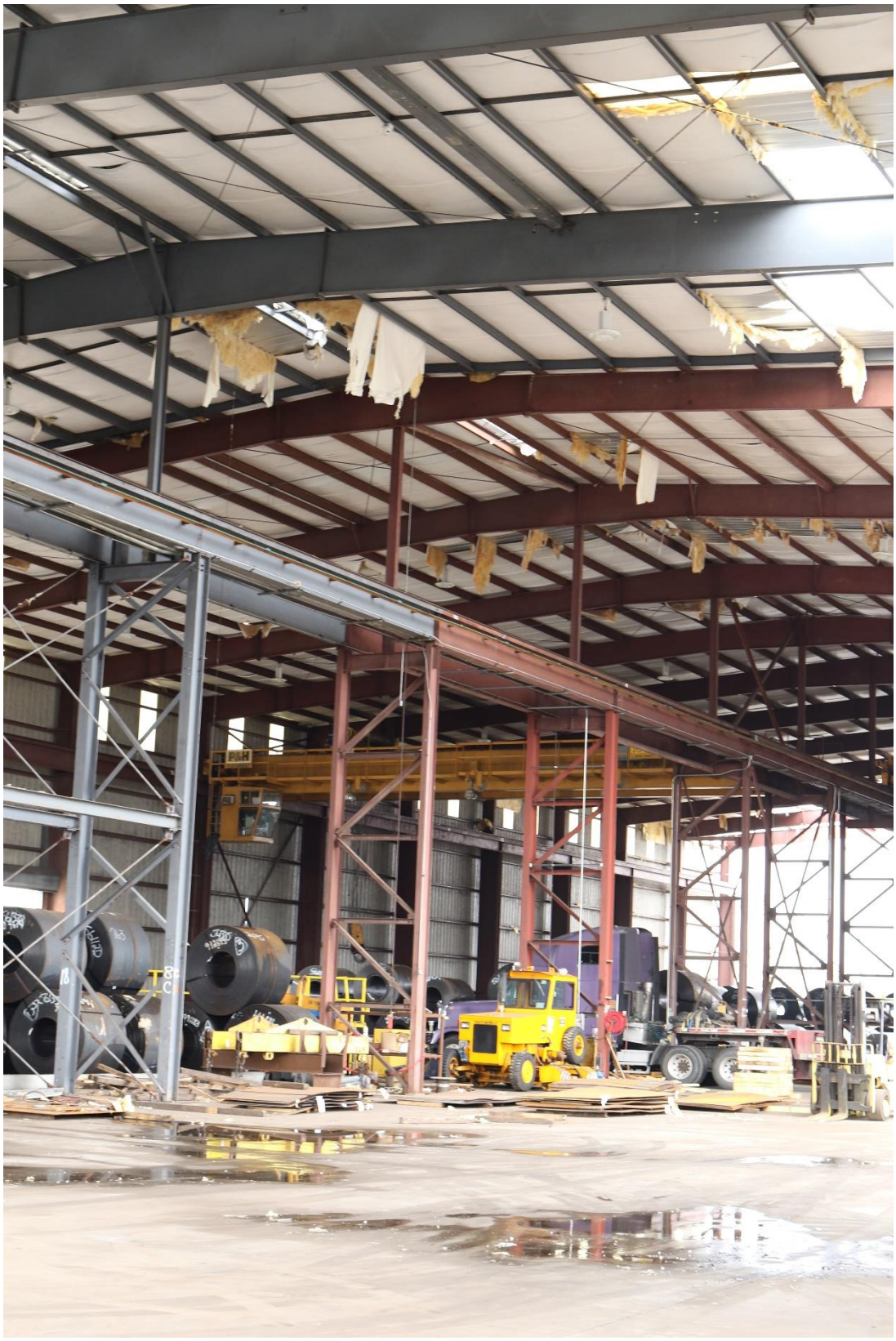

Figure 3.17. The framing system of Cargill Distribution Center.

Figure 3.18. The collapsed side of Cargill Distribution Center.

Figure 3.19. Other damage to Cargill Distribution Center.

3.3.5 *Tyndall Air Force Base: Hangar 5*

Hangar 5 is the only building with an arched framing system in this dataset and therefore it is possible to keep the whole floor space empty. The arches are truss girders spanning the shorter dimension of the building, and connected perpendicular to them are much smaller truss girders acting in the longitudinal direction, shown in Figure 3.20 and Figure 3.21. Cross bracing can be found in every other span, going into every slot along the direction of the arches.

The structural system did not suffer from any obvious damages, but the roofing was torn off in well over half the building as demonstrated in Figure 3.22 and Figure 3.23.

Figure 3.20. Roof framing in Hangar 5.

Figure 3.21. Roof framing in Hangar 5.

Figure 3.22. Overview of roof damage on the south facing side of Hangar 5.

Figure 3.23. Overview of roof damage on the north facing side of Hangar 5.

3.3.6 *Tyndall Air Force Base: Building 316*

Building 316 is one of the smaller buildings in this set and has a very simple geometry with a rectangular plan view. The roof has a relatively tall pitch and is spanned by large, tapered, wide flange beams which are interconnected by purlins. These beams then connect into columns on the long edges, while the short edges have almost no direct support as they have large openings. All of these features can be seen in Figure 3.24. There is a smaller room on the outside of the northernmost side of the building that was not scanned, but it can be seen on the right side of Figure 3.25.

The damage to Building 316 can be described as a total removal of the roof as can be seen in Figure 3.24 and Figure 3.25, but no clear damage to the structural system could be observed.

Figure 3.24. The roof system of Building 316.

Figure 3.25. The roof damage to Building 316.

3.3.7 *Tyndall Air Force Base: Building 333*

Building 333 has only a small portion of it scanned, but if the information gathered from the scanned end is assumed to be repeated throughout the building, it can be described sufficiently. The building is relatively long and has wide flange beams spanning the whole width of the roof and into columns on the sides. The roof has a gentle pitch towards the center that can be seen in Figure 3.26 and the beams are interconnected with purlins. There are cross-braces visible between the columns in the third span. No photographs were taken from within the building, so the observations made here are based on the point cloud models.

The least amount of damage of all the buildings discussed here was observed in Building 333 at Tyndall Air Force Base, with slight damages to the outside cladding visible in Figure 3.27 and Figure 3.28.

Figure 3.26. Front view of Building 333.

Figure 3.27. Paneling damages to Building 333.

Figure 3.28. More paneling damages to Building 333.

3.3.8 *Tyndall Air Force Base: Building 375*

Building 375 is similar to 316 and 333 as it has a rectangular plan and relatively simple moment frames. Wide flange beams span the whole roof from side to side where they connect into columns. The roof pitch is quite gentle, but clearer than in 333, and the roof beams are interconnected with purlins as is demonstrated in Figure 3.29. Cross braces are also visible here in between columns on the longitudinal sides. An elevated platform containing a room of some sorts is located in one of the corners and scans were taken from atop it, but none from the inside.

Much like the other buildings scanned at Tyndall Air Force Base, Building 375 suffered mostly from cladding damages to the roof, shown in Figure 3.30, with no clearly visible damages to the structural system.

Figure 3.29. The framing system in Building 375.

Figure 3.30. The roof damage to Building 375.

3.3.9 *Parthenon*

Parthenon is a low-rise, high volume storage facility, and is the only building of this set to have scans from inside various rooms. Those scans could not be registered so when the building is discussed, it is in reference to the main space. The frames are made of wide flange sections in both the beams and columns, and the beams are interconnected with purlins as can be seen in Figure 3.31 . The ridge of the roof is offset from the center, much like Westrock East Terminal, and under the ridge is a mid-span row of columns supporting the roof also seen in Figure 3.31, with the central row of columns being the row further away.

The damages to Parthenon included the collapse of the north facing wall shown in Figure 3.32 and large deformations to the roof-spanning beam along the second column line demonstrated in Figure 3.33. In addition, the roofing was torn off in the second bay and damages to the concrete side walls were recorded towards the north side, shown in Figure 3.34.

All the information about the structural failures gathered from Parthenon should be taken with a grain of salt, as the demolition process was well under way and therefore it is unclear what damages were caused by the hurricane and what was collateral damage in the clean-up process.

Figure 3.31. The framing system in Parthenon.

Figure 3.32. The collapsed side of Parthenon.

Figure 3.33. View of the collapsed beam in Parthenon.

Figure 3.34. View of the damaged wall in Parthenon.

3.3.10 *Miller Distribution Center*

Miller Distribution Center was not thoroughly scanned, and the part of the building visible in the scans is only a small part of the whole structure. It consists of various rectangular zones that can be identified from aerial photographs as either closed off spaces or overhangs of some sort. The area that was scanned has wide flange beams spanning the roof with smaller purlins in between, and the beams connecting into columns on the sides as can be seen in Figure 3.35.

The damage observed included the complete collapse of the roofing system, five bays into the structure from the north side, and large deformations of the side walls supporting the roof over the same distance. Those damages can be seen in Figure 3.35 and a closer view of the buckled purlins between the beams spanning the roof in Figure 3.36.

Figure 3.35. Overview of the damages to Miller Distribution Center.

Figure 3.36. Another view of the damages to Miller Distribution Center.

3.3.11 *Pirates Cove Marina*

Pirates Cove Marina has the worst quality scan of all the buildings in the dataset, as the field crew could not get close enough with their scanners. Therefore, most of the information gathered comes from photographs taken with a drone.

It is a steel frame building, and much like Watson Landings Marina, boat racks appear to be an integral part of the structural system. There is a single file of racks on either edge along with two rows in the middle. The roof is spanned by wide flange beams which are interconnected by purlins, and they connect to the central boat rack along with rows of columns on either side. The roof appears to have a gentle pitch towards the center, but due to the quality of scans it is difficult to tell. The framing system is most clearly demonstrated in Figure 3.38.

The roofing suffered a complete collapse between the westernmost side and the central row of columns, approximately five bays in from the north along with more minor cladding damages between bays five and nine as demonstrated in Figure 3.37. In addition, there were signs of buckling of roof purlins in the first bay between the easternmost side and the central row of columns which can be seen in Figure 3.39.

Figure 3.37. Pirates Cove Marina seen from the west.

Figure 3.38. Pirates Cove Marina seen from the northwest.

Figure 3.39. Pirates Cove Marina seen from the north.

3.4 SCAN LOCATION MAPS

Maps were made to illustrate where the lidar scanners were set up within each building. It is worth noting that the BLK360 scanners always do a single scan from each location whereas the XR3 scanners sometimes do two scans of varying resolutions from the same spot. That is denoted by a point that is double the area of a single scan location. Each scan location has a number that corresponds with the ones on DesignSafe, e.g. “XR3_1” for XR3 scans and “BLK_4” for BLK360 scans. The scan locations maps can be seen in Figure 3.40 through Figure 3.50.

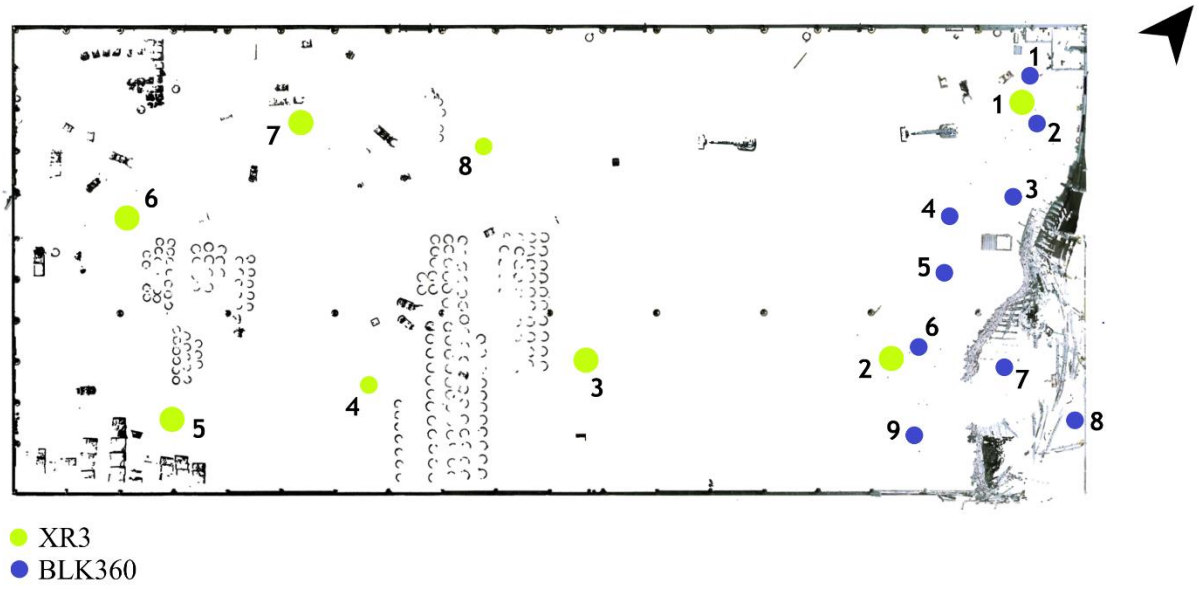

Figure 3.40. Locations of scans for Westrock East Terminal

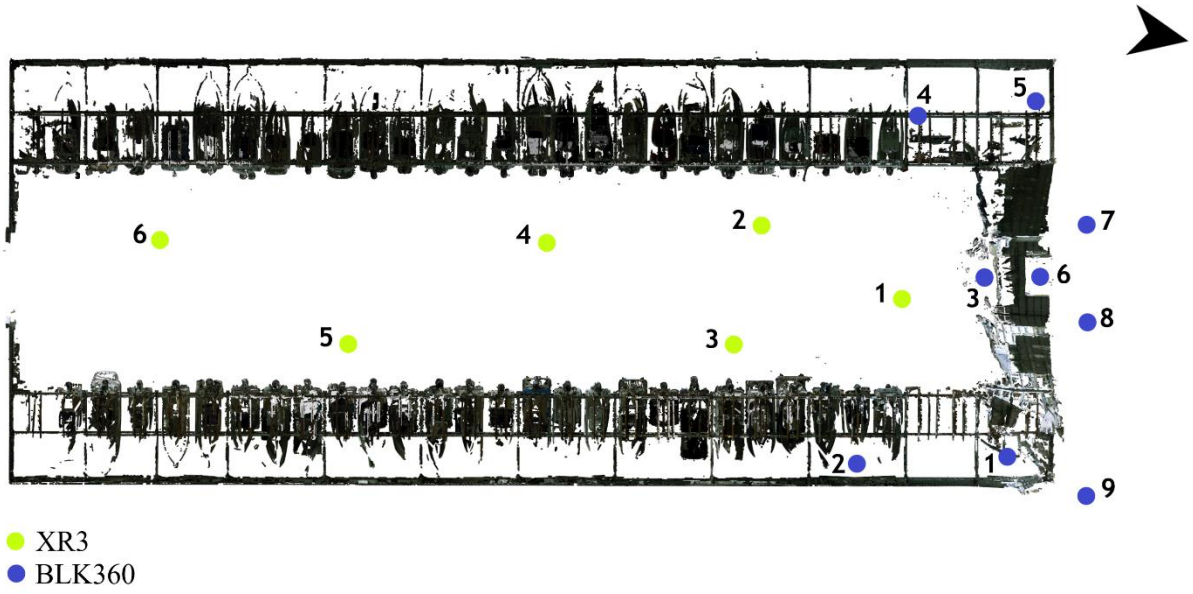

Figure 3.41. Locations of scans for Watson Landings Marina

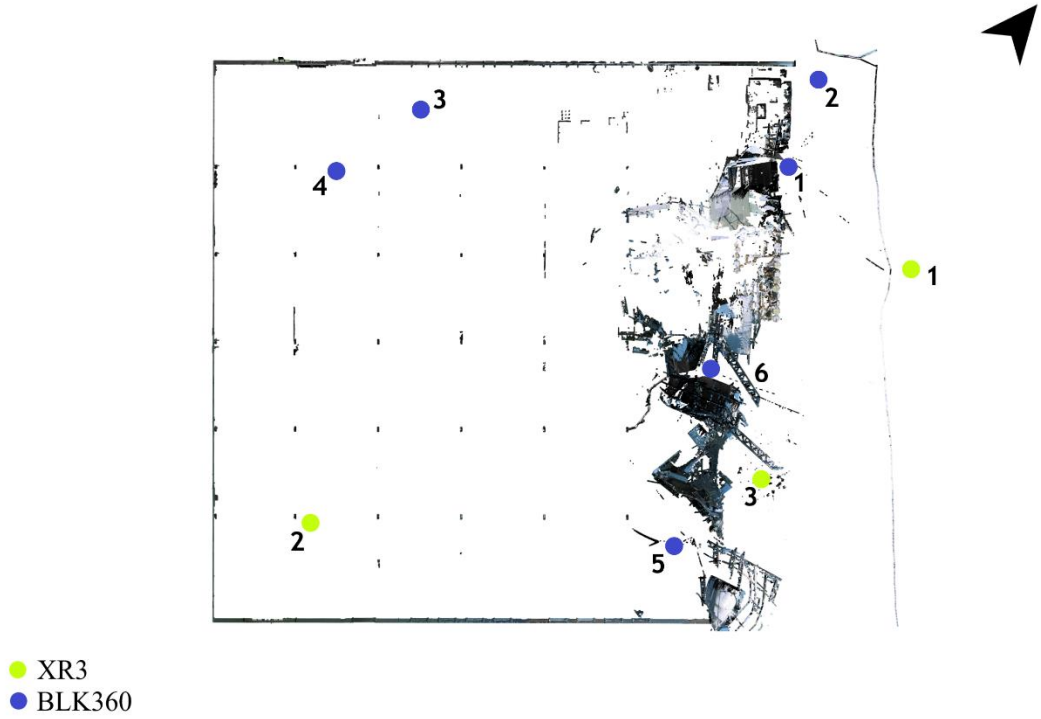

Figure 3.42. Locations of scans for Intermodal Distribution Center

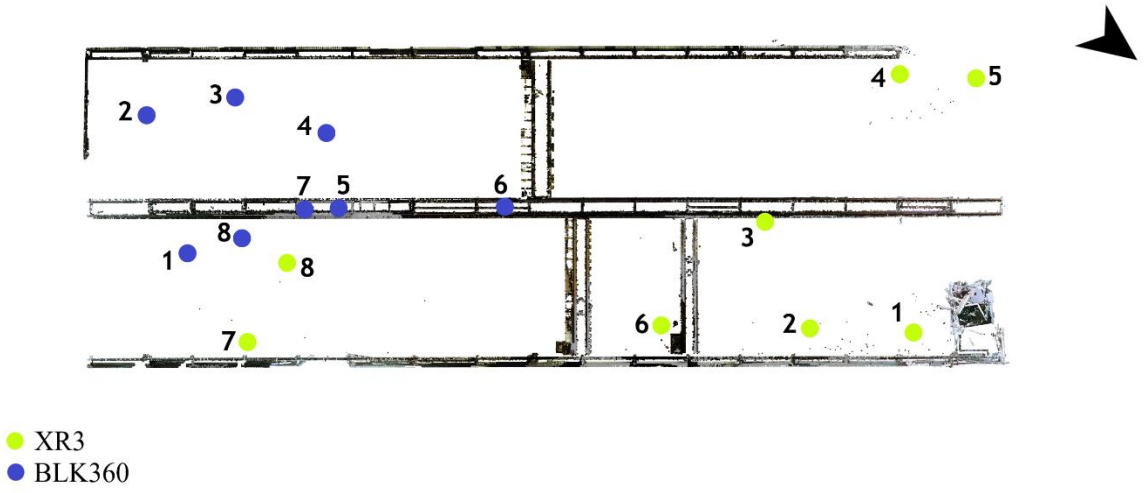

Figure 3.43. Locations of scans for Cargill Distribution Center

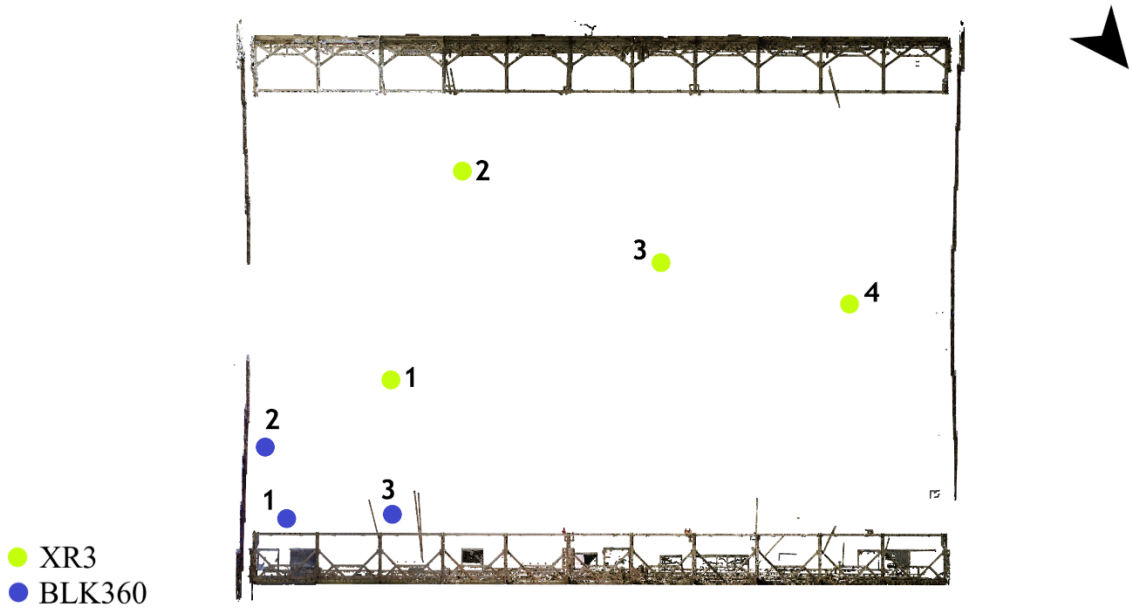

Figure 3.44. Locations of scans for Tyndall Air Force Base: Hangar 5

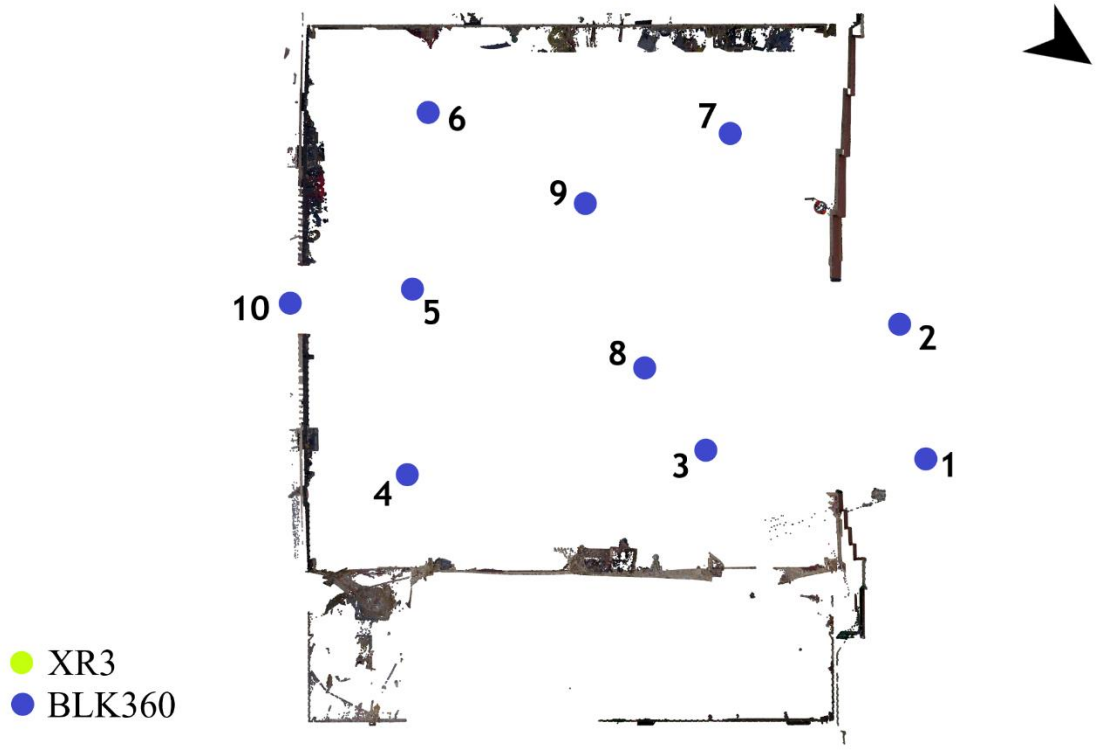

Figure 3.45. Locations of scans for Tyndall Air Force Base: Building 316

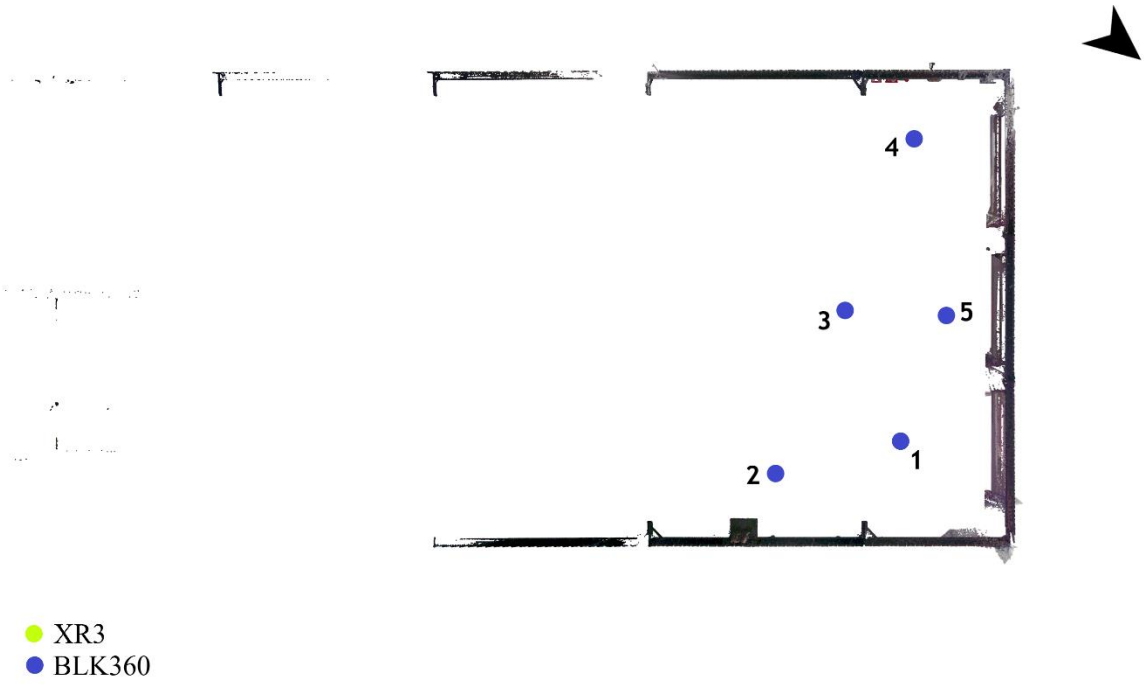

Figure 3.46. Locations of scans for Tyndall Air Force Base: Building 333

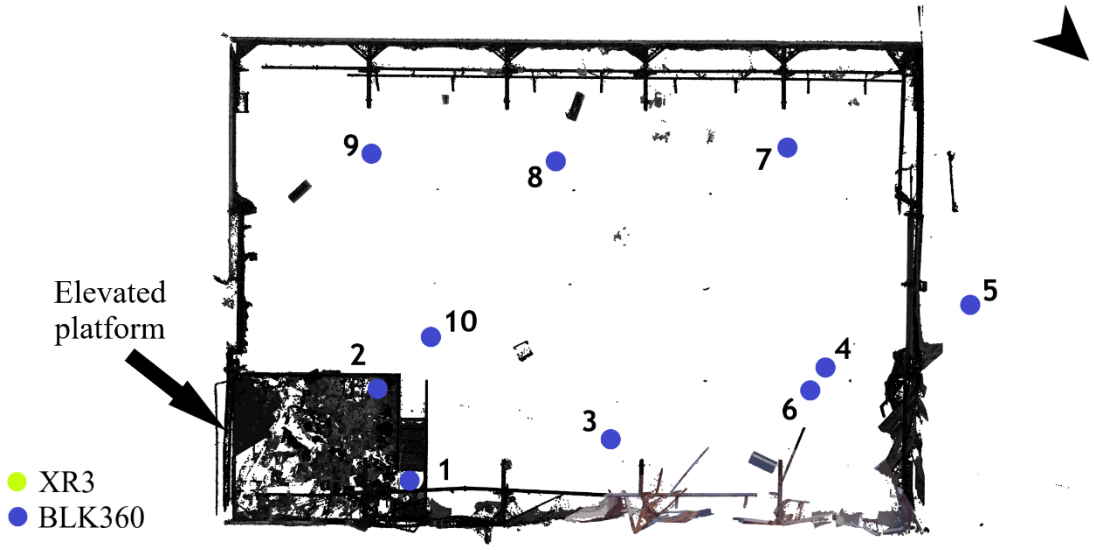

Figure 3.47. Locations of scans for Tyndall Air Force Base: Building 375

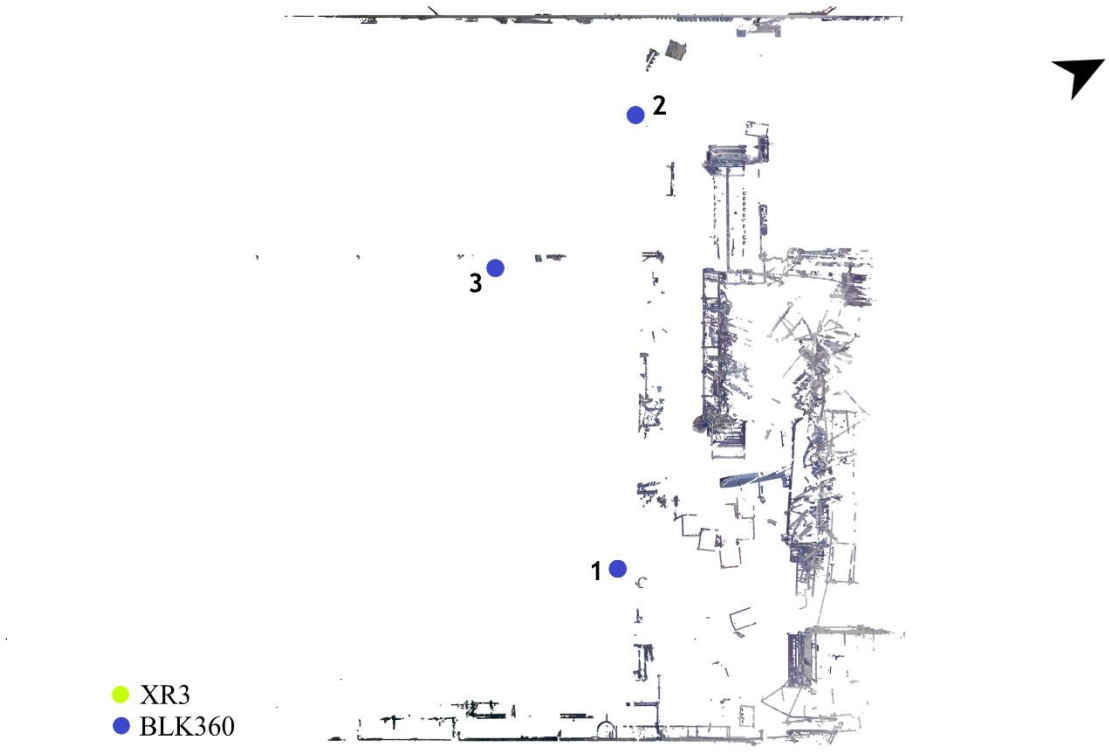

Figure 3.48. Locations of scans for Parthenon.

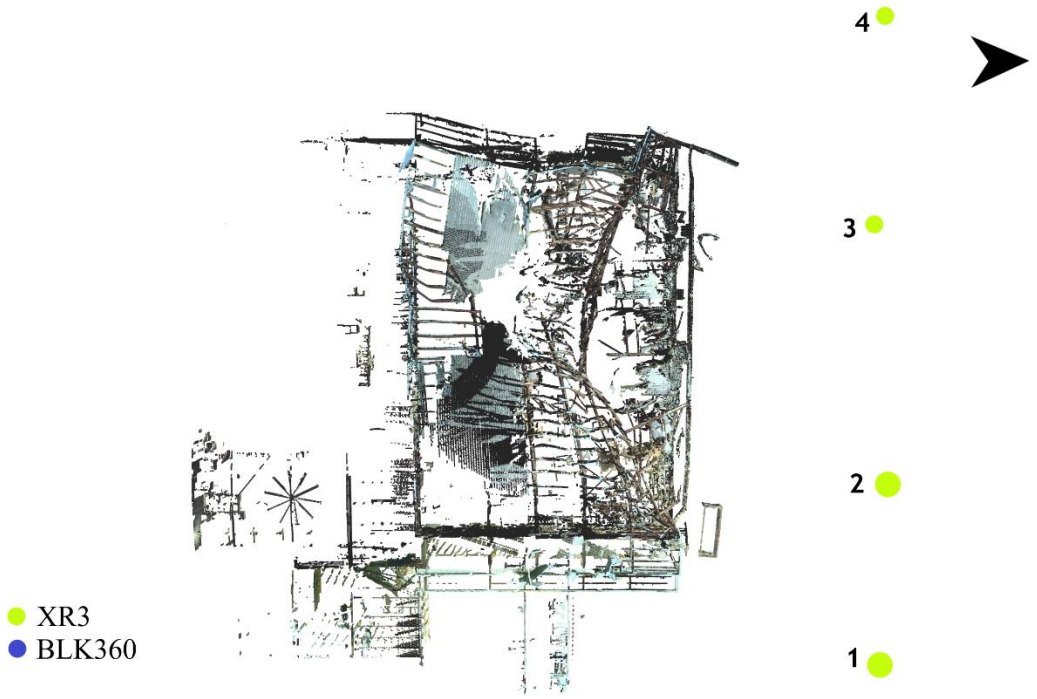

Figure 3.49. Locations of scans for Miller Distribution Center

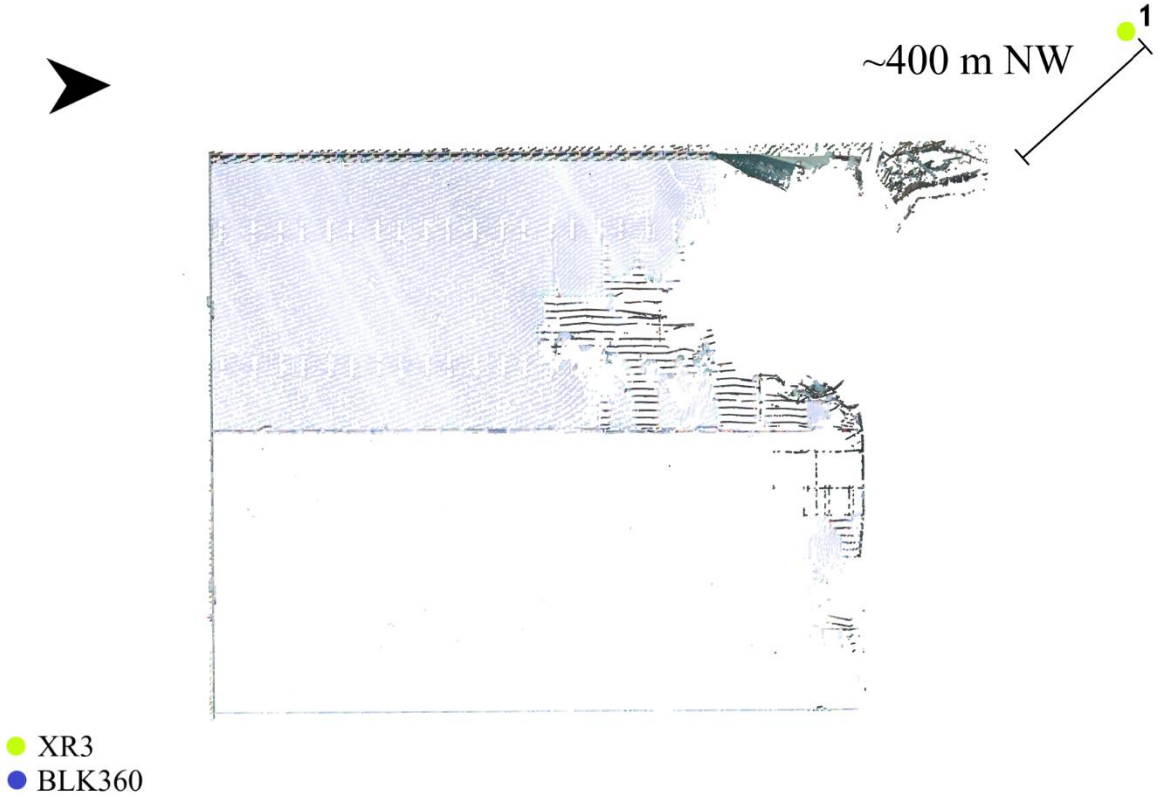

Figure 3.50. Locations of scans for Pirates Cove Marina

3.5 INSTRUMENTATION

Two types of scanners were used to gather data. Firstly, the Leica BLK360 Imaging Scanner and those scans are referred to as BLK360 or short-range scans, and secondly the Maptek I-Site XR3 which will be referred to as XR3 or long-range scans. The specifications for each are described below.

3.5.1 *Leica BLK360 Imaging Scanner*

Distance measurement system:	High speed time of flight enhanced by WFD technology.
Laser class:	1 (in accordance with IEC 60825-1:2014)
Wavelength:	830 nm
Field of view:	360° (horizontal) / 300° (vertical)
Range*:	min. 0.6 - up to 60 m
Point measurement rate:	up to 360,000 pts/sec
Ranging accuracy*:	4mm @ 10m / 7mm @ 20m
Measurement modes:	3 user selectable resolution settings.

Figure 3.51. Picture of the BLK360 scanner from Leica.

3.5.2 *Maptek I-Site XR3 Scanner*

Maximum range:	2400m off reflector
Minimum range:	2.5m
Range accuracy:	5mm
Repeatability:	±4mm
Exit aperture:	<8mm
Beam divergence:	0.25mrad
Acquisition rate:	200 kHz 100 kHz 50 kHz
Product laser class:	Class 1 IEC60825-1:2014
Wavelength:	Near IR
Intensity measurement:	Yes
Angular step selectable:	0.2° to 0.0125°
Angular scanning range:	100° vertical (-40° to +60° with no camera), 360° horizontal.

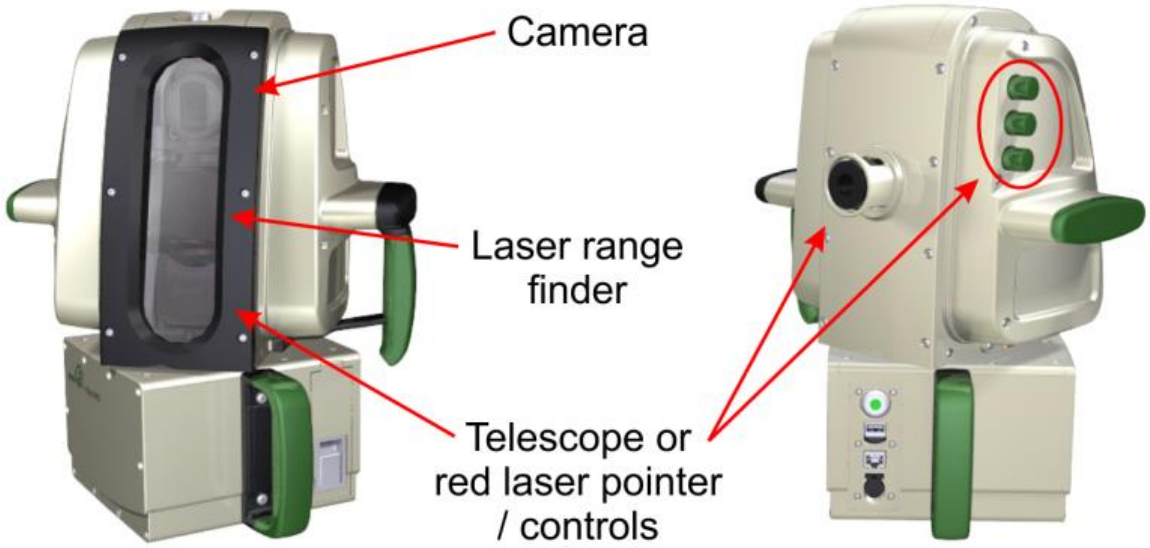

Figure 3.52. Picture of the XR3 scanner from Maptek.

3.6 DATA TYPES

The Leica BLK360 scanner uses the .blk file format that stores X, Y and Z coordinated in space in relation to the scan location, along with an RGB color value for each point.

Maptek's XR3 scanner stores its scans in an r3s format and to register them, they are imported into a maptekdb database format to be registered and processed within Maptek PointStudio.
When point clouds are merged it is necessary to have them readable by the same program. In this case the BLK360 scans are registered first and then exported in the e57 file format, which is a 3D image file. It keeps the point clouds from each scan location separate, so the user can turn individual scans on and off, depending on what the intentions are.
The e57 file can then be directly imported into Maptek PointStudio, and simultaneously into the maptekdb where the XR3 scans are registered, to combine them into a single point cloud.

When the processing is complete, the point clouds are exported in an LAS file format for viewing and future use. In this case LAS 1.4 was used and all the models referenced are accessible on DesignSafe in that format.

3.7 DATA REGISTRATION TOOLS

Point cloud registration is the process of gathering multiple scans in software designed for that purpose and relating them to each other. This is done through targets that the surveyors set up to have a spatial relation between scan, or through objects that are common with multiple scans. These objects can be anything that stays stationary between scans, like beams, columns or other structural elements.

Like virtually all the resources used here, the data registration tools were supplied by NHERI RAPID. That applies to both the processing computers used to register and manipulate data, and the software licenses needed to do so.

3.7.1 *Software*

The software used in the point cloud processing is mainly from Leica and Maptek, who are the manufacturers of the scanning equipment too. In addition to that, the open source 3D point cloud processing software, CloudCompare, was used for extracting information from the clouds after they had been registered and adjusted in the other programs.

Leica Cyclone 3D Point Cloud Processing Software was used to register BLK360 data, and in some cases, Leica Cyclone REGISTER 360. The REGISTER 360 version takes the user step-by-step through the registration process, while the original Cyclone is not as intuitive but offers more possibilities for the user to manually interfere with the process as is deemed necessary.

Maptek PointStudio was used in registering the long range XR3 as well as combining different types of scans together. Familiar users might not recognize the PointStudio software, as it was formerly known as I-Site Studio before November 2018 when the name changed along with the user interface (Maptek, 2018).

CloudCompare is an open source 3D point cloud processing software where most of the measurements were done. This was done so that users that do not have licenses for Leica or Maptek software can visualize and manipulate processed point clouds demonstrated here.

3.7.2 *Hardware*

During the course of the research, two processing computers were used. When data processing limitations such as maneuverability within the model are discussed, the newer computer specifications apply, but some of the initial data processing was done on the older one.

3.7.2.1 Older Processing Machine

OS: Microsoft Windows 10 Home, 10.0.18362, x64
CPU: Intel® Core™ i9-7900X CPU @ 3.30 GHz, 10 Cores, 20 Logical Processors.
RAM: 128 GB DDR4
GPU: 2x NVIDIA GeForce GTX 1080 Ti.

3.7.2.2 Newer Processing Machine

OS: Microsoft Windows 10 Enterprise, 10.0.18362, x64

CPU: Intel® Core™ i9-9980XE CPU @ 3.00 GHz, 18 Cores, 36 Logical Processors.

RAM: 128 GB DDR4

GPU: NVIDIA GeForce RTX 2080 Ti.

Chapter 4. LIDAR REGISTRATION, CLEANING AND FEATURE EXTRACTION.

4.1 INTRODUCTION

The process of registering lidar scans together is described in this chapter. A quick overview of the steps taken in each of the programs used to register data will be given here for future reference and repeatability.

All the raw data used in Chapter 4 is available here:
https://doi.org/10.17603/ds2-3jpz-sk97 (Berman et al., 2020).
The processed models will be available in the same directory in spring 2020.

Leica

1. Import raw BLK360 files into Leica Cyclone REGISTER360.
2. Use the automatic link creation to establish a model.
3. Visually examine the links, make adjustments as needed, and add missing links between individual scan locations if needed.
4. Export an e57 file along with an error report.

Maptek

1. Import raw XR3 scan files into Maptek PointStudio.
2. Choose two scans in close proximity to each other.
3. Use the free transform tool to visually align these two scans.
    a. Use section view to increase the accuracy of the visual alignment.
    b. Use elevation view to make sure the scans are in the same elevation.
4. Globally register the scans together using one of them as a reference.
5. Repeat for all other scans, using the already registered scans as a reference.
6. Import the e57 file exported from Leica Cyclone REGISTER360.
7. Treat that registration as a single scan and repeat steps 3 and 4.
8. Check section views in X, Y and Z directions to confirm the registration.

4.2 WESTROCK EAST TERMINAL

4.2.1 *Review of available lidar data*

Westrock East Terminal was scanned relatively extensively, compared to the other ten buildings, with 18 Maptek XR3 scans, of which 3 were unusable due to an incomplete registration. There were 19 available BLK360 scans, which can theoretically be loaded into Maptek PointStudio with the processing computer setup used here. However, for optimization purposes the number was lowered to 14 by removing scans in extreme proximity to other scan locations, and by removing scans located where the area of interest was beyond the range 30 meter range of the BLK360 scanners. The scan locations can be seen in Figure 3.40.After importing all scans and prior to any cleaning, the Maptek database file containing all the scans is 52.3 GB.

4.2.2 *Data registration overview and challenges*

Registration was done with 15 XR3 scans and 14 BLK360 scans. However, registration was hampered by a water over much of the floor of the building, which caused a reflection in most of the scans. Therefore, the number of scans was lowered to 14 XR3 and 9 BLK360 scans. This might have something to do with the registration algorithm taking into account the mirror image of the building within the floor, but that complication is not the subject of this thesis. The final registration contained 140,562,527 points from XR3 and 349,518,195 from BLK360, totaling 490,080,722 points. A point cloud of that size can take quite substantial time to work with and therefore a “minimum separation” filter with a 0.5 cm distance was applied, displaying only points who have no neighbors within that distance. After applying the filter 278,691,049 remained, of which 113,924,520 were XR3 and 164,766,529 were BLK360. This technique allows the user to observe everything on a macro scale, e.g. observing failure modes, but this is not optimal when looking at sections and other micro scaled procedures so other techniques must be used to reduce the number of points in the model.

4.2.3 *Point cloud cleaning*

The cleaning process was relatively straight forward for this building and mostly consisted of removing items that were stored in the building and temporary machinery from the view to better

observe the damaged face from inside the building. Standard procedures of removing everything from outside the building were used in addition and after these steps were taken 205,152,478 points remained, 44,765,459 from the XR3 and 160,387,019 from the BLK360.

Figure 4.1 through Figure 4.10 show the cleaning process from various angles, demonstrating the differences between XR3 and BLK360 data. The figures come in pairs where the untouched model is showed first and the fully cleaned version follows. When looking at the pictures from inside Westrock East Terminal, the floor looks like it has been cut out of the cleaned versions, but there is technically no floor to begin with. There is only the reflection in the water which looks like it is in floor height, but, is a mirrored version of the roof below the floor.

Figure 4.11 and Figure 4.12 show a single bay extracted from Westrock East Terminal, demonstrating the slicing abilities of PointStudio to get a clearer view of elements of interest.

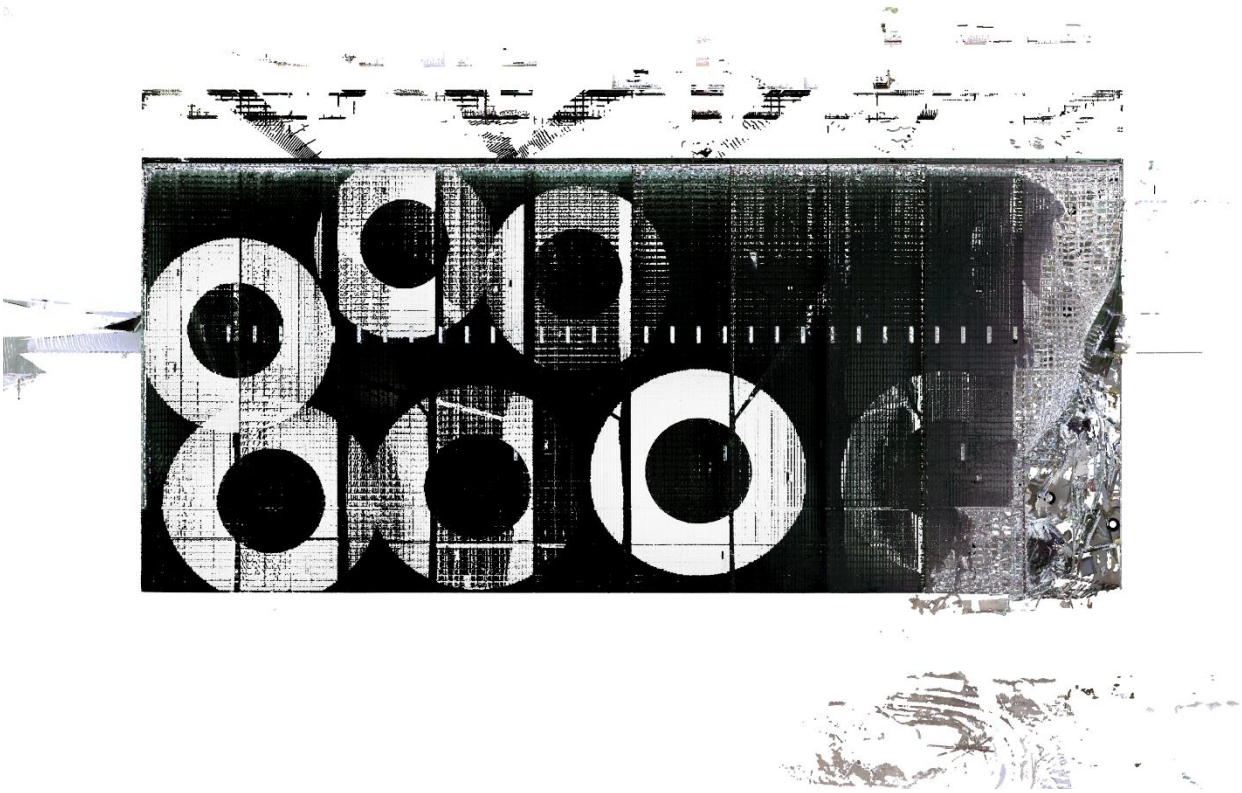

Figure 4.1. Aerial view before any modifications were done to the point cloud.

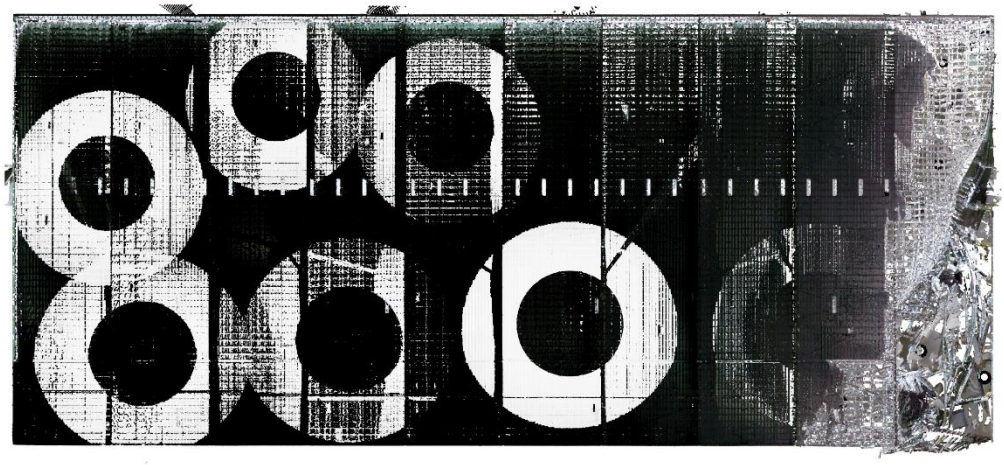

Figure 4.2. Aerial view after cleaning.

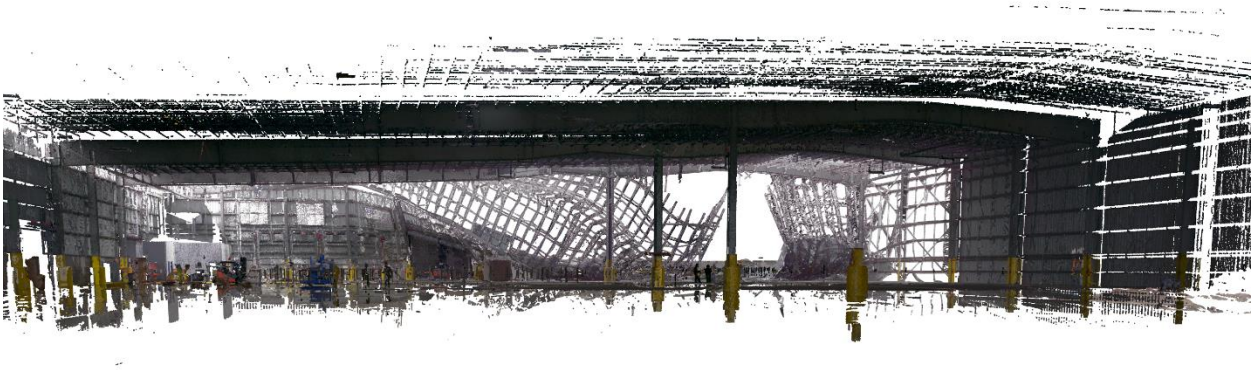

Figure 4.3. Inside view before cleaning showing only BLK360 data.

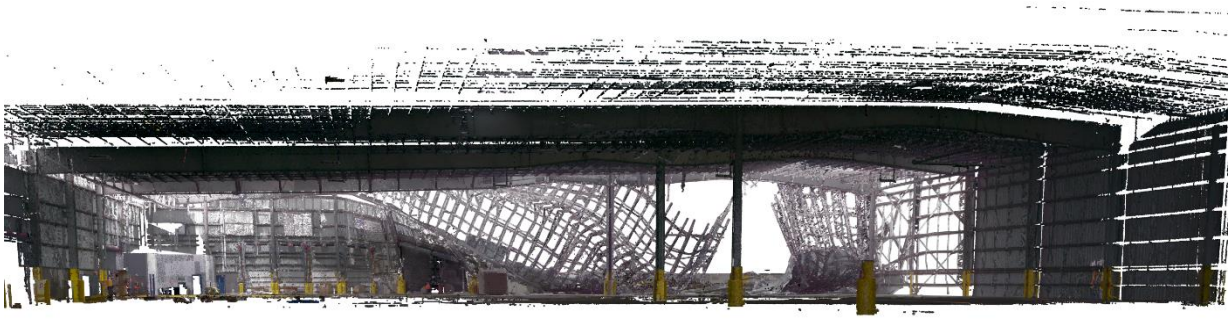

Figure 4.4. Inside view after cleaning showing only BLK360 data.

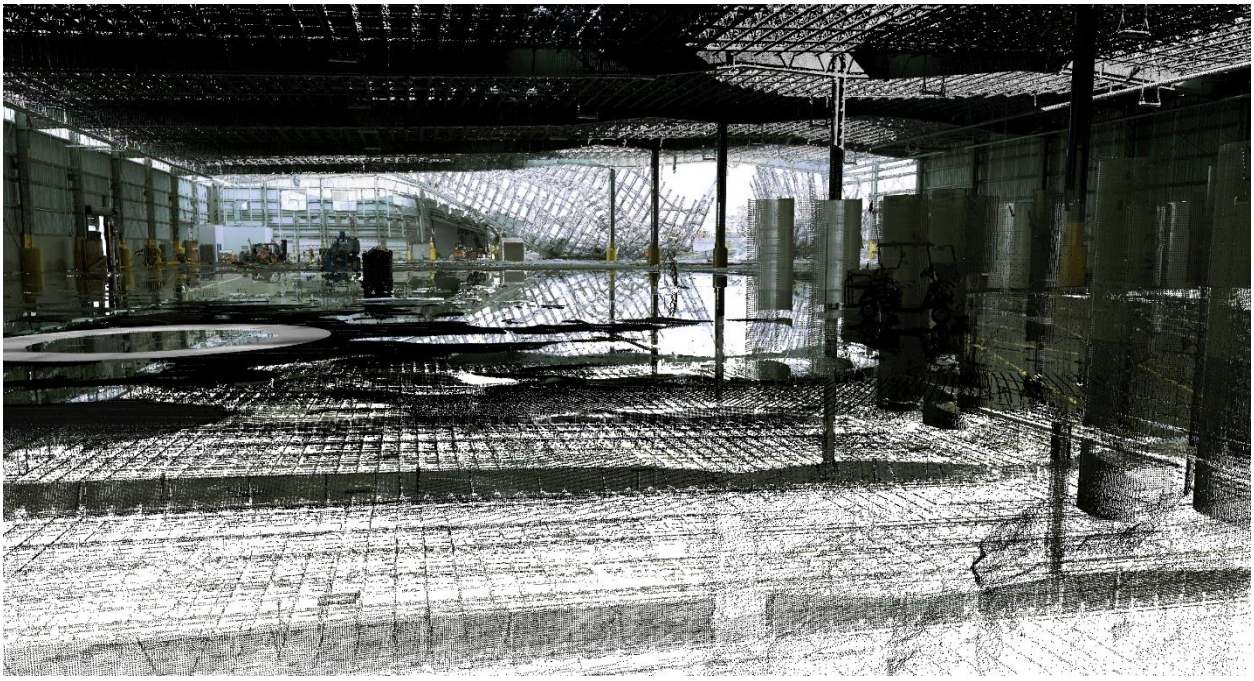

Figure 4.5. Inside view before cleaning showing only XR3 data.

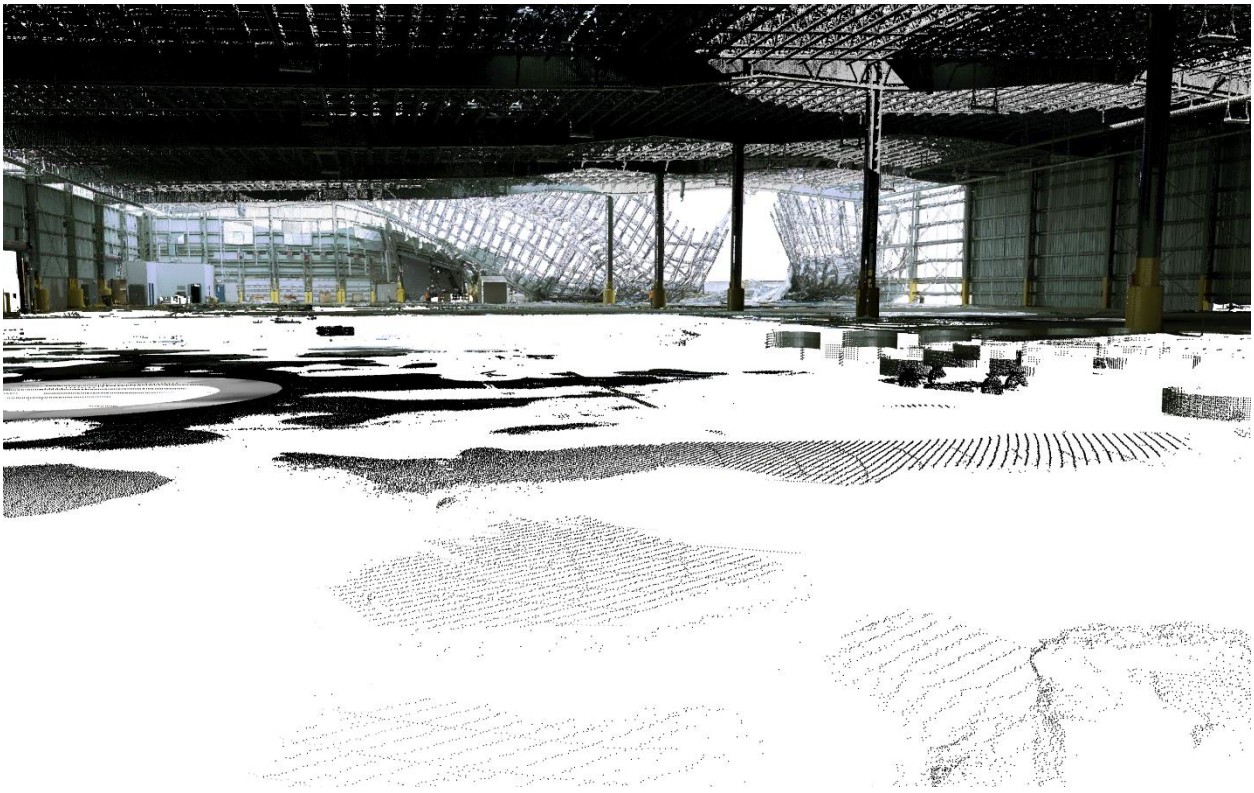

Figure 4.6. Inside view after cleaning showing only XR3 data.

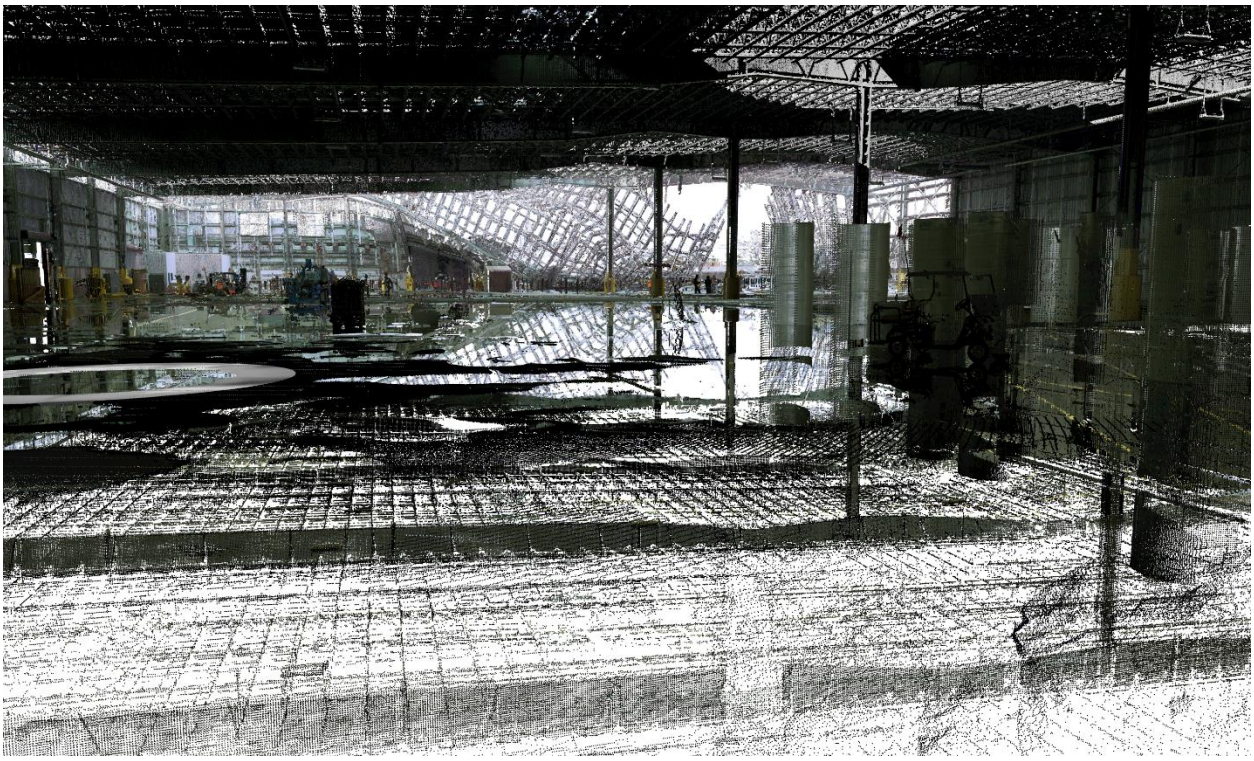

Figure 4.7. Inside view before cleaning with both XR3 and BLK360

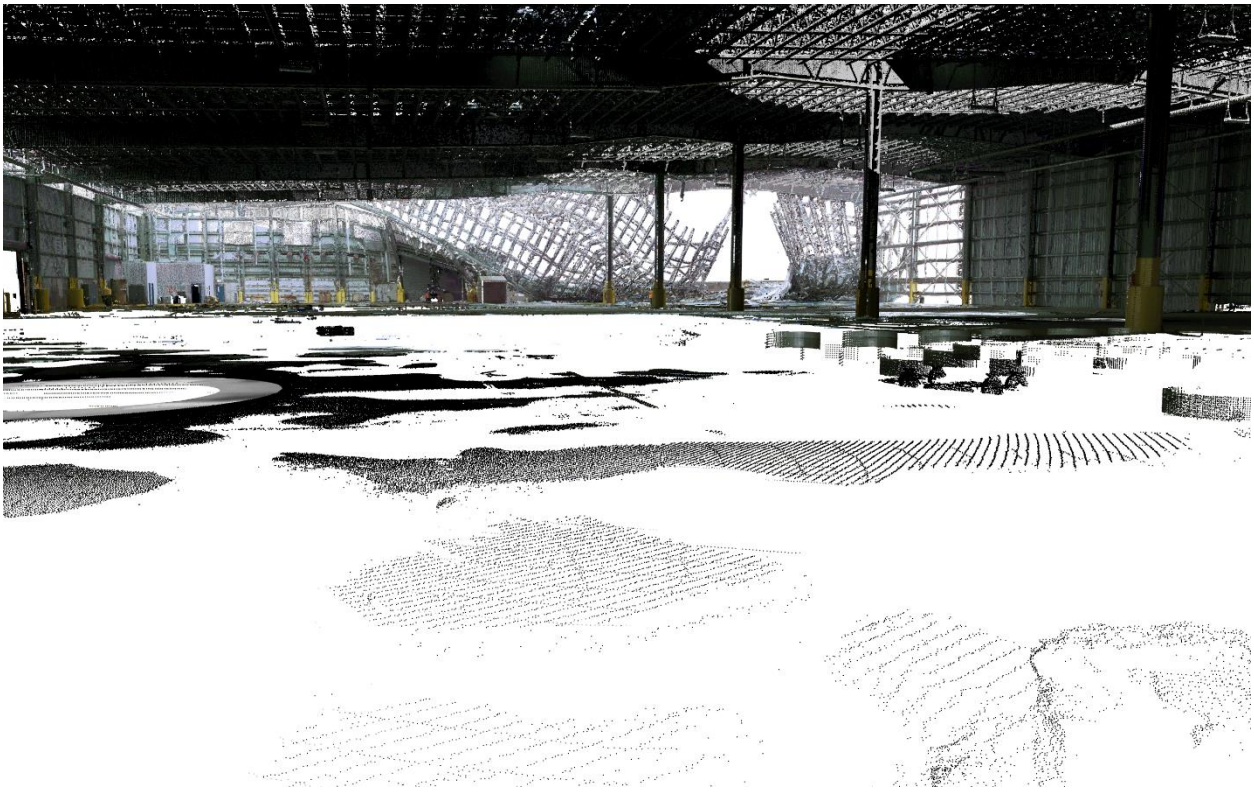

Figure 4.8. Inside view after cleaning with both XR3 and BLK360

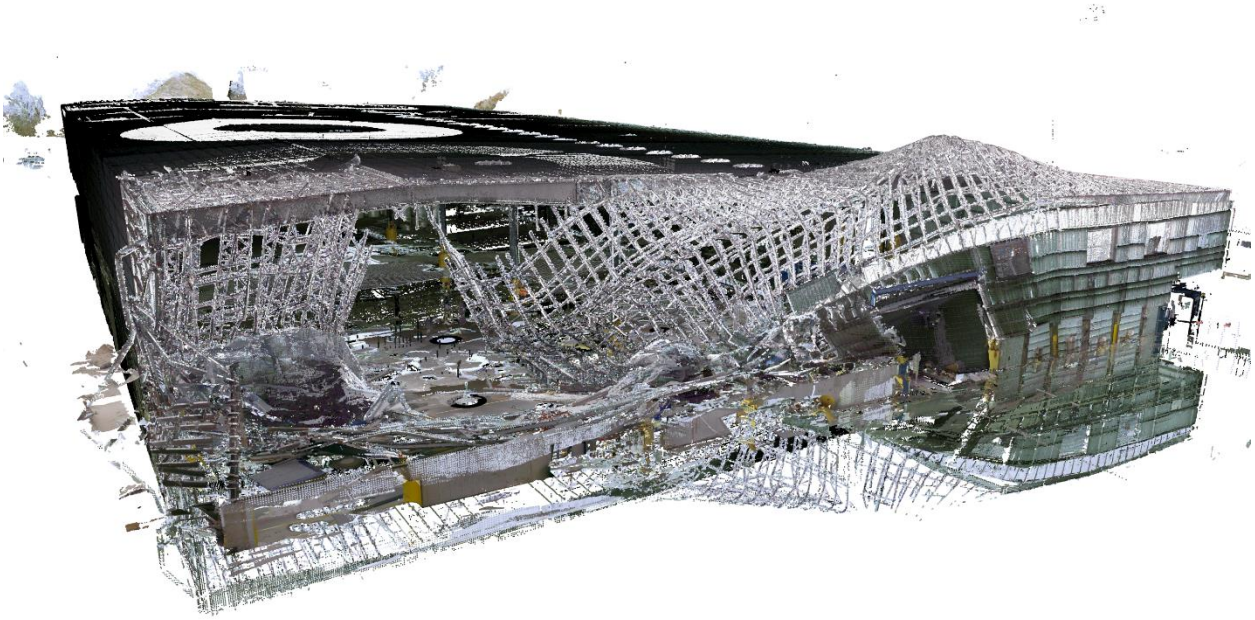

Figure 4.9. Outside view before cleaning showing both BLK360 and XR3 data.

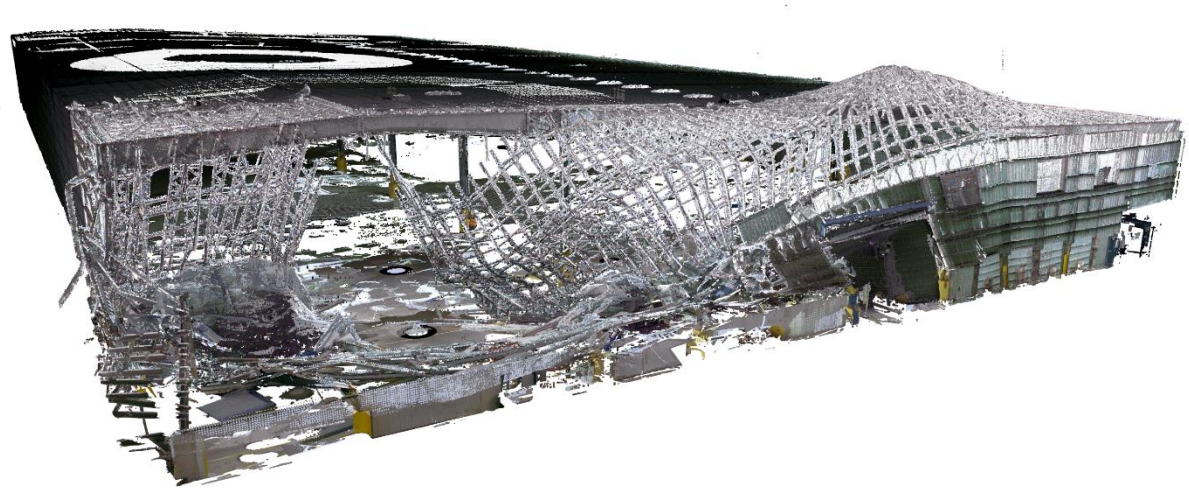

Figure 4.10. Outside view after cleaning showing both BLK360 and XR3 data.

Figure 4.11. A single bay from Westrock East Terminal using XR3 data only.

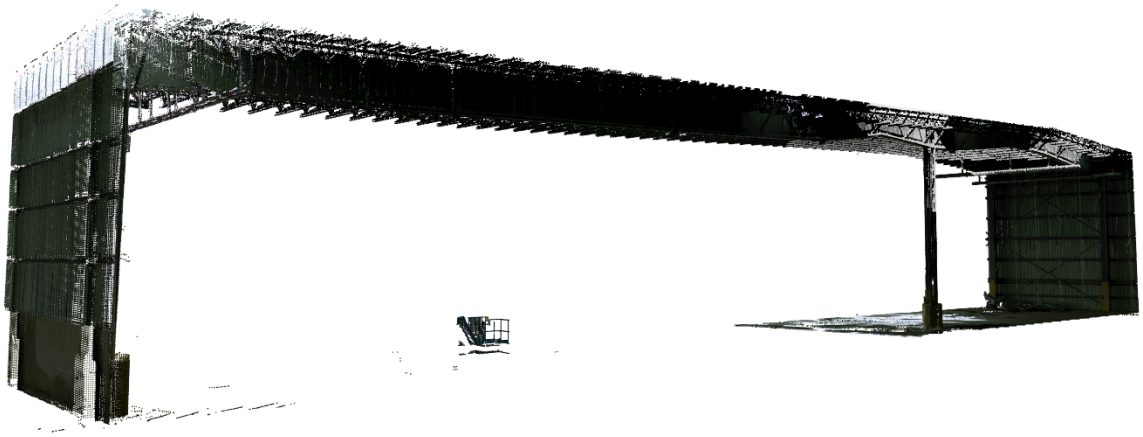

Figure 4.12. A single bay from Westrock East Terminal using XR3 data only.

4.2.4 *Other observations*

No other observations were made.

4.3 WATSON LANDINGS MARINA

4.3.1 *Review of available lidar data*

Watson Landings Marina was scanned more extensively than all the other buildings in this eleven building set from Panama City, FL. It consists of eleven Maptek XR3 scans, two of which were incomplete and thus nine remained. After some iteration a decision was made to reduce to the number of scans for this model due to the sheer number of them, so double scan locations were reduced to single ones and with that, 6 scans from the Maptek XR3 were used for the final registration. There were a total of 30 BLK360 scans available, but it is not feasible to use that many in a registration due to hardware limitations, so a subjective assessment of which scans to use was done. There were 17 scans outside the damaged face of the building, but the point density does not need to be this high since outside scans capture mostly the cladding. Only 4 scans were used from the outside, with a focus on areas where structural elements were exposed i.e. centrally by the door. Inside there were 13 scans, of which 4 were disregarded due to proximity to other BLK360 scans, and 4 due to heavily obstructed views which results in unnecessary density in very specific locations. The final number of BLK360 scans was 9. The scan locations can be seen in Figure 3.41.
The Maptek database containing all the scans is 28.9 GB.

4.3.2 *Data registration overview and challenges*

The final registration contained 297,956,363 points from the XR3 and 401,172,053 from the BLK360. The total number of points in the cloud is 699,128,4166 , which is too many for the processing machine used here to effectively work with, so an extra step had to be taken where a “minimum separation” filter with 5 cm as the input was utilized forcing PointStudio to display only points that have no neighboring points within that distance. This technique allows the user to observe everything on a macro scale, e.g. observing failure modes, but this is not optimal when

looking at sections and other micro scaled procedures so other techniques must be used to reduce the number of points in the model.

4.3.3 *Point cloud cleaning*

The cleaning process was relatively straightforward for this building and mostly consisted of removing debris and equipment from the floor, along with the standard procedures of removing everything from outside the building. After these steps were taken 473,220,825 points remained, 170,847,864 from the XR3 and 302,372,983 from the BLK360. A further reduced and cleaned model with the previously mentioned minimum separation filter of 5 cm is much smaller, at 9,460,357 points, of which 7,065,740 are XR3 and 2,394,617 BLK360, and can therefore be opened and manipulated in much less powerful processing computers.

Figure 4.13 through Figure 4.22 show the cleaning process from various angles, demonstrating the differences between XR3 and BLK360 data. The figures come in pairs where the untouched model is showed first and the fully cleaned version follows

Figure 4.23 and Figure 4.24 show a single frame extracted from Watson Landings Marina, demonstrating the slicing abilities of PointStudio to get a clearer view of elements of interest.

Figure 4.13. Aerial view before any modifications were done to the point cloud.

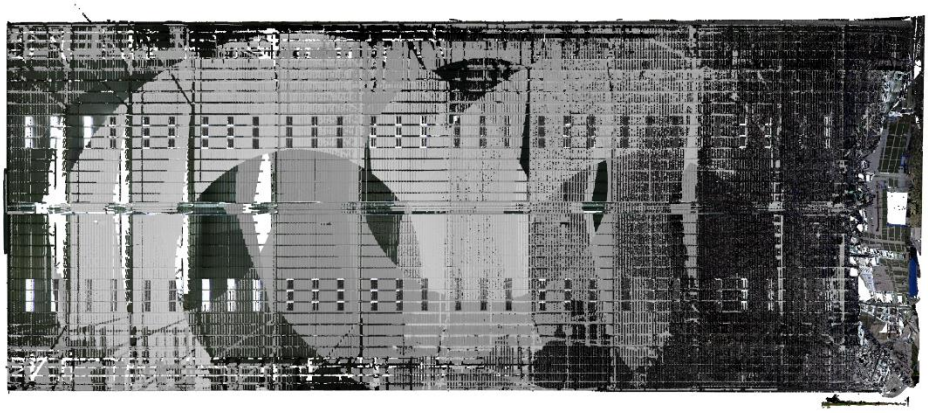

Figure 4.14. Aerial view after cleaning.

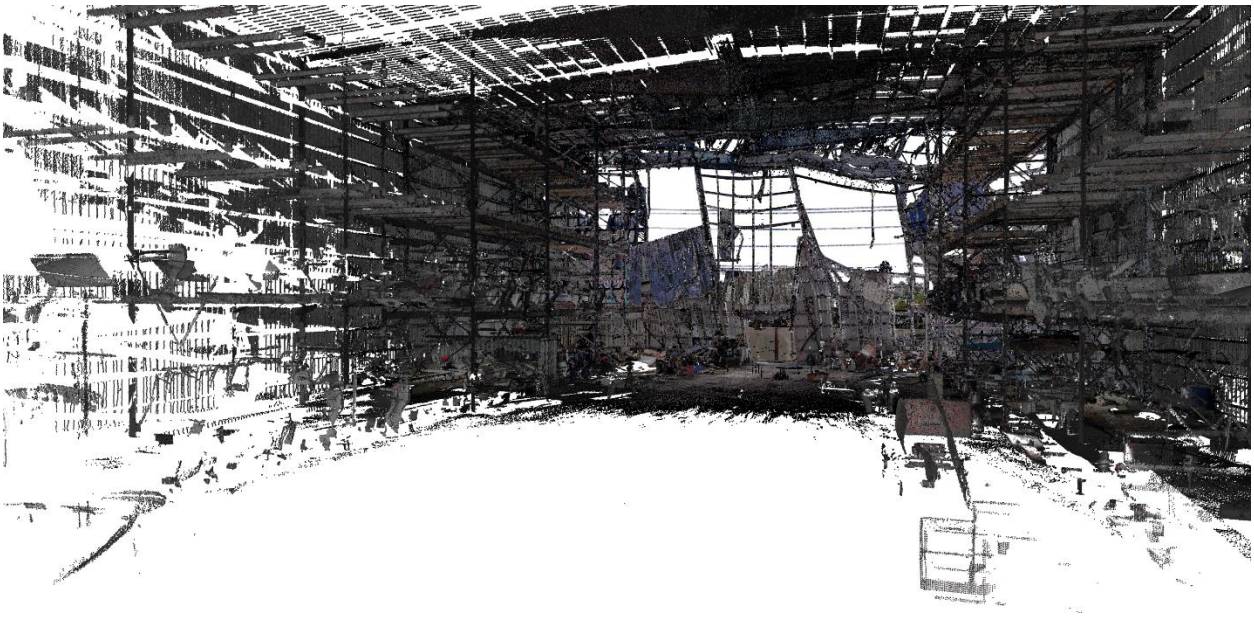

Figure 4.15. Inside view before cleaning showing only BLK360 data.

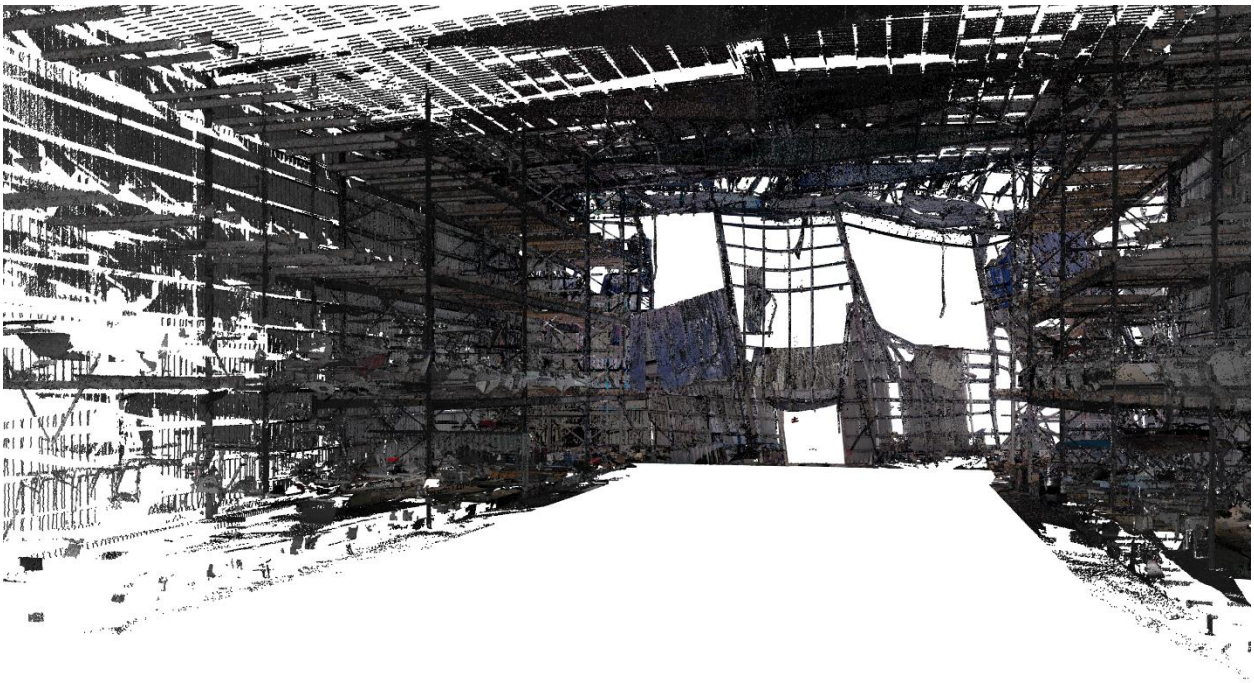

Figure 4.16. Inside view after cleaning showing only BLK360 data.

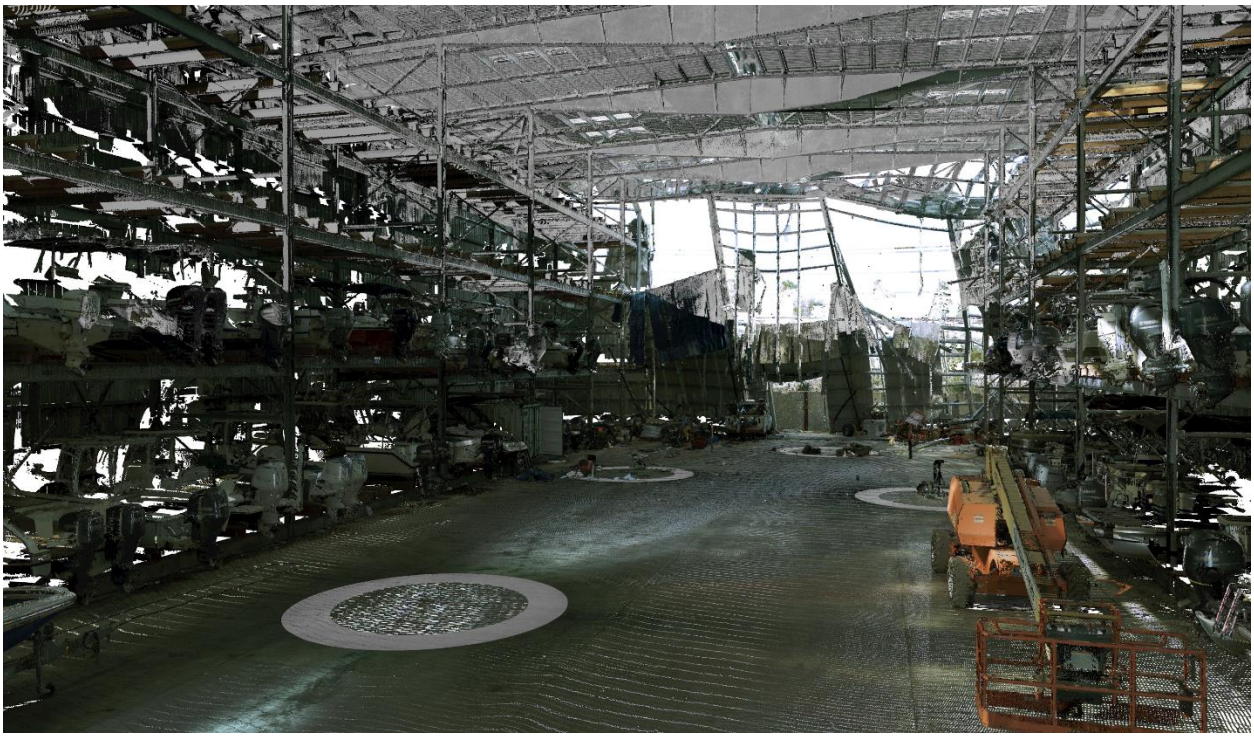

Figure 4.17. Inside view before cleaning showing only XR3 data.

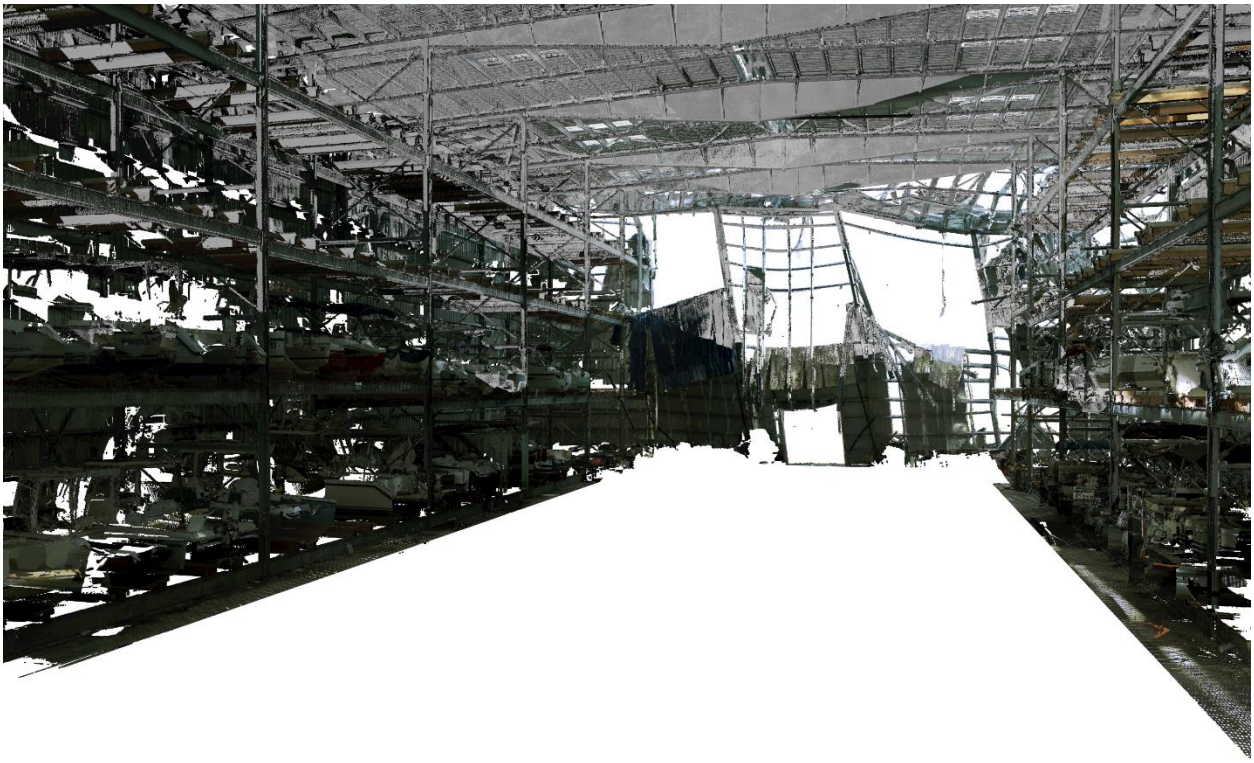

Figure 4.18. Inside view after cleaning showing only XR3 data.

Figure 4.19. Inside view before cleaning with both XR3 and BLK360

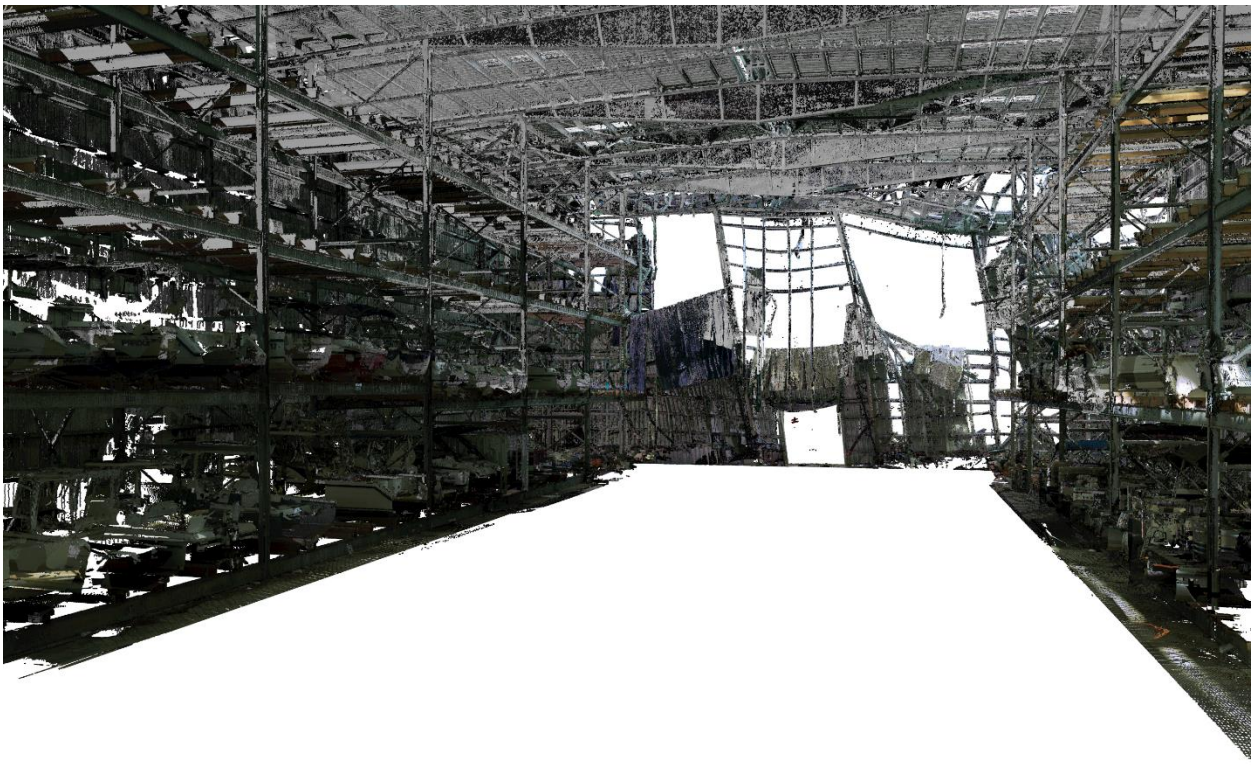

Figure 4.20. Inside view after cleaning with both XR3 and BLK360

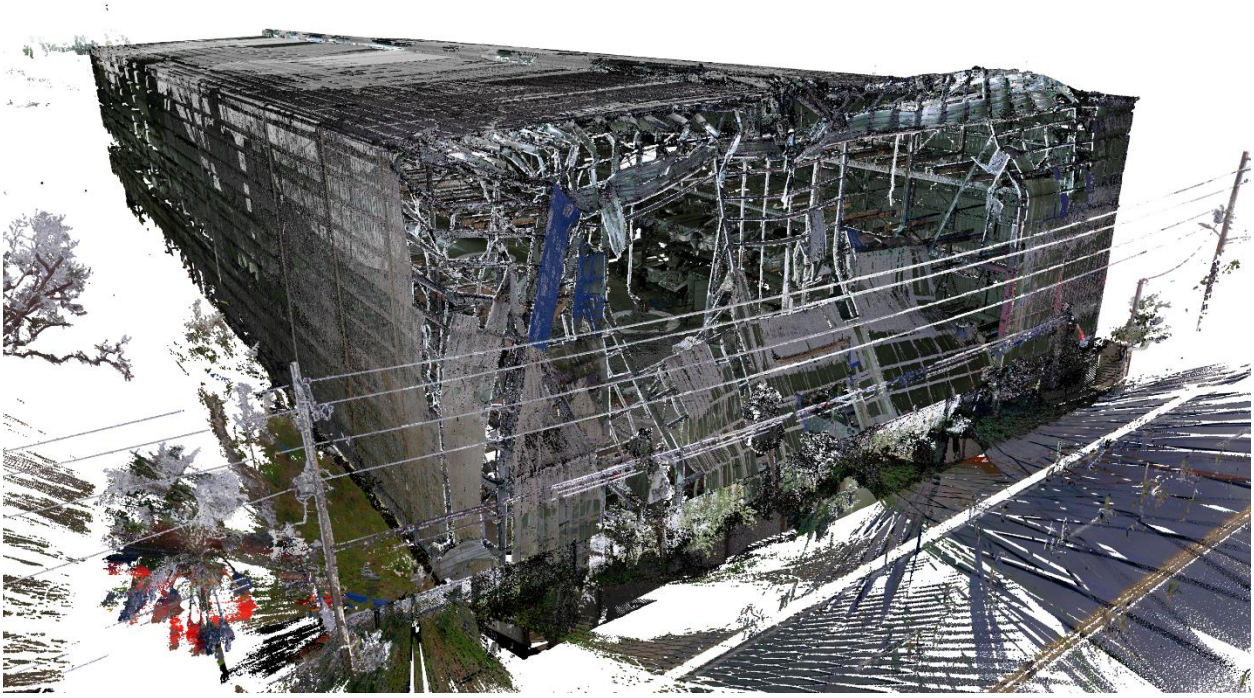

Figure 4.21. Outside view before cleaning showing both BLK360 and XR3 data.

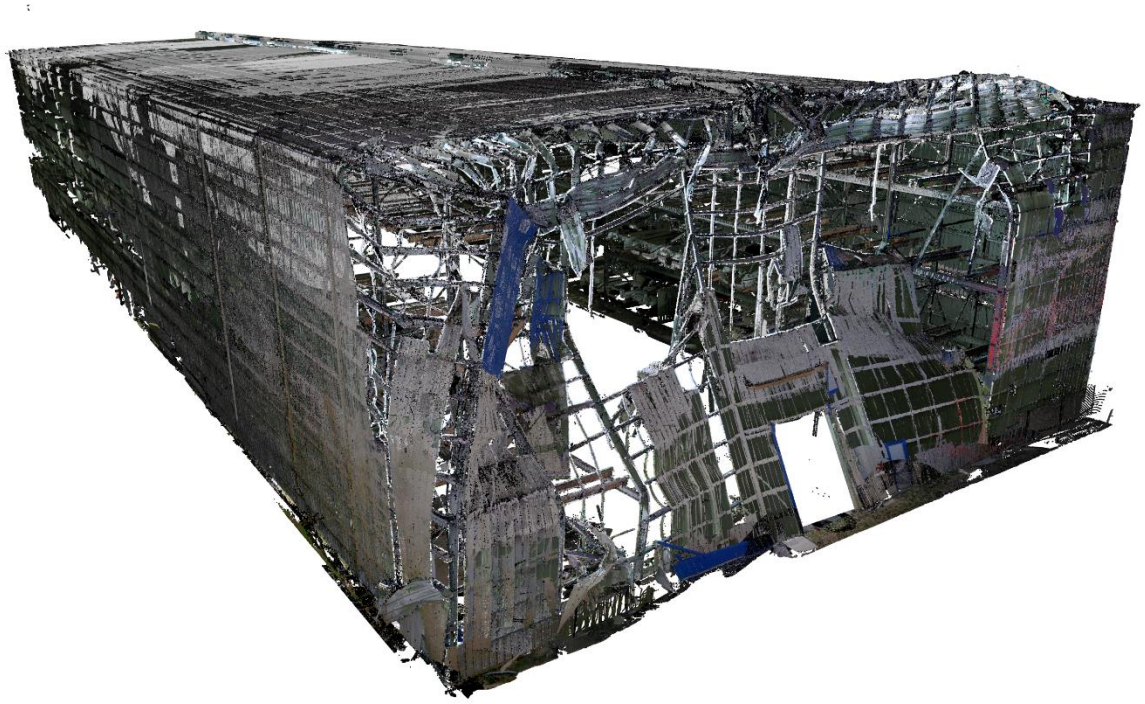

Figure 4.22. Outside view after cleaning showing both BLK360 and XR3 data.

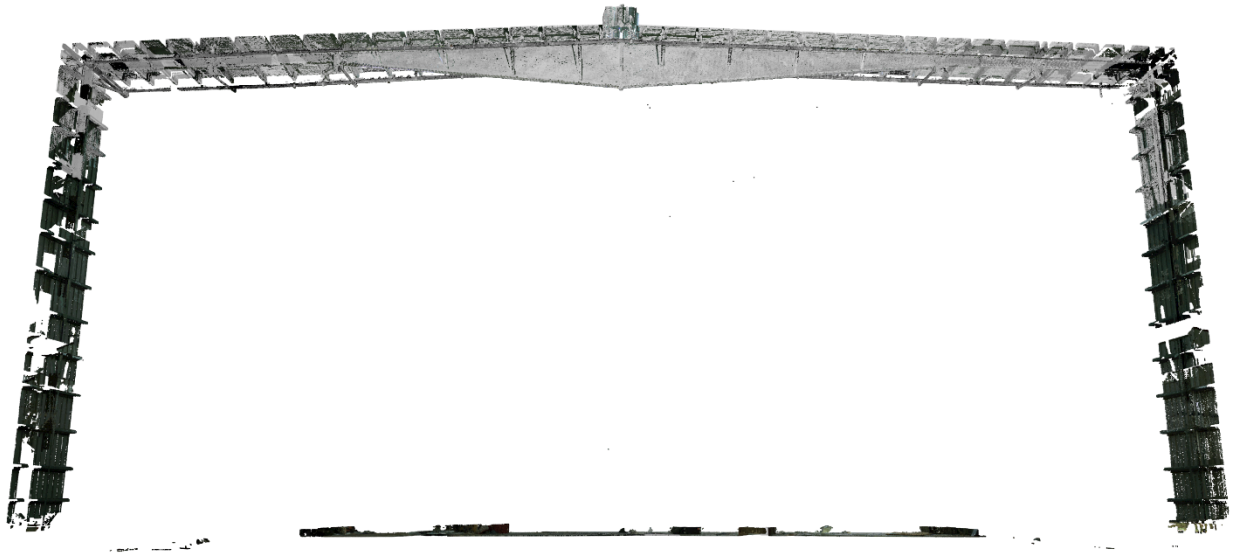

Figure 4.23. A single frame from Watson Landings Marina using XR3 data only.

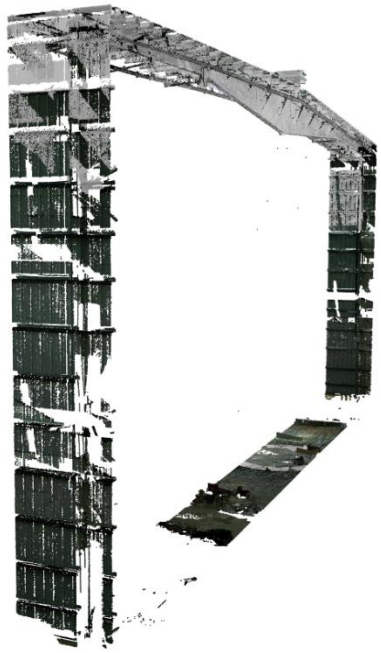

Figure 4.24. A single frame from Watson Landings Marina using XR3 data only.

4.3.4 *Other observations*

No other observations were made.

4.4 INTERMODAL DISTRIBUTION CENTER

4.4.1 *Review of available lidar data*

The Intermodal Distribution Center is along with Westrock East Terminal and Watson Landings Marina, the main focus of this thesis, due to the fact that extensive building drawings and schematics were made available to researchers. It differs from the other two due to not having been scanned as extensively and therefore provides challenges that the other two might not.
There were a total of 4 XR3 scans, 1 of which was incomplete and therefore disregarded. A total of 6 BLK360 scans were available and all of them were used, but due to the locations of them, they could not be registered all together but rather in clusters of two at a time. The scan locations can be seen in Figure 3.42.
The Maptek database containing all the scans is 23.4 GB.

4.4.2 *Data registration overview and challenges*

The final registration contained 86,976,207 points from the XR3 scans and 247,337,624 from the BLK360. This is within a reasonable range for the processing machine to handle and therefore no filters were needed to proceed.
As mentioned before, the technique employed with the BLK360 scans differed from the one used previously due to the fact that all the scans could not be linked together with any accuracy. Instead the XR3 scans formed a base layer to which the BLK360 scans were linked to in clusters of two, hereafter referred to as the north cluster (top right on the map), west cluster (top left) and east cluster (bottom left).

4.4.3 *Point cloud cleaning*

The cleaning of the Intermodal Distribution Center was relatively straightforward and consisted only of removing items such as cardboard boxes from the inside and irrelevant points outside the

building. The collapsed tilt-up wall on the northeast face of the building were kept in the scan, and not disregarded as rubble, because of how well they kept their shape and therefore might provide structural information.

After the cleaning process, a total of 309,478,518 points remained, of which 80,026,122 were XR3 and 229,452,396 BLK360. This is approaching the upper limits of what the processing machine can reasonably handle.

A macro model with 5 cm minimum separation was also made and contains a total of 10,424,030 points, of which 5,415,847 are XR3 and 5,008,183 are BLK360.

Figure 4.25 through Figure 4.34 show the cleaning process from various angles, demonstrating the differences between XR3 and BLK360 data. The figures come in pairs where the untouched model is showed first and the fully cleaned version follows.

Figure 4.35 shows a front view of a single frame from IDC and Figure 4.36 shows the bay following that frame, demonstrating the slicing abilities of PointStudio to get a clearer view of elements of interest.

Figure 4.25. Aerial view before any modifications were done to the point cloud.

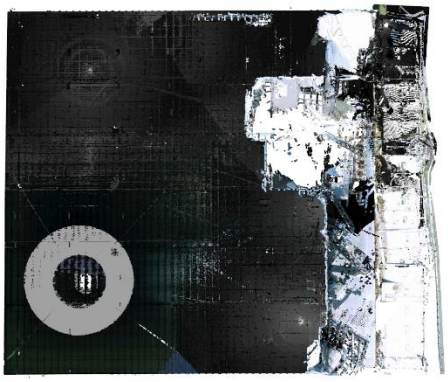

Figure 4.26. Aerial view after cleaning.

Figure 4.27. Inside view before cleaning showing only BLK360 data.

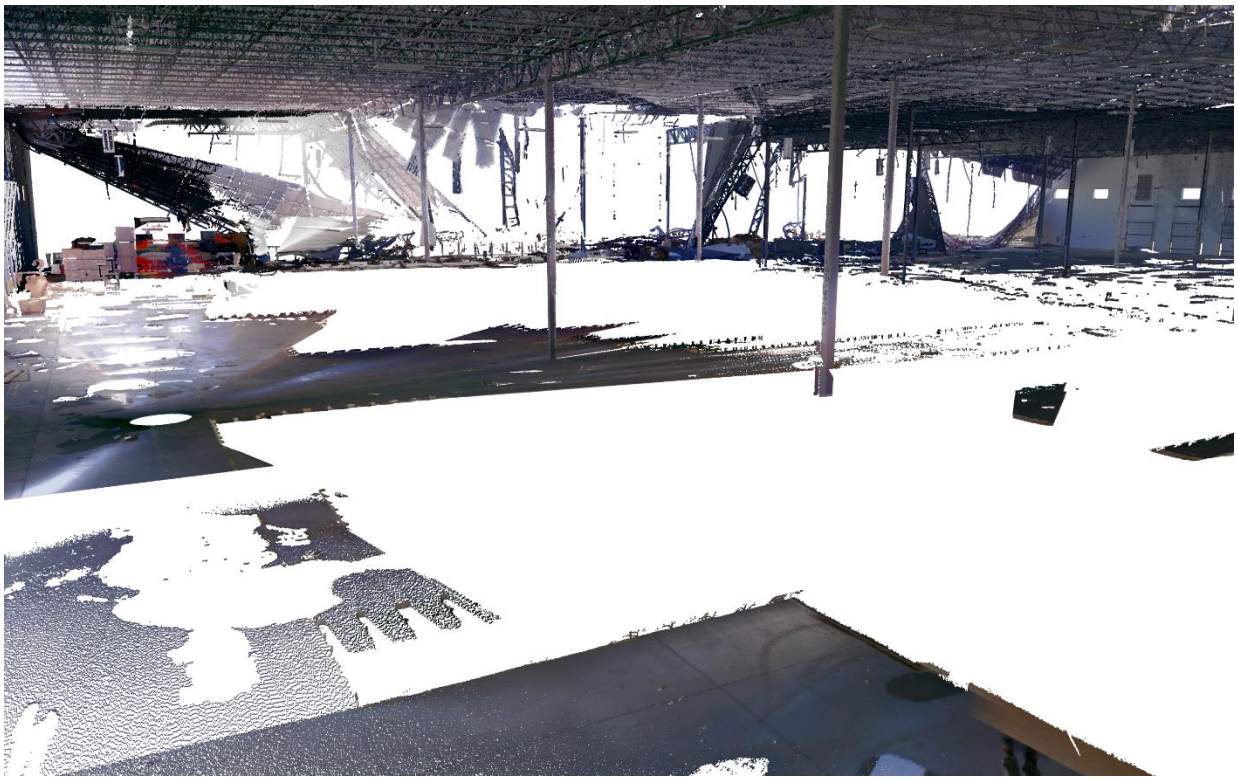

Figure 4.28. Inside view after cleaning showing only BLK360 data.

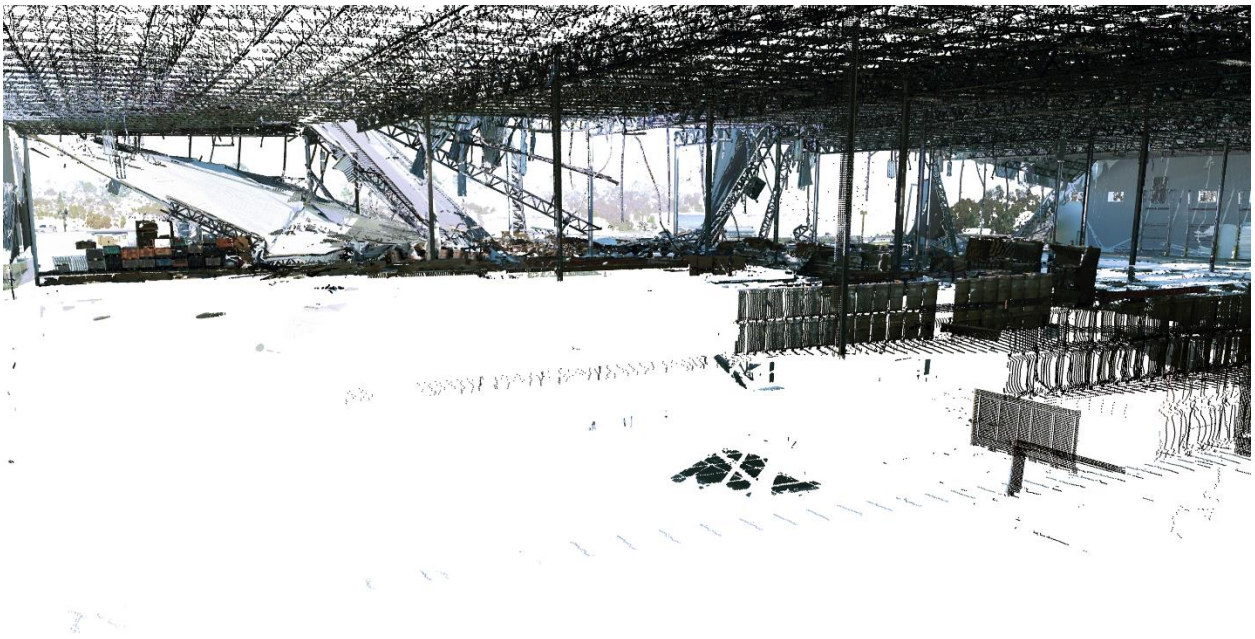

Figure 4.29. Inside view before cleaning showing only XR3 data.

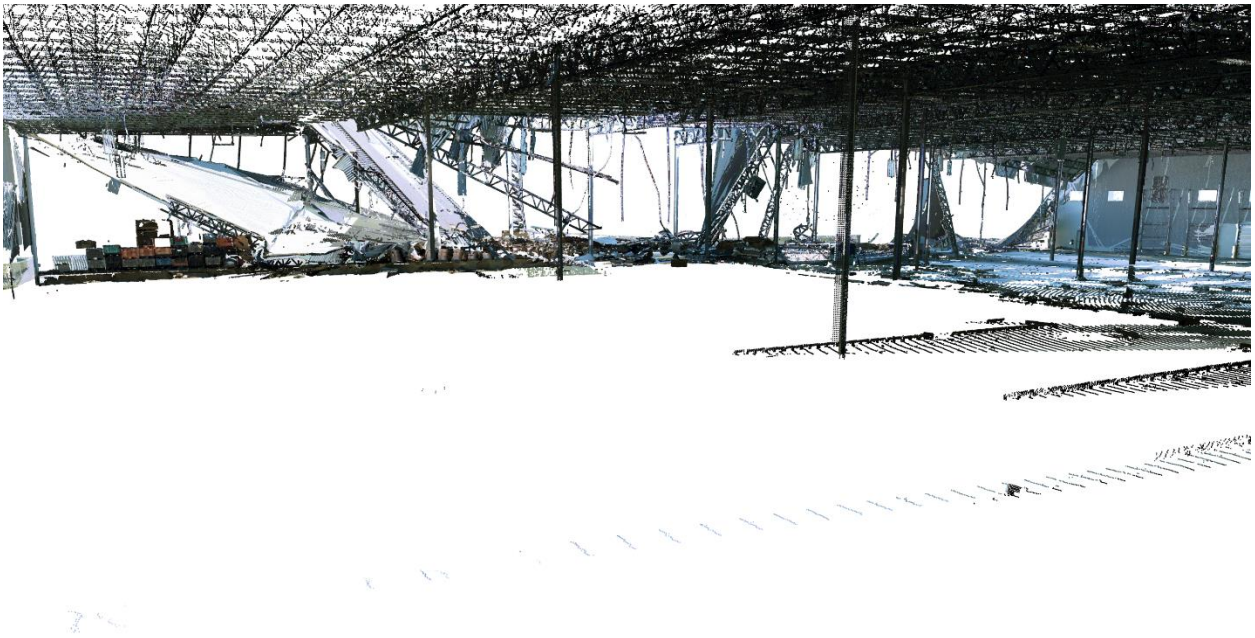

Figure 4.30. Inside view after cleaning showing only XR3 data.

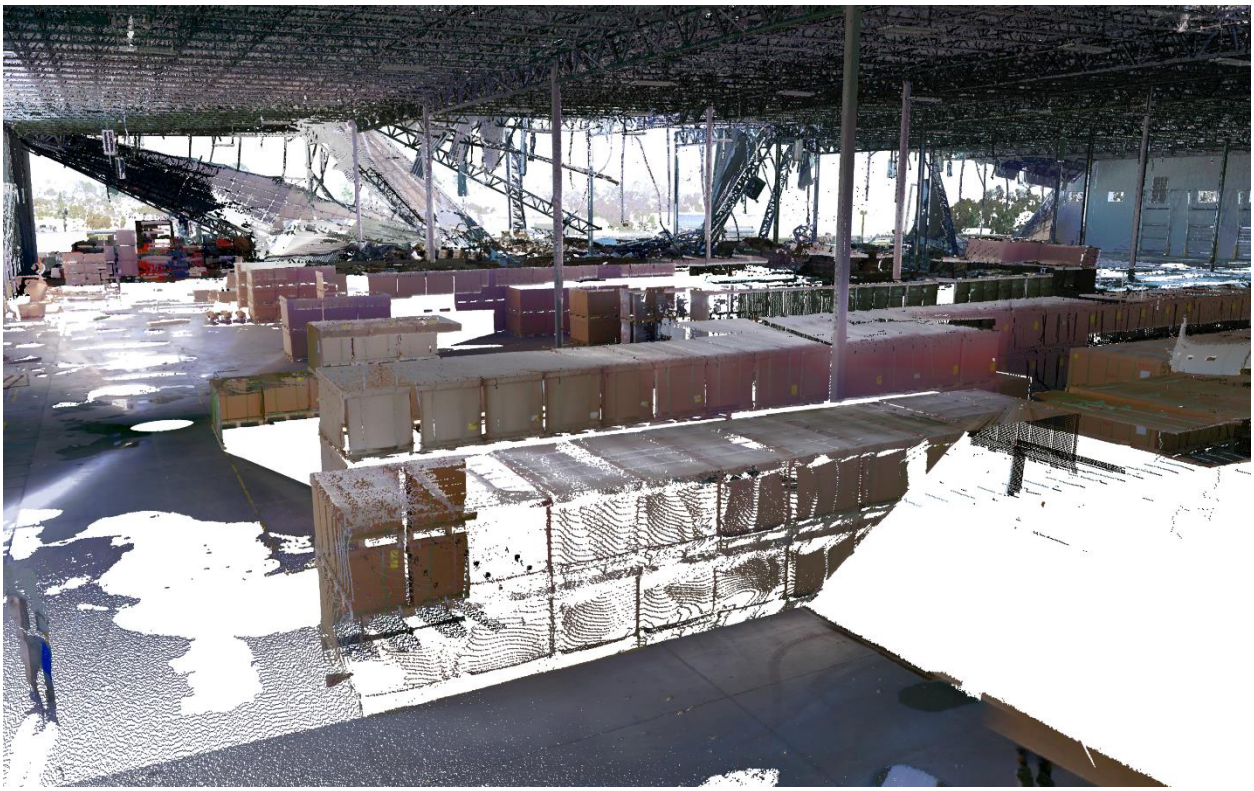

Figure 4.31. Inside view before cleaning with both XR3 and BLK360

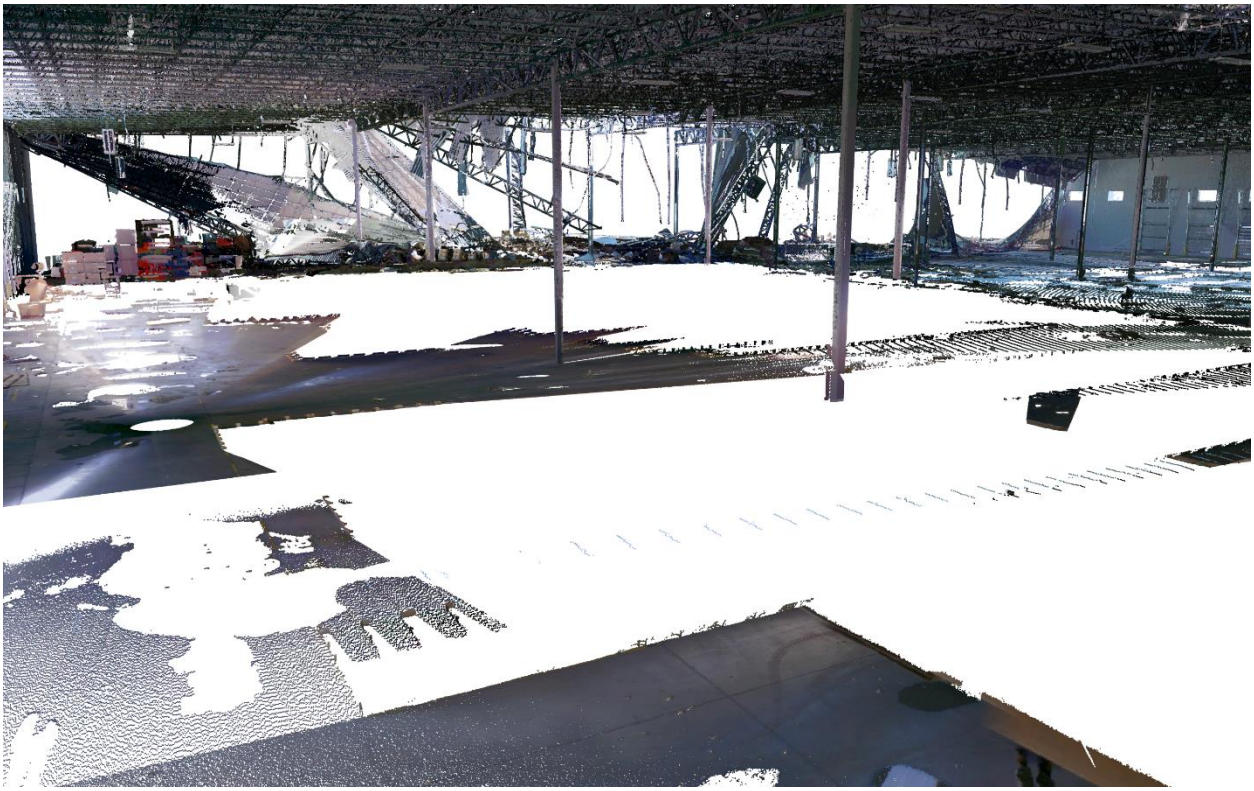

Figure 4.32. Inside view after cleaning with both XR3 and BLK360

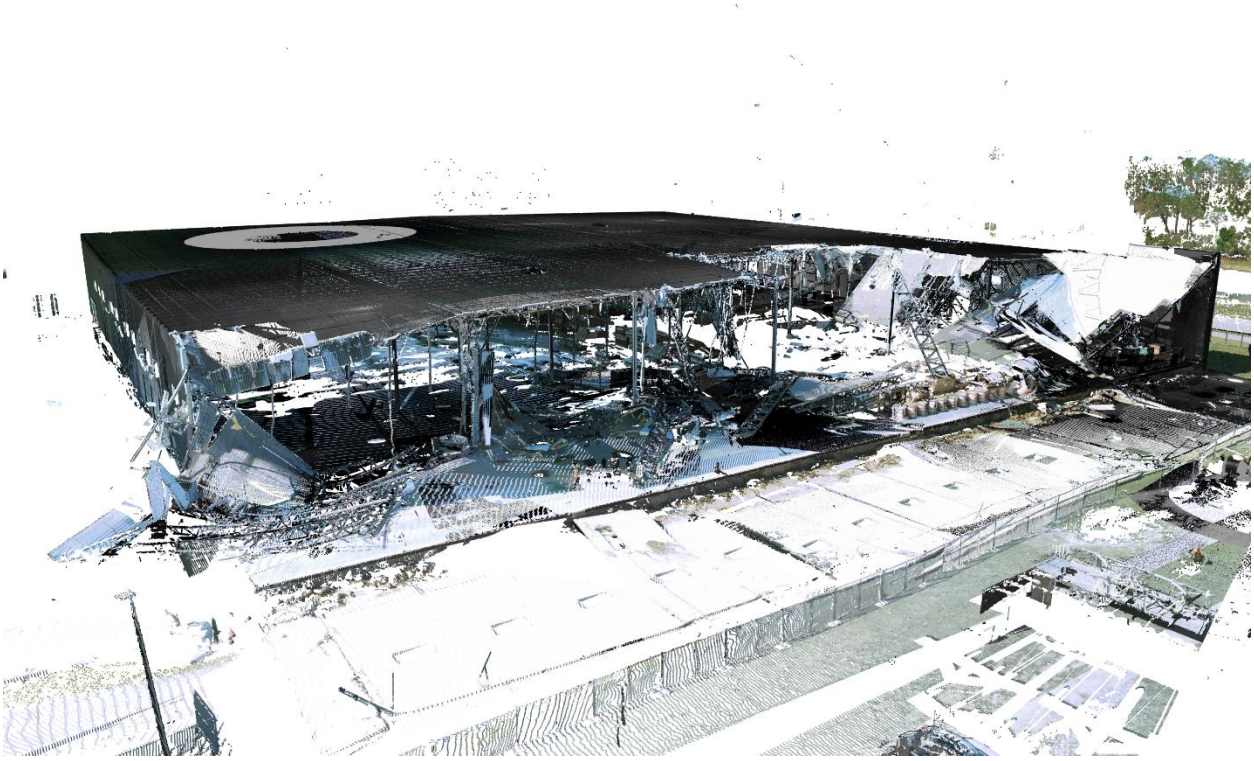

Figure 4.33. Outside view before cleaning showing both BLK360 and XR3 data.

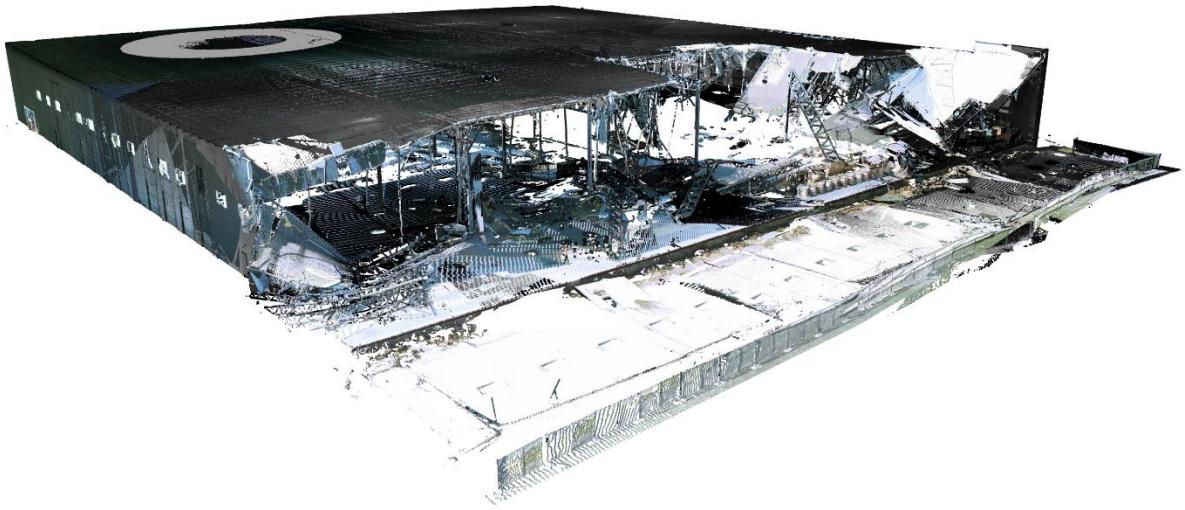

Figure 4.34. Outside view after cleaning showing both BLK360 and XR3 data.

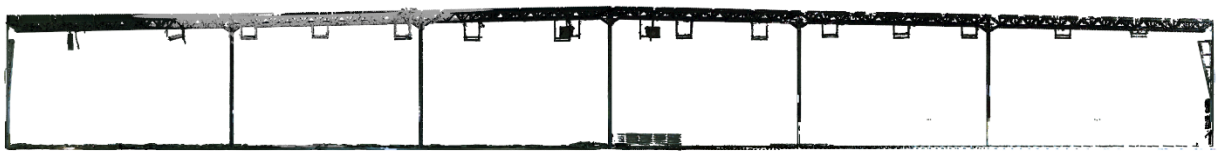

Figure 4.35. A single frame from Intermodal Distribution Center using XR3 data only.

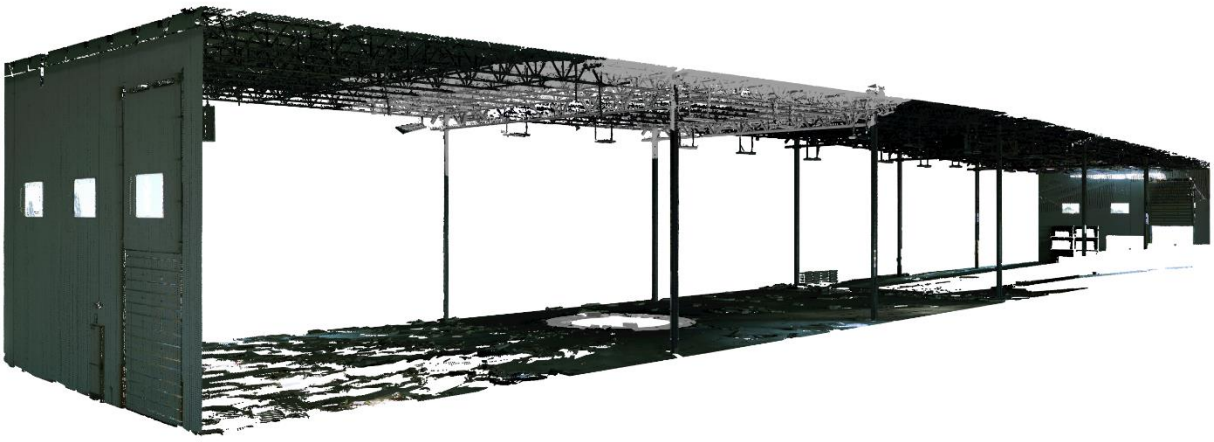

Figure 4.36. A single bay from Intermodal Distribution Center using XR3 data only.

4.4.4 *Other observations*

No other observations were made.

4.5 CARGILL DISTRIBUTION CENTER

4.5.1 *Review of available lidar data*

Cargill Distribution Center was scanned relatively extensively, and in a rather uniform manner, i.e. not particularly focused on the heavily damaged side like most of the other buildings. That is an understandable decision by the field crew since this building suffered damages on the back side along with a hole in the wall on the long side. A total of 10 XR3 scans were made and all of them used without problems. The same number of BLK360 scans were made, 10, but only 8 of them were used due to 2 of them being incomplete and unusable. The scan locations can be seen in Figure 3.43.
The Maptek database containing all the scans is 19.3 GB.

4.5.2 *Data registration overview and challenges*

The final registration contained 324,084,917 points from the XR3 scans and 425,618,967 from the BLK360 scans. That is a total of 749,703,884 points which is reaching the upper bounds of what can reasonably be worked with in the processing machine here. With patience it is possible, but applying a minimum separation filter would be beneficial or slicing areas of interest and work with them separately.

4.5.3 *Point cloud cleaning*

The cleaning process consisted of removing the points outside the building, ghosts of people from the field crew and various items and rubble from the ground. After the process a total of 643,579,263 points remained, of which 273,935,582 were XR3 and 369,643,681 were BLK360. The macro model with a 5 cm minimum separation filter contains 10,831,139 points, of which 5,946,256 are XR3 and 4,884,883 BLK360.

Figure 4.37 through Figure 4.46 show the cleaning process from various angles, demonstrating the differences between XR3 and BLK360 data. The figures come in pairs where the untouched model is showed first and the fully cleaned version follows.

Figure 4.47 shows a front view of a single frame from Cargill Distribution Center and Figure 4.48 shows the bay following that frame, demonstrating the slicing abilities of PointStudio to get a clearer view of elements of interest.

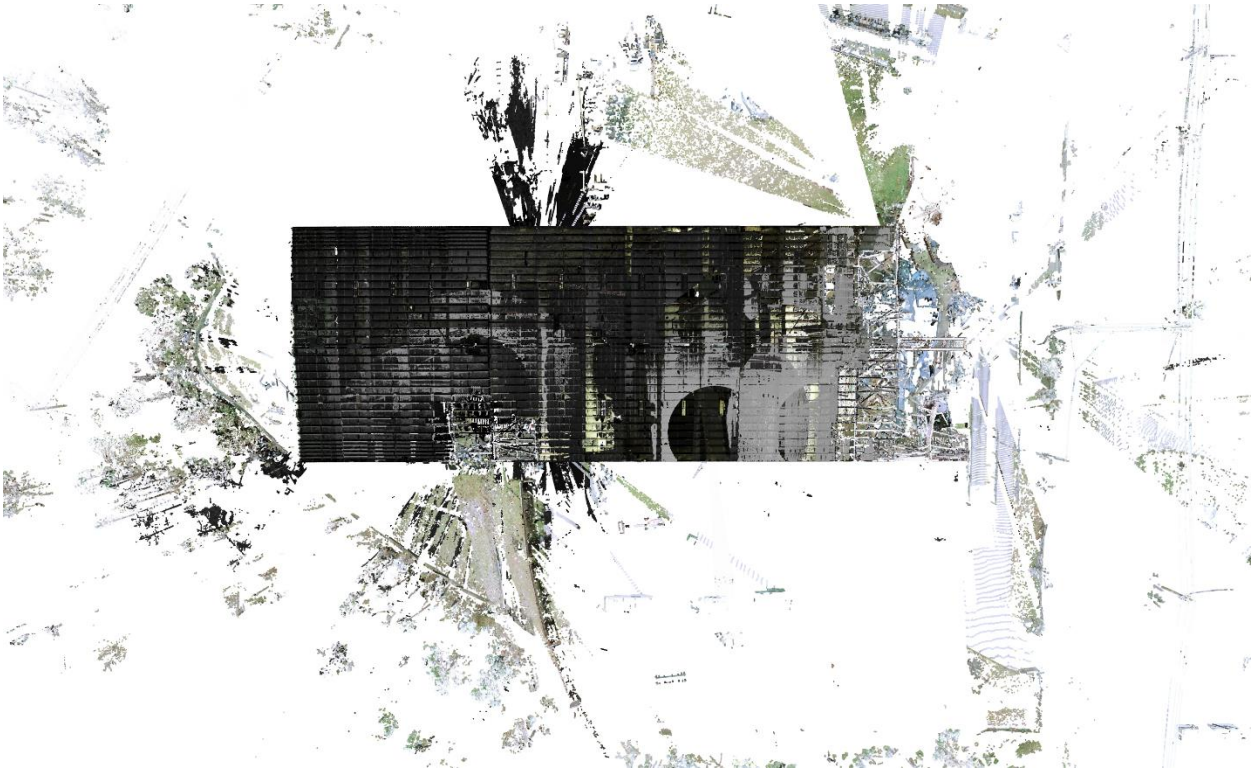

Figure 4.37. Aerial view before any modifications were done to the point cloud.

Figure 4.38. Aerial view after cleaning.

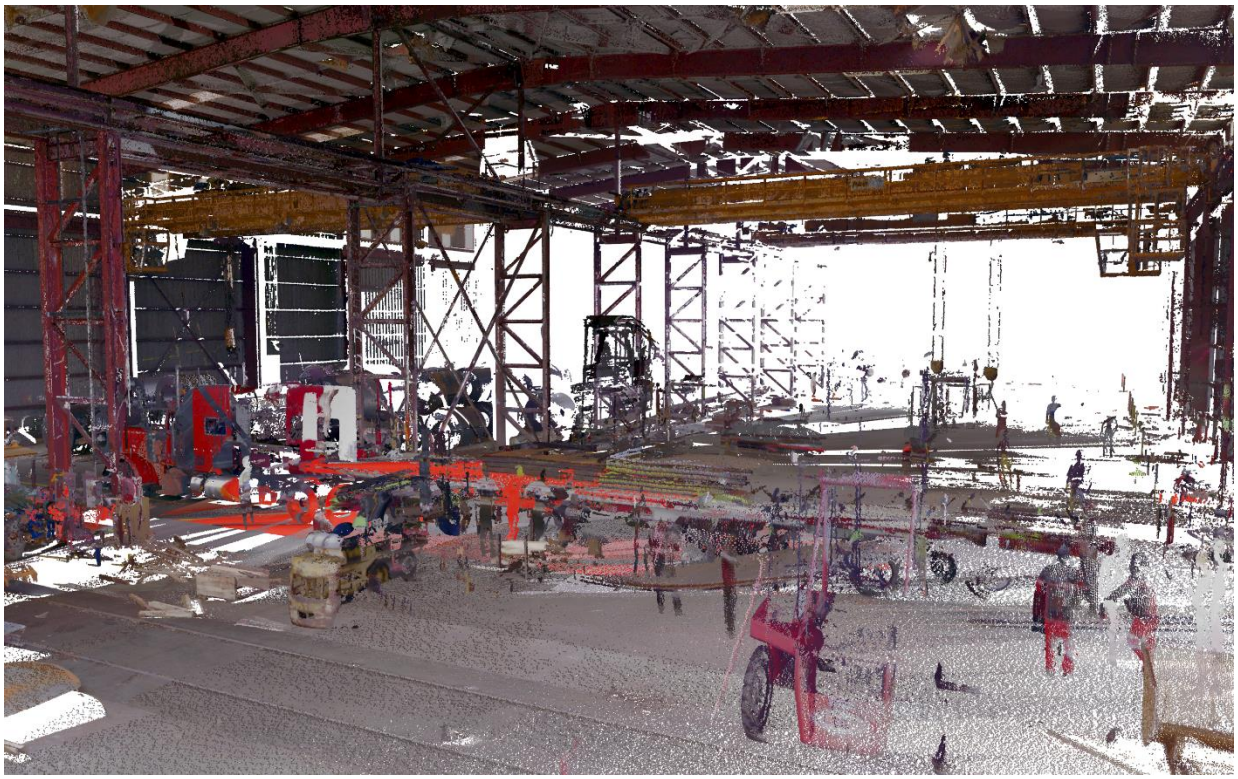

Figure 4.39. Inside view before cleaning showing only BLK360 data.

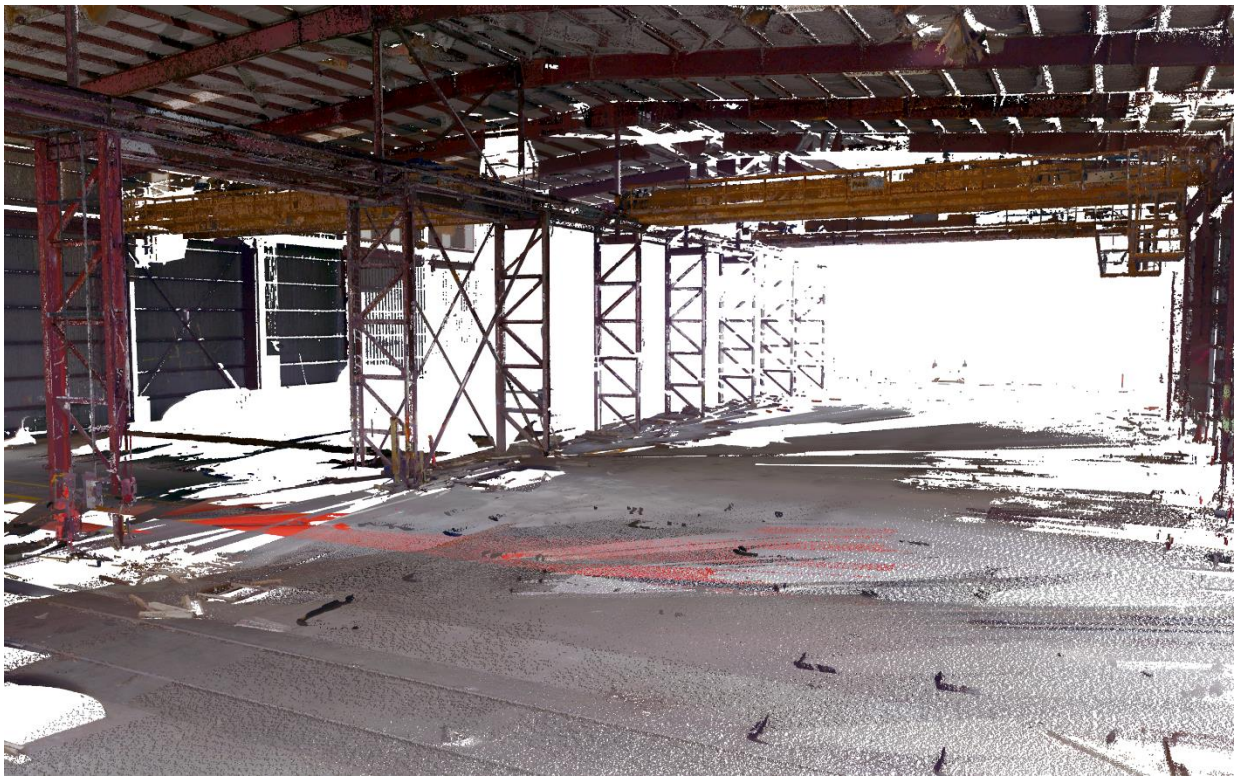

Figure 4.40. Inside view after cleaning showing only BLK360 data.

Figure 4.41. Inside view before cleaning showing only XR3 data.

Figure 4.42. Inside view after cleaning showing only XR3 data.

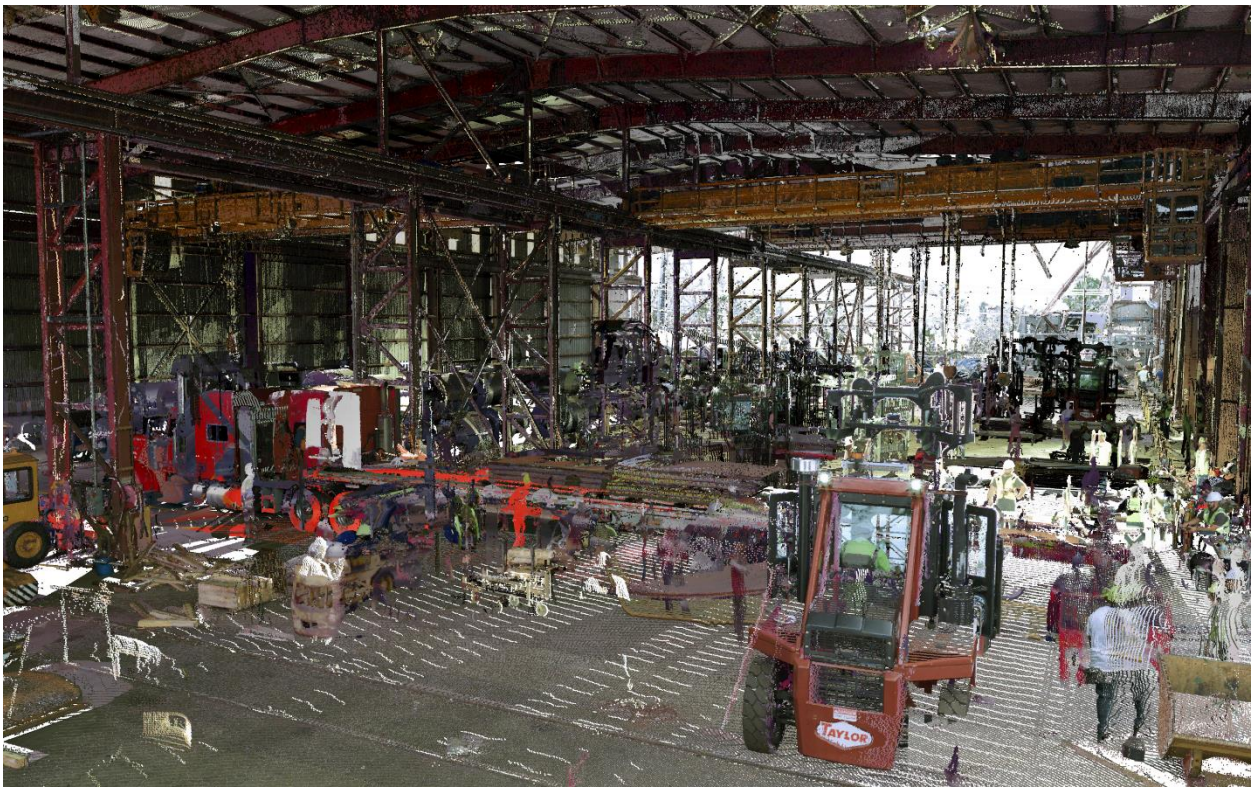

Figure 4.43. Inside view before cleaning with both XR3 and BLK360

Figure 4.44. Inside view after cleaning with both XR3 and BLK360

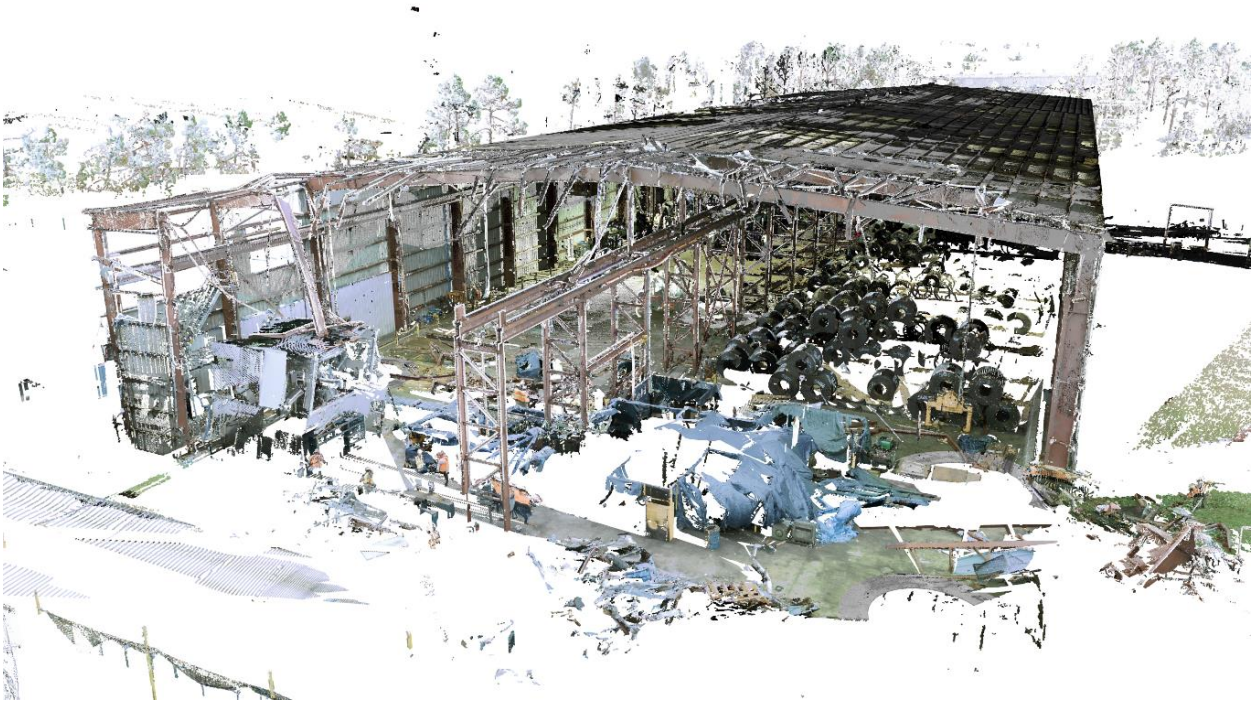

Figure 4.45. Outside view before cleaning showing both BLK360 and XR3 data.

Figure 4.46. Outside view after cleaning showing both BLK360 and XR3 data.

Figure 4.47. A single frame from Cargill Distribution Center using XR3 data only.

Figure 4.48. A single bay from Cargill Distribution Center using XR3 data only.

4.5.4 *Other observations*

No other observations were made.

4.6 TYNDALL AIR FORCE BASE: HANGAR 5

4.6.1 *Review of available lidar data*

Available data for Hangar 5 consists of 4 XR3 scans, all of them used, and 4 BLK360 scans, but only 3 were used due to 1 being incomplete and unusable. As can be seen in the scan location map and is apparent in the overview pictures of the model, the BLK360 scans are all located in the same corner and therefore cannot reach the whole building. Furthermore, an airplane is located in that corner which blocks the view even further. This was not done to survey any localized damaged as has been the case, but rather to save time as XR3 is more suitable for a tall, open building like this one with no specific area of interest. The scan locations can be seen in Figure 3.44.
The Maptek database containing all the scans is 21.2 GB.

4.6.2 *Data registration overview and challenges*

The final registration contained a total of 345,030,002 points, of which 181,246,646 came from the XR3 scanners and 167,783,356 from the BLK360 ones. Due to the fact that all the BLK360 scans were done in the same corner, the point density there is much higher than elsewhere in the building.

4.6.3 *Point cloud cleaning*

Minimal cleaning was done since there was no rubble congested area and the damage mostly to the outside of the building. As before, the points outside the building were removed along with various loose items inside the building. A total of 324,902,943 points remained, 176,242,764 from XR3 and 148,660,179 from BLK360.

Figure 4.49 through Figure 4.58 show the cleaning process from various angles, demonstrating the differences between XR3 and BLK360 data. The figures come in pairs where the untouched model is showed first and the fully cleaned version follows.

Figure 4.59 shows a front view of a single frame from Hangar 5 and Figure 4.60 shows the bay following that frame, demonstrating the slicing abilities of PointStudio to get a clearer view of elements of interest.

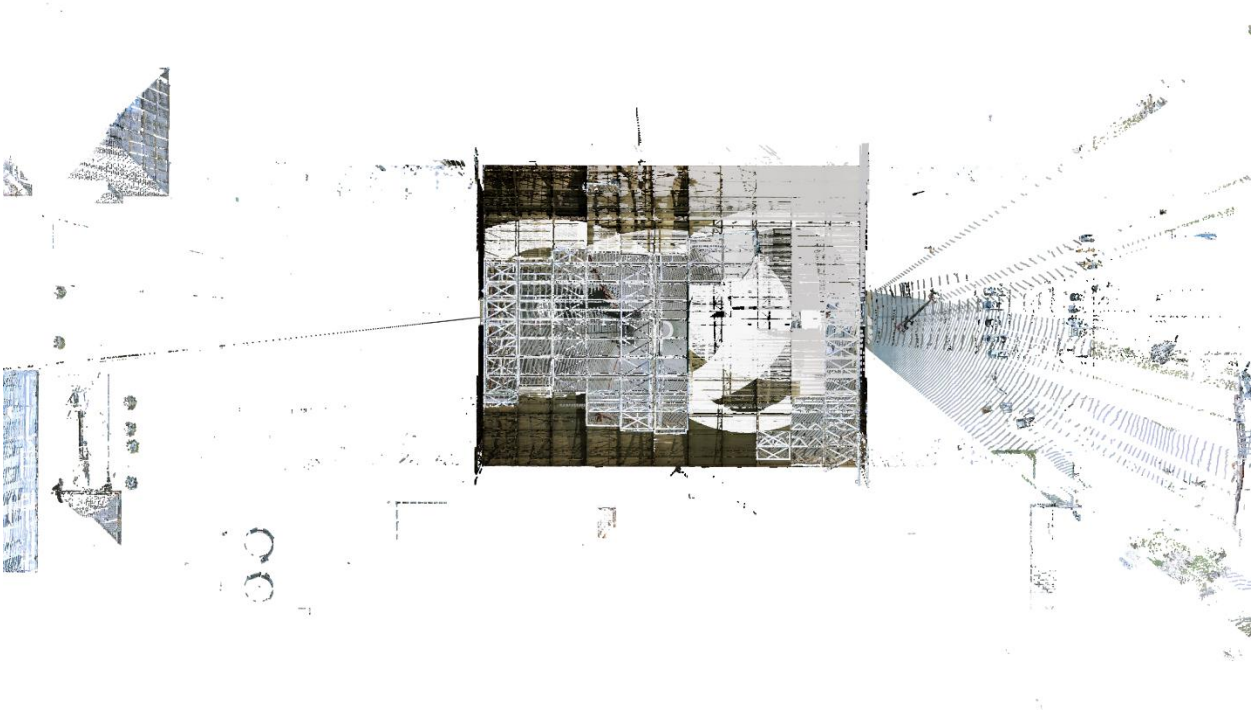

Figure 4.49. Aerial view before any modifications were done to the point cloud.

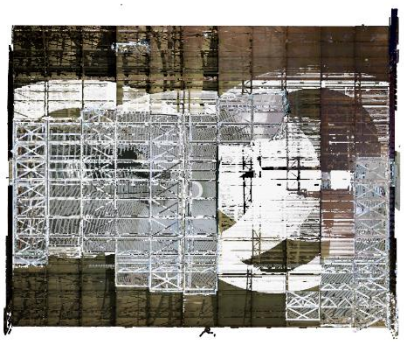

Figure 4.50. Aerial view after cleaning.

Figure 4.51. Inside view before cleaning showing only BLK360 data.

Figure 4.52. Inside view after cleaning showing only BLK360 data.

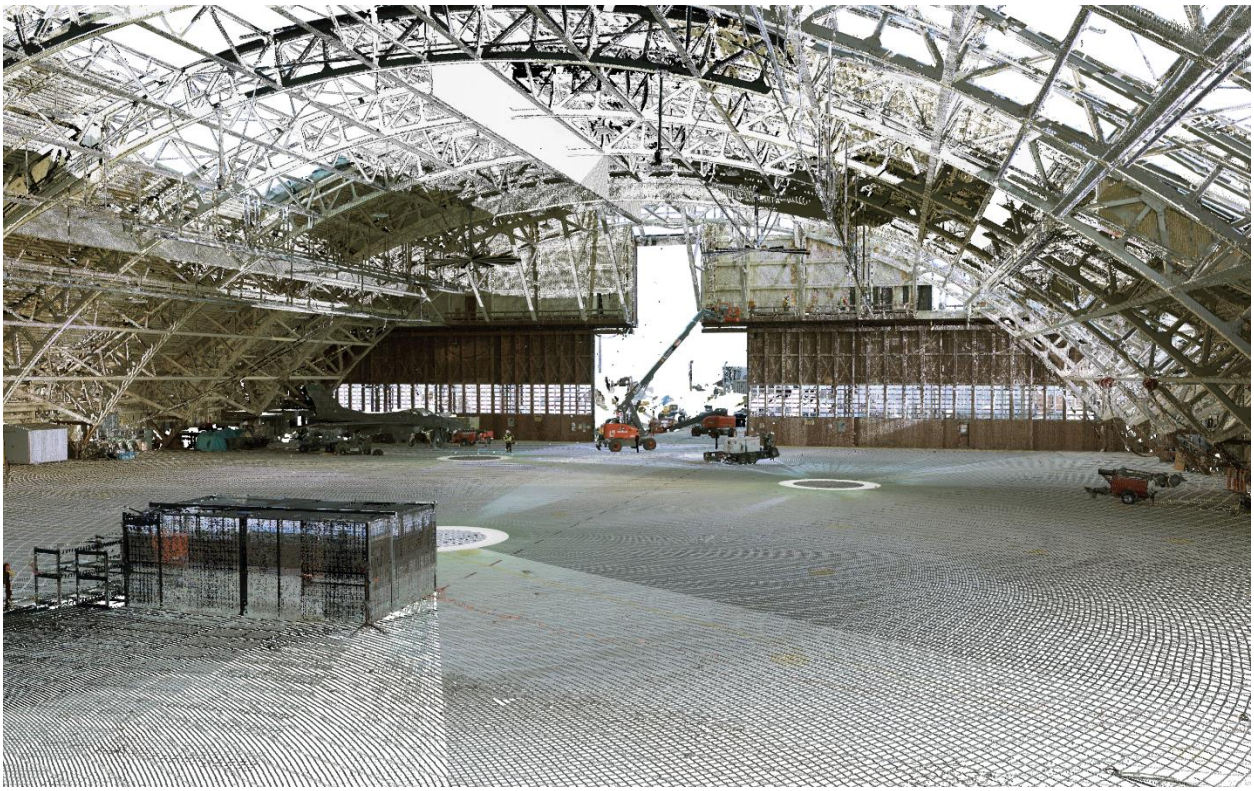

Figure 4.53. Inside view before cleaning showing only XR3 data.

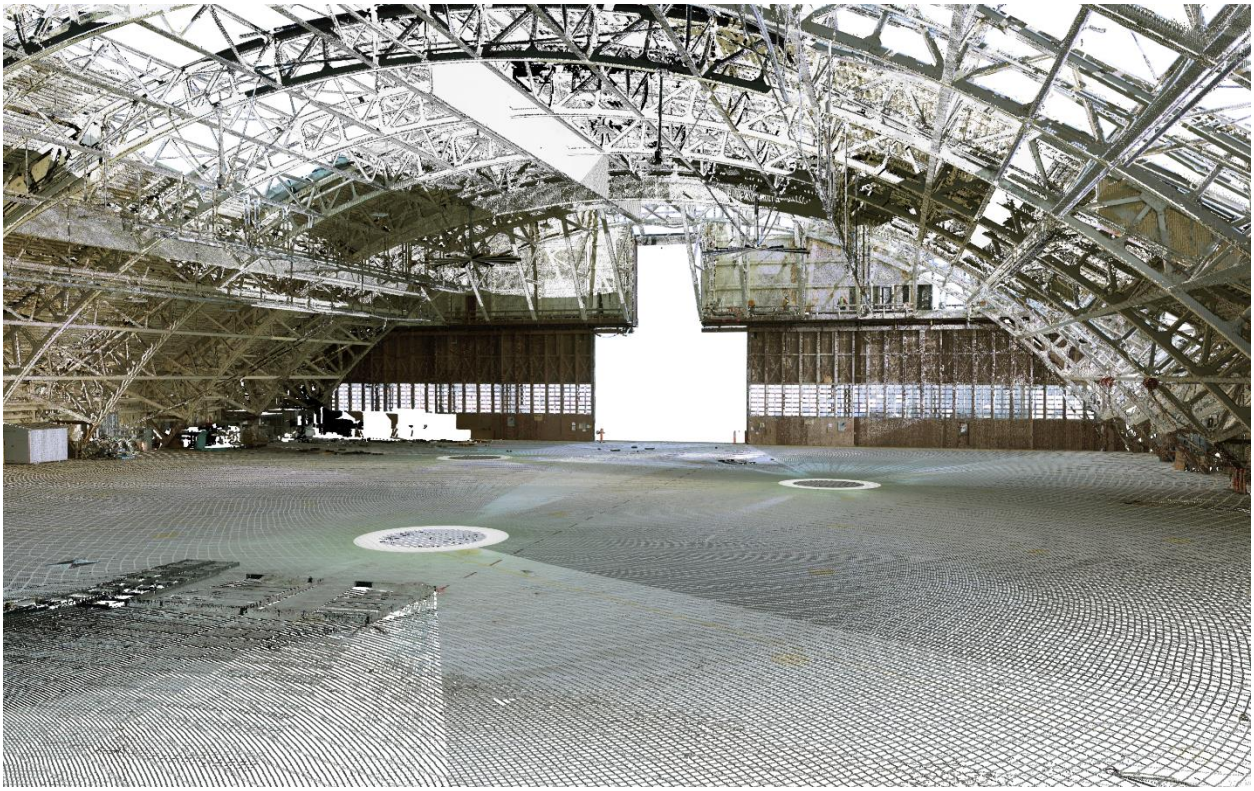

Figure 4.54. Inside view after cleaning showing only XR3 data.

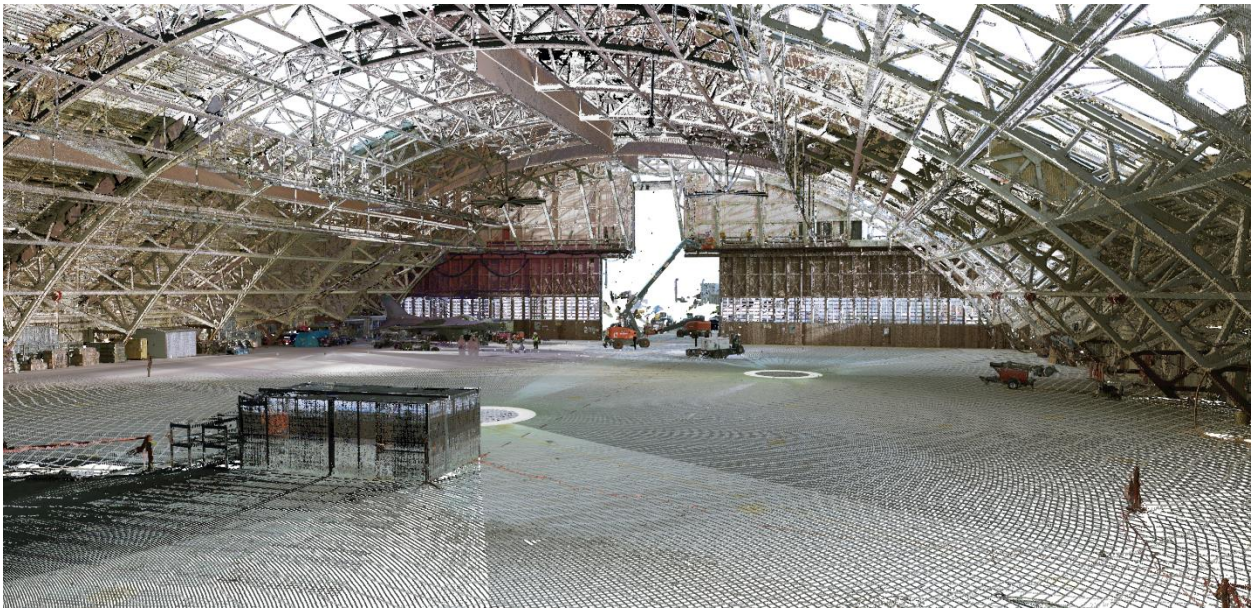

Figure 4.55. Inside view before cleaning with both XR3 and BLK360

Figure 4.56. Inside view after cleaning with both XR3 and BLK360

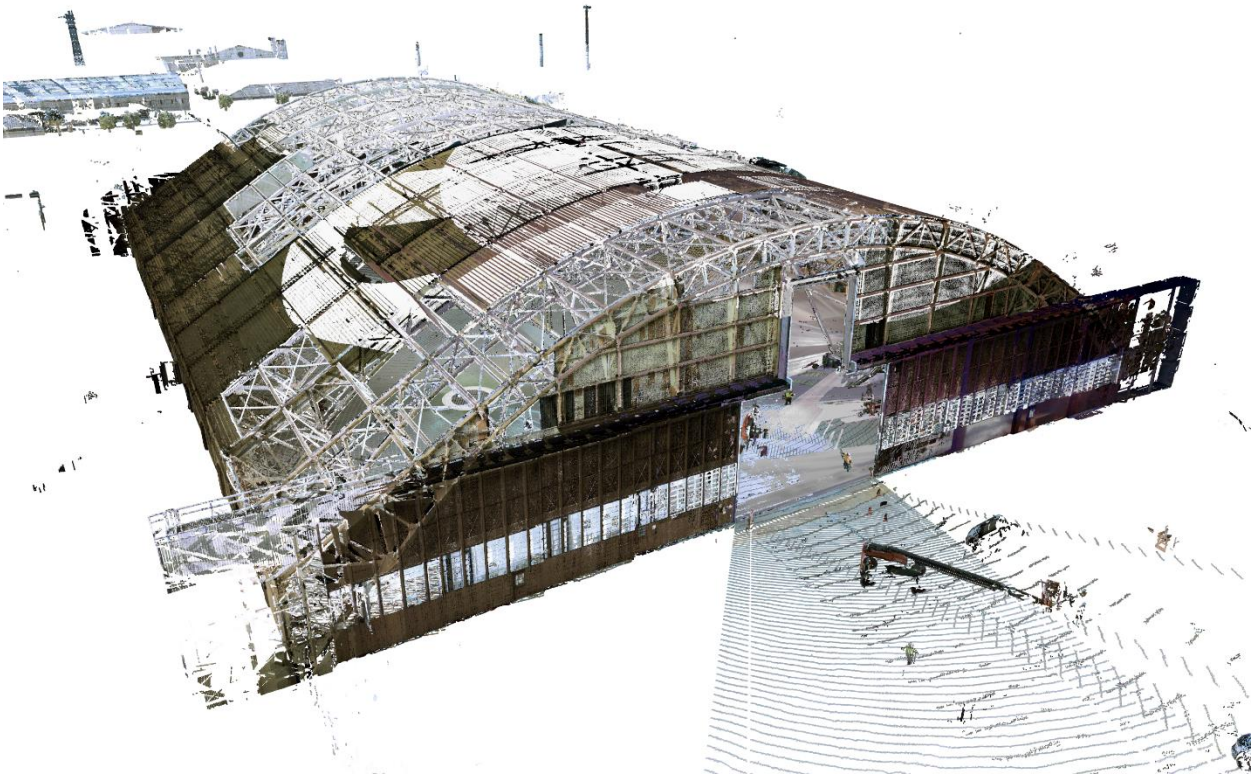

Figure 4.57. Outside view before cleaning showing both BLK360 and XR3 data.

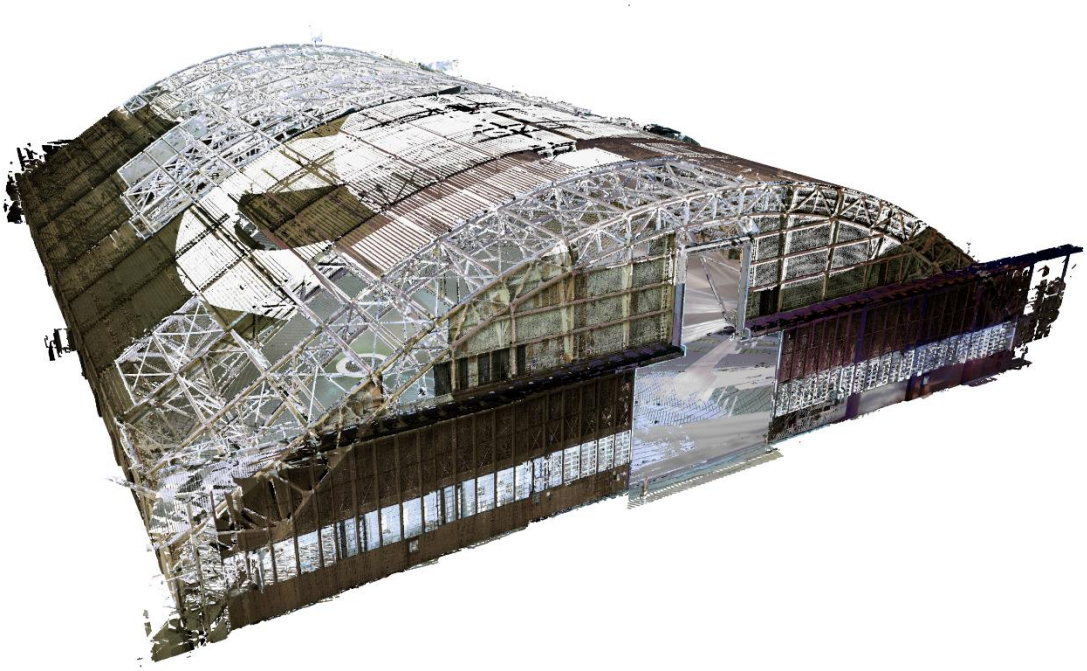

Figure 4.58. Outside view after cleaning showing both BLK360 and XR3 data.

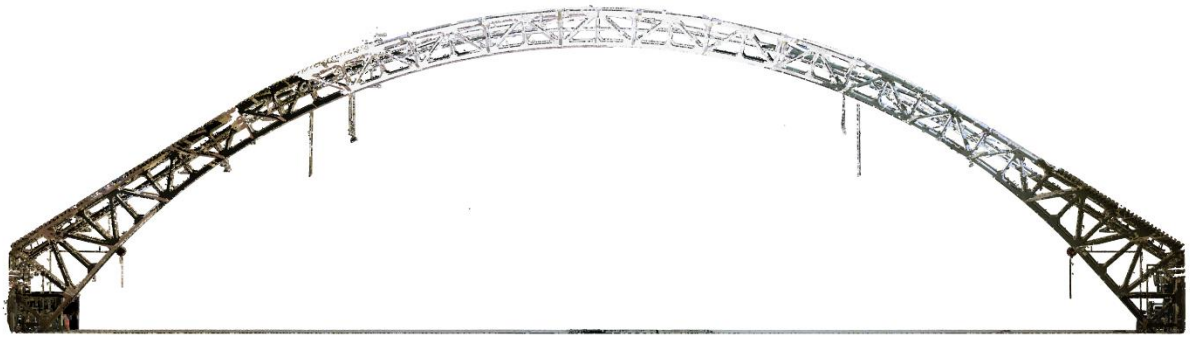

Figure 4.59. A single frame from Hangar 5 using XR3 data only.

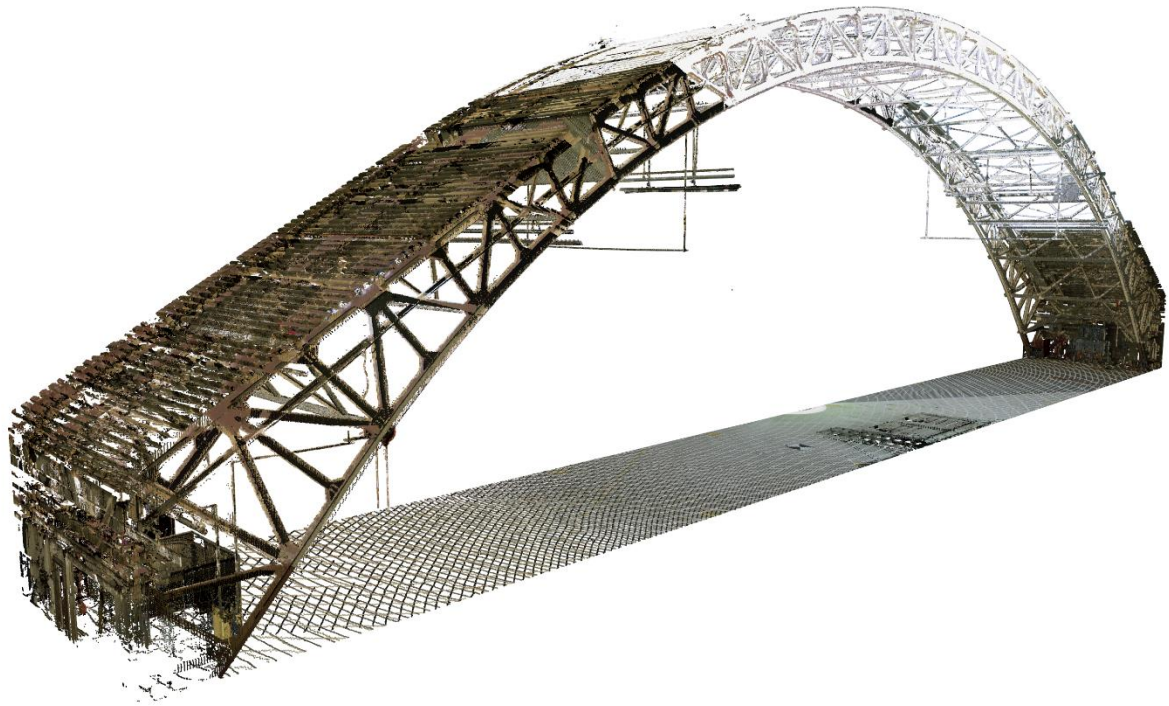

Figure 4.60. A single bay from Hangar 5 using XR3 data only.

4.6.4 *Other observations*

No other observations were made.

4.7 TYNDALL AIR FORCE BASE: BUILDING 316

4.7.1 *Review of available lidar data*

Building 316 was only scanned with BLK360 scanners and not XR3. A total of 10 scans were made and all of them used in the registration. The scans are relatively uniformly distributed around the building as there is no specific side of more interest than another. The scan locations can be seen in Figure 3.45.
The Maptek database containing all the scans is 15.6 GB.

4.7.2 *Data registration overview and challenges*

The final registration contained 395,557,797 points from the BLK360 scans. No filters were needed to process this building, but it could not afford to contain many more points.

4.7.3 *Point cloud cleaning*

The cleaning process included removing the points outside the building and various items and ghosts from the floor inside. After cleaning 337,471,678 points remained.

Figure 4.61 through Figure 4.66 show the cleaning process from various angles. Those figures come in pairs where the untouched model is showed first and the fully cleaned version follows.

Figure 4.67 and Figure 4.68 show a single bay from Building 316, demonstrating the slicing abilities of PointStudio to get a clearer view of elements of interest.

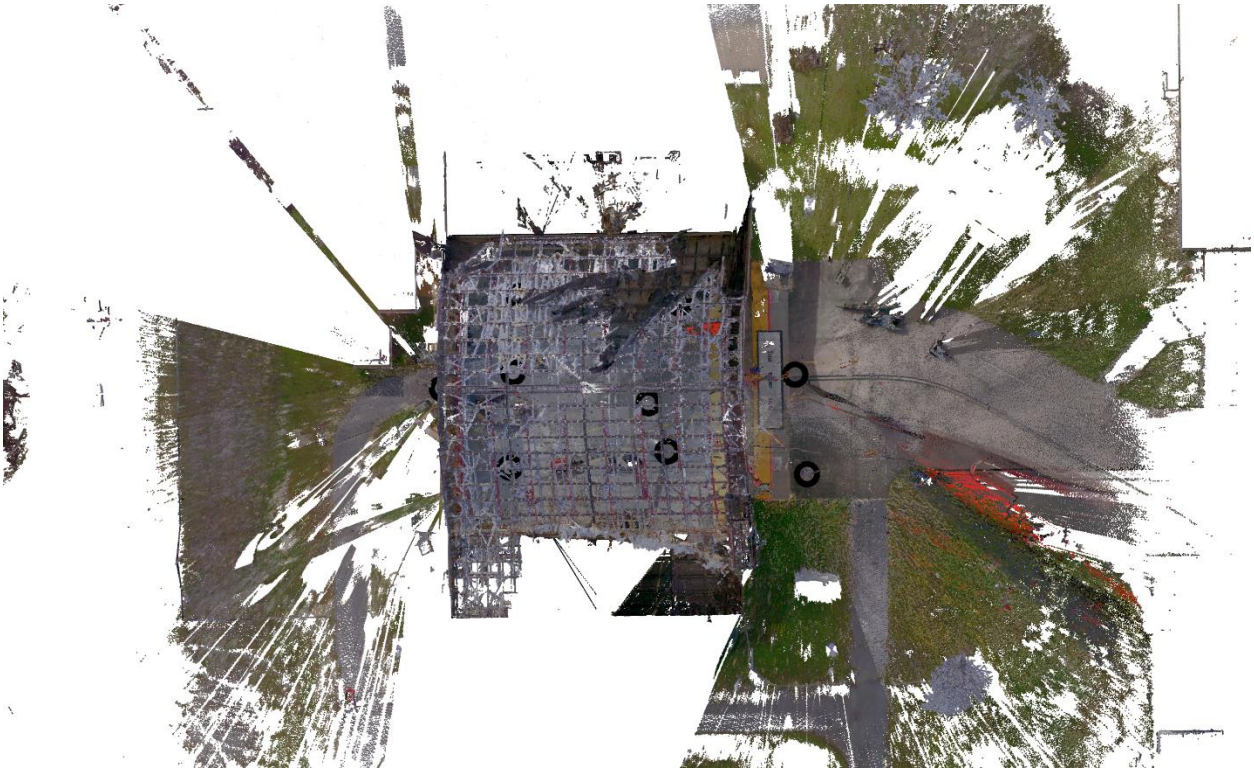

Figure 4.61. Aerial view before any modifications were done to the point cloud.

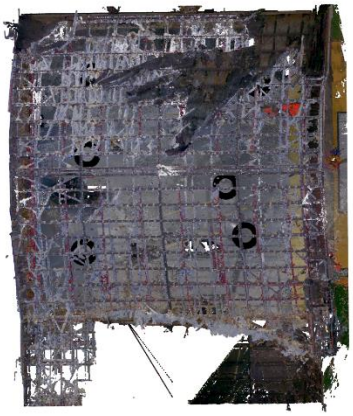

Figure 4.62. Aerial view after cleaning.

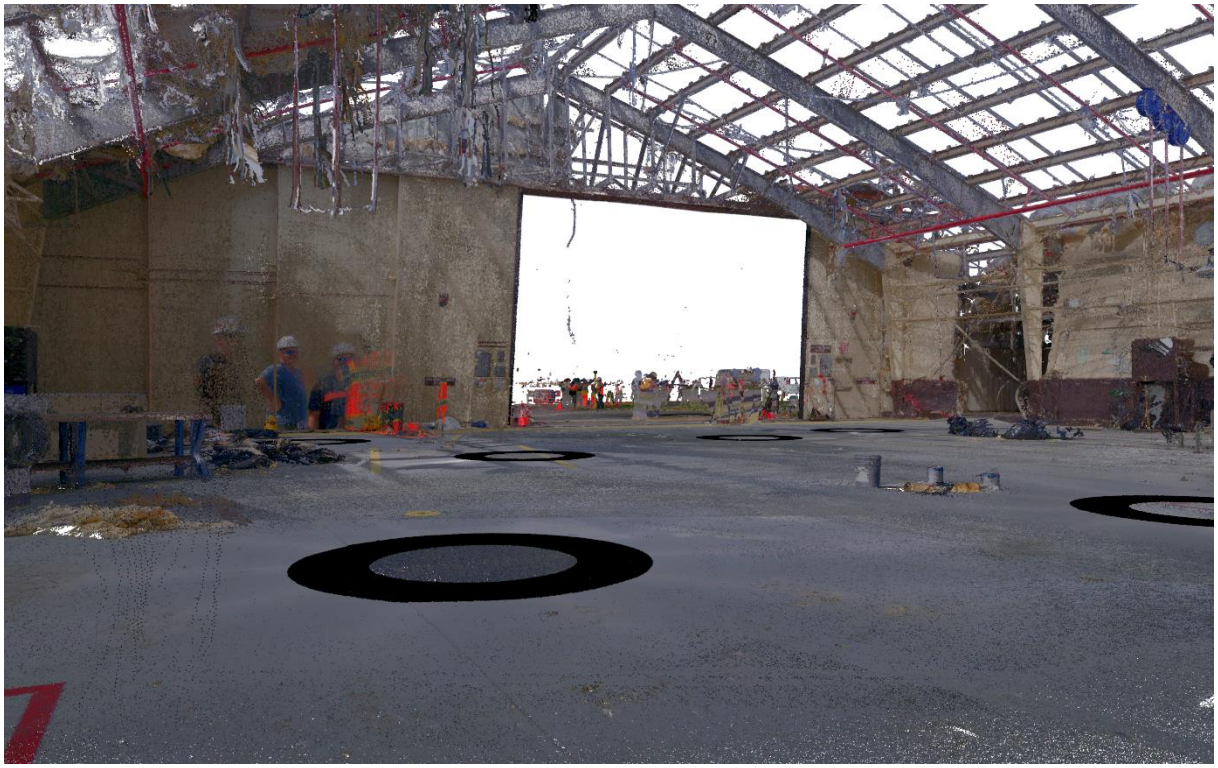

Figure 4.63. Inside view before cleaning showing only BLK360 data.

Figure 4.64. Inside view after cleaning showing only BLK360 data.

Figure 4.65. Outside view before cleaning showing BLK360 data.

Figure 4.66. Outside view after cleaning showing BLK360 data.

Figure 4.67. A single bay from Building 316.

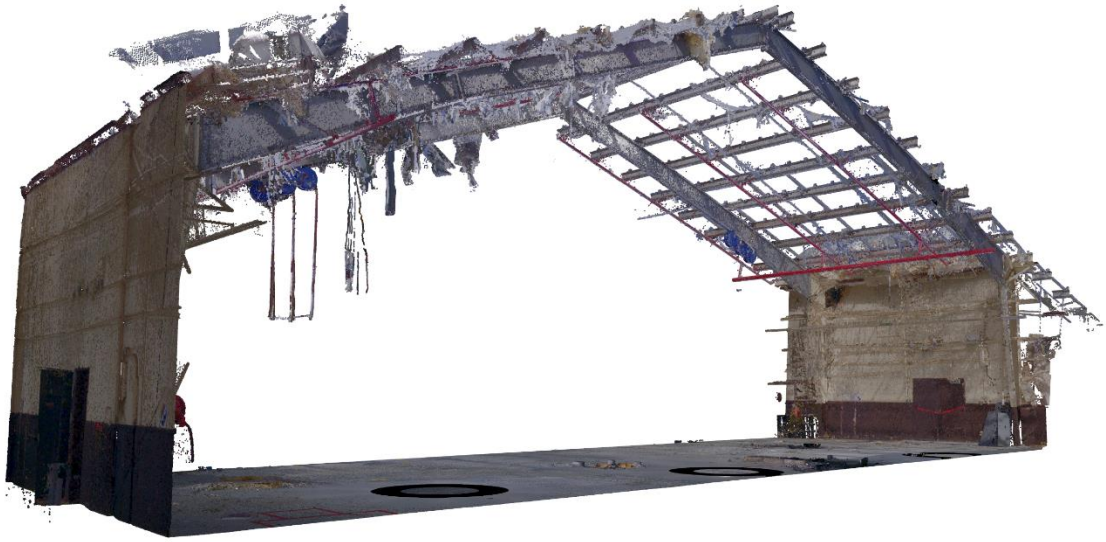

Figure 4.68. A single bay from Building 316.

4.7.4 *Other observations*

No other observations were made.

4.8 TYNDALL AIR FORCE BASE: BUILDING 333

4.8.1 *Review of available lidar data*

Building 333, like Building 316 in the Tyndall Air Force Base, was scanned with BLK360 scanners exclusively. A total of 5 scans were made, all of which were used in the registration. All of those scans were made close to the entrance on the northwest side due to the fact that the rest of the building was inaccessible as can be seen in the overview pictures. The scan locations can be seen in Figure 3.46.
The Maptek database containing all the scans is 11.9 GB.

4.8.2 *Data registration overview and challenges*

The final registration contained 291,571,664 points, which is reasonable for processing and therefore no filters were applied.

4.8.3 *Point cloud cleaning*

The cleaning process here was more extensive than in other buildings since all the scans are in one end and tanks block the view towards the opposite end. Therefore, the part of the building barely visible in the point cloud was removed, and due to the repetitive nature of the frames the one end clearly visible in the point cloud will be used exclusively. Along with that process, the points registered outside the building were removed.
After cleaning a total of 248,517,125 points remained, all of which are BLK360.

Figure 4.69 through Figure 4.74 show the cleaning process from various angles. Those figures come in pairs where the untouched model is showed first and the fully cleaned version follows.

Figure 4.75 shows a single frame from Building 333 and Figure 4.76 shows the following bay, demonstrating the slicing abilities of PointStudio to get a clearer view of elements of interest.

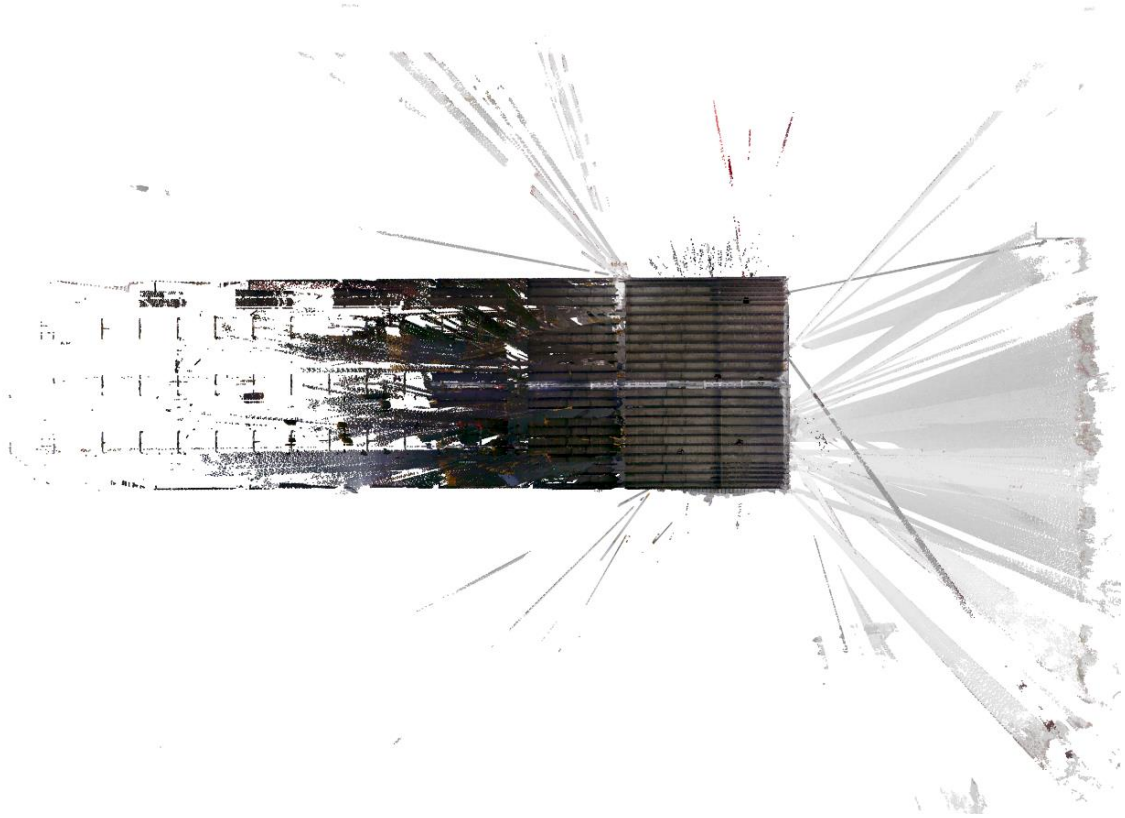

Figure 4.69. Aerial view before any modifications were done to the point cloud.

Figure 4.70. Aerial view after cleaning.

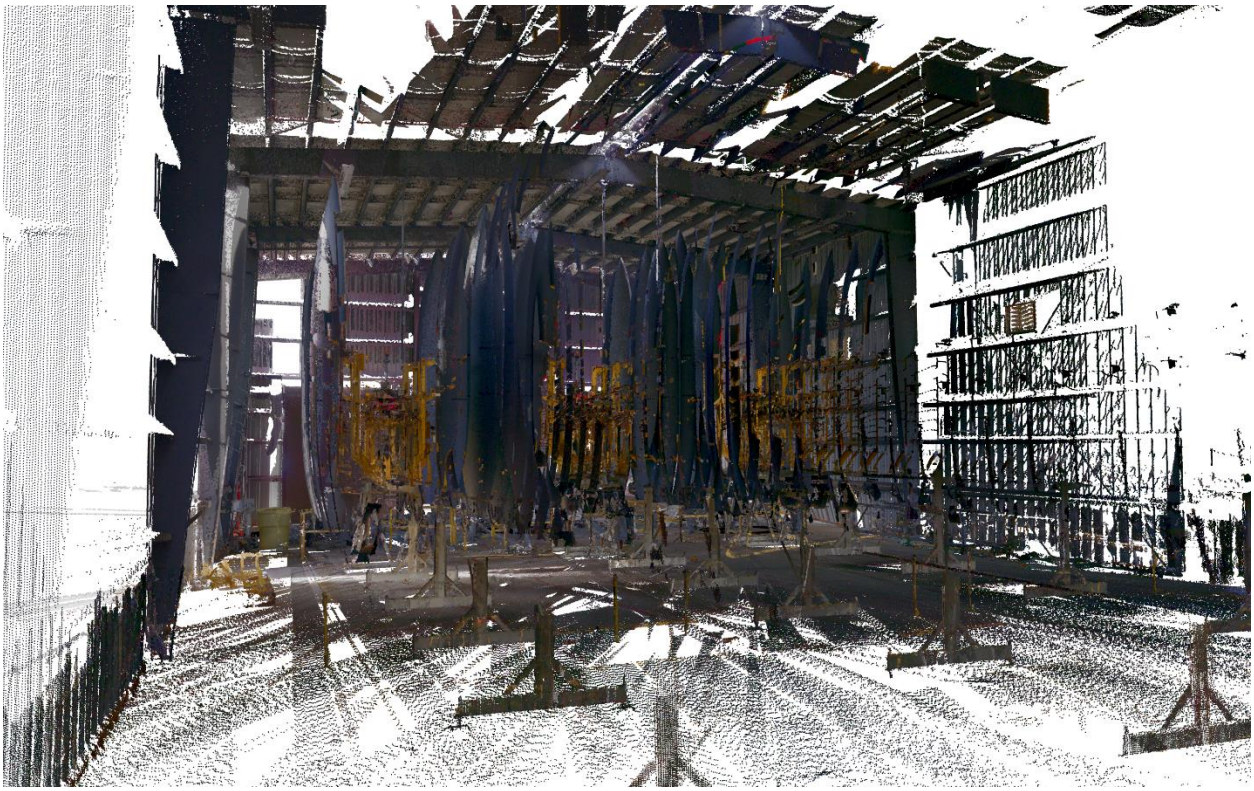

Figure 4.71. Inside view before cleaning showing only BLK360 data.

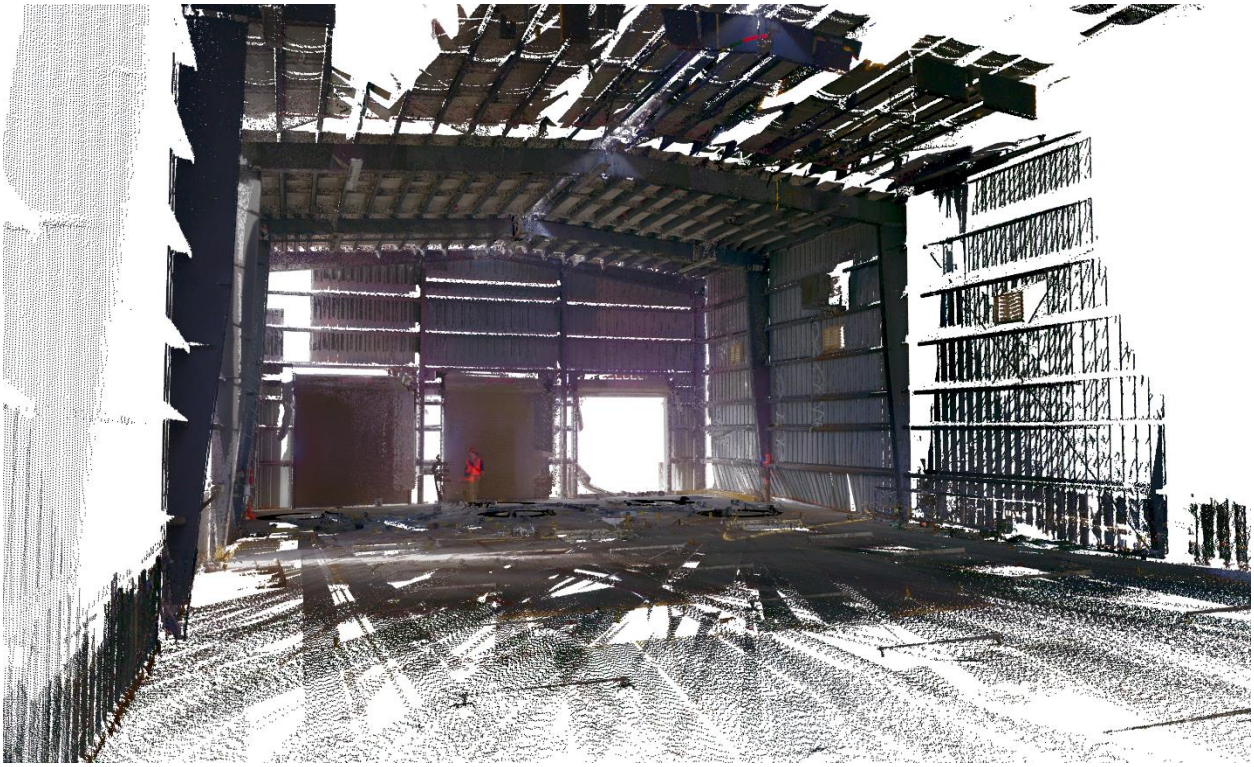

Figure 4.72. Inside view after cleaning showing only BLK360 data.

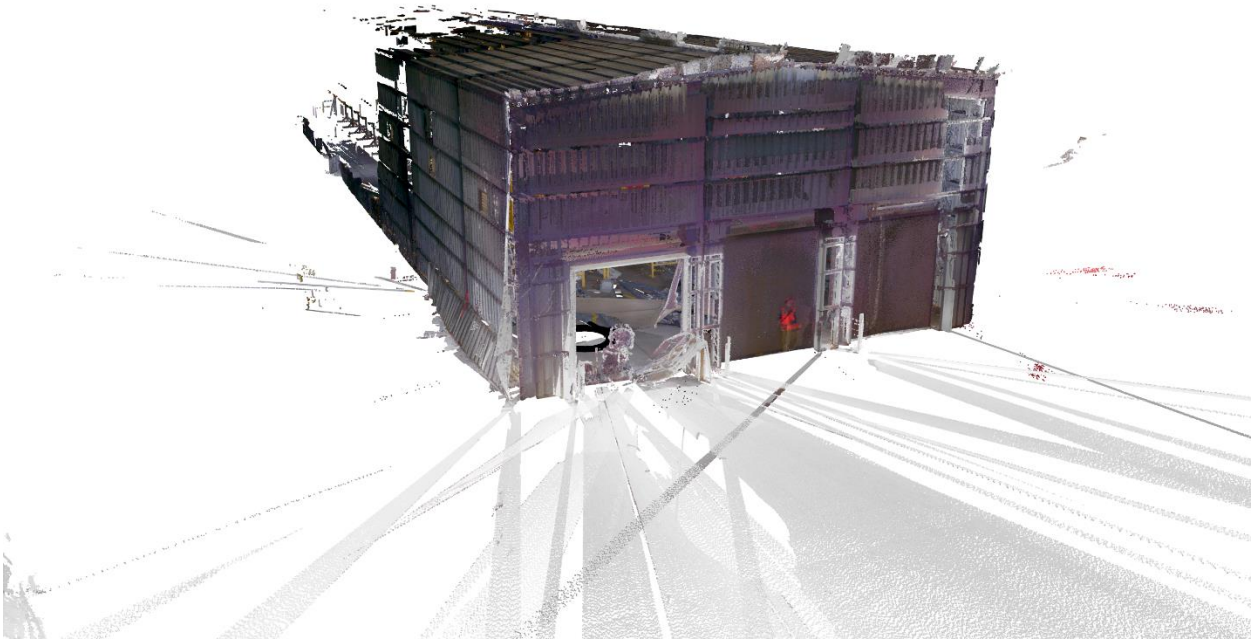

Figure 4.73. Outside view before cleaning showing BLK360 data.

Figure 4.74. Outside view after cleaning showing BLK360 data.

Figure 4.75. A single frame from Building 333.

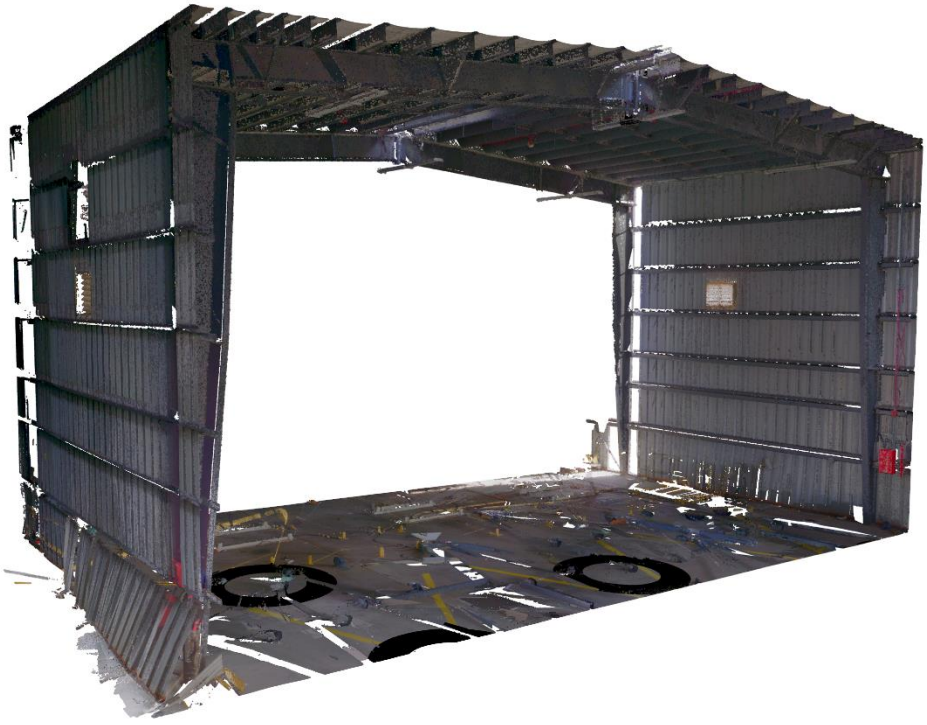

Figure 4.76. A single bay from Building 333.

4.8.4 *Other observations*

No other observations were made.

4.9 TYNDALL AIR FORCE BASE: BUILDING 375

4.9.1 *Review of available lidar data*

Like the previous two buildings from Tyndall Air Force Base, Building 375 was scanned with BLK360 exclusively. A total of 10 scans were made and all of them used in the registration. The scan locations can be seen in Figure 3.47.
The Maptek database containing all the scans is 20.1 GB.

4.9.2 *Data registration overview and challenges*

The final registration contained 412,493,667 points and no filters were applied to reduce that number. Two of the scans were done on an elevated platform as can be seen on the scan location map and therefore the built-in registration tools from Leica did not detect that those were done in the same room, which complicated the registration process slightly. The only action that had to be taken was to manually move those scans to the approximate height and then the automatic process took over.

4.9.3 *Point cloud cleaning*

The cleaning process was relatively straight forward as rubble was removed from the floor along with points outside the building. After cleaning, 380,773,450 points remained and for the 5 cm macro model a total of 1,400,580 were used.

Figure 4.77 through Figure 4.82 show the cleaning process from various angles. Those figures come in pairs where the untouched model is showed first and the fully cleaned version follows.

Figure 4.83 shows a single frame from Building 375 and Figure 4.84 shows the following bay, demonstrating the slicing abilities of PointStudio to get a clearer view of elements of interest.

Figure 4.77. Aerial view before any modifications were done to the point cloud.

Figure 4.78. Aerial view after cleaning.

Figure 4.79. Inside view before cleaning showing only BLK360 data.

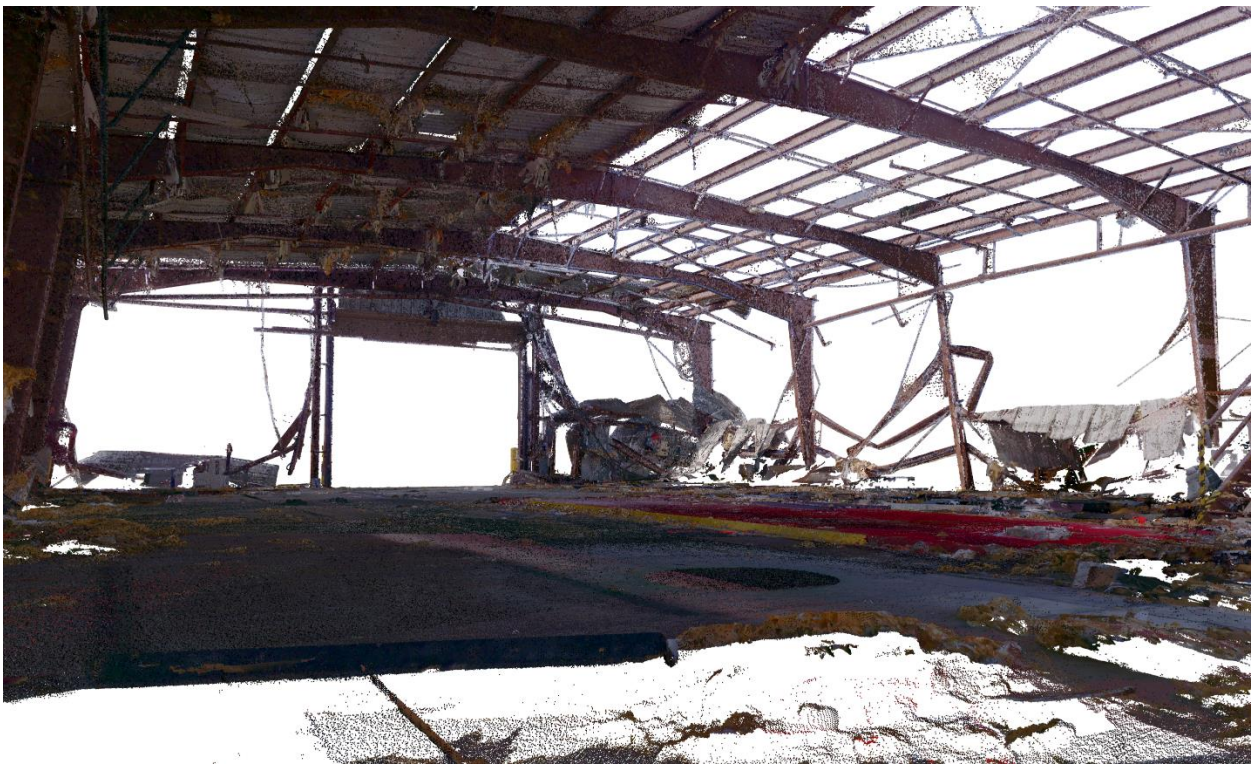

Figure 4.80. Inside view after cleaning showing only BLK360 data.

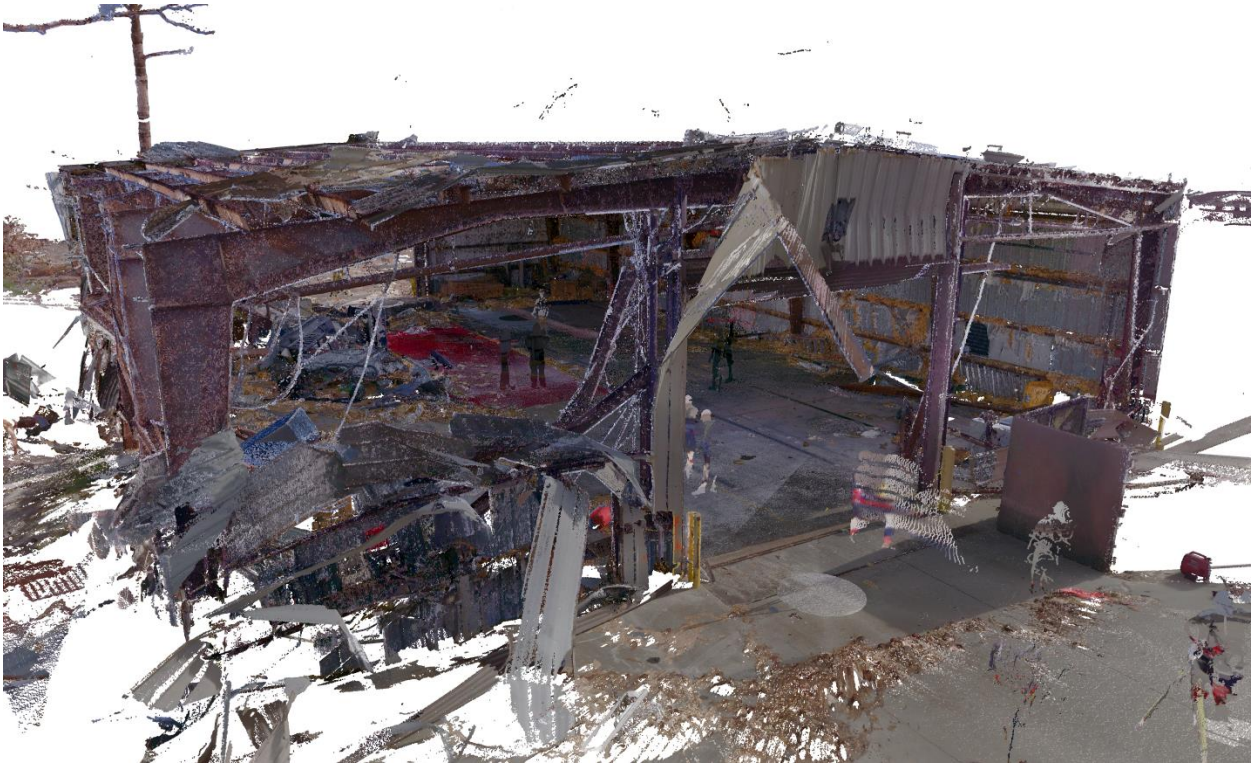

Figure 4.81. Outside view before cleaning showing BLK360 data.

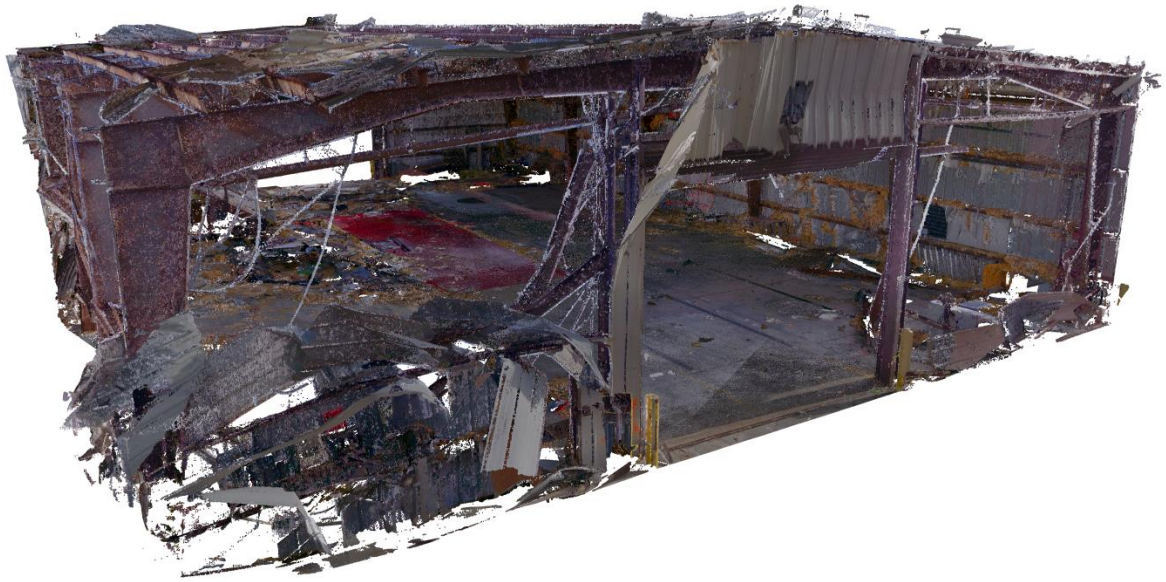

Figure 4.82. Outside view after cleaning showing BLK360 data.

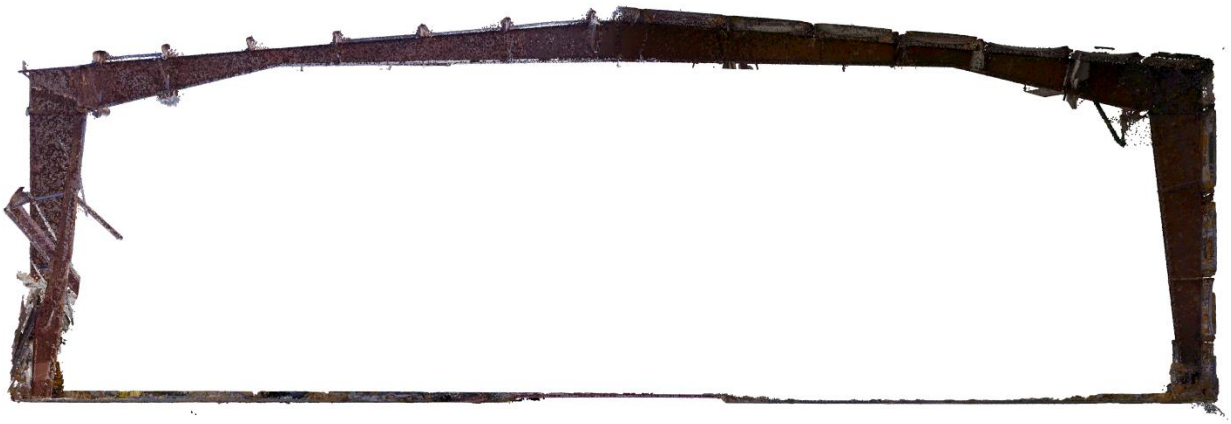

Figure 4.83. A single frame from Building 375.

Figure 4.84. A single bay from Building 375.

4.9.4 *Other observations*

No other observations were made.

4.10 PARTHENON

4.10.1 *Review of available lidar data*

Parthenon was scanned exclusively with BLK360 scanners, a total of 6 scans. Of those, 3 were in the main area around the collapsed side of the building, but 3 were taken in rooms at the back. They are not interlinked so in practice the point cloud relies only on the 3 in the main area. The scan locations can be seen in Figure 3.48.
The Maptek database containing all the scans is 15.1 GB.

4.10.2 *Data registration overview and challenges*

The final registration contained 346,335,418 points with 172,308,774 in the main area. There was not enough overlap with the other scans to even accurately place those rooms, and with no drawings available for this building, they had to be mostly disregarded. A case where they could become useful is the identification of various structural elements due to the repeating nature of the framing. Another note is that during the scanning process there was no access in front of the building due to the cleaning of rubble, so the point cloud is lacking from that direction.

4.10.3 *Point cloud cleaning*

The cleaning process was relatively straight forward as merchandise stored in the building was removed from the scans. After that process the number of points within the main registration was 131,151,721. Minimal rubble was removed from the floor since it consisted largely of structural elements such as beams and purlins and therefore has the possibility of being measured.

Figure 4.85 through Figure 4.90 show the cleaning process from various angles. Those figures come in pairs where the untouched model is showed first and the fully cleaned version follows. Figure 4.93 shows the approximate locations of the rooms discussed, but as they were not registered to the rest of the cloud their exact orientation is unclear.

Figure 4.91 shows a single frame from Parthenon and Figure 4.92 shows the following bay, demonstrating the slicing abilities of PointStudio to get a clearer view of elements of interest.

Figure 4.85. Aerial view before any modifications were done to the point cloud.

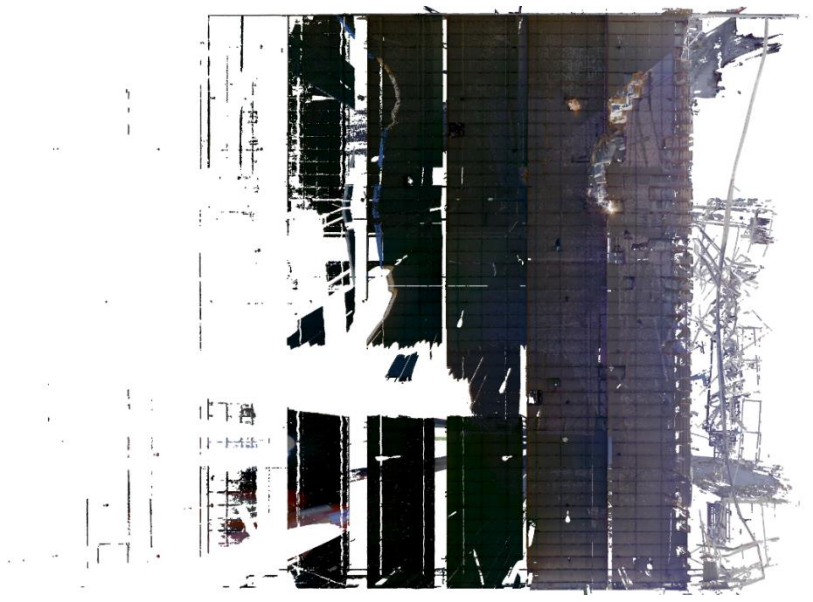

Figure 4.86. Aerial view after cleaning.

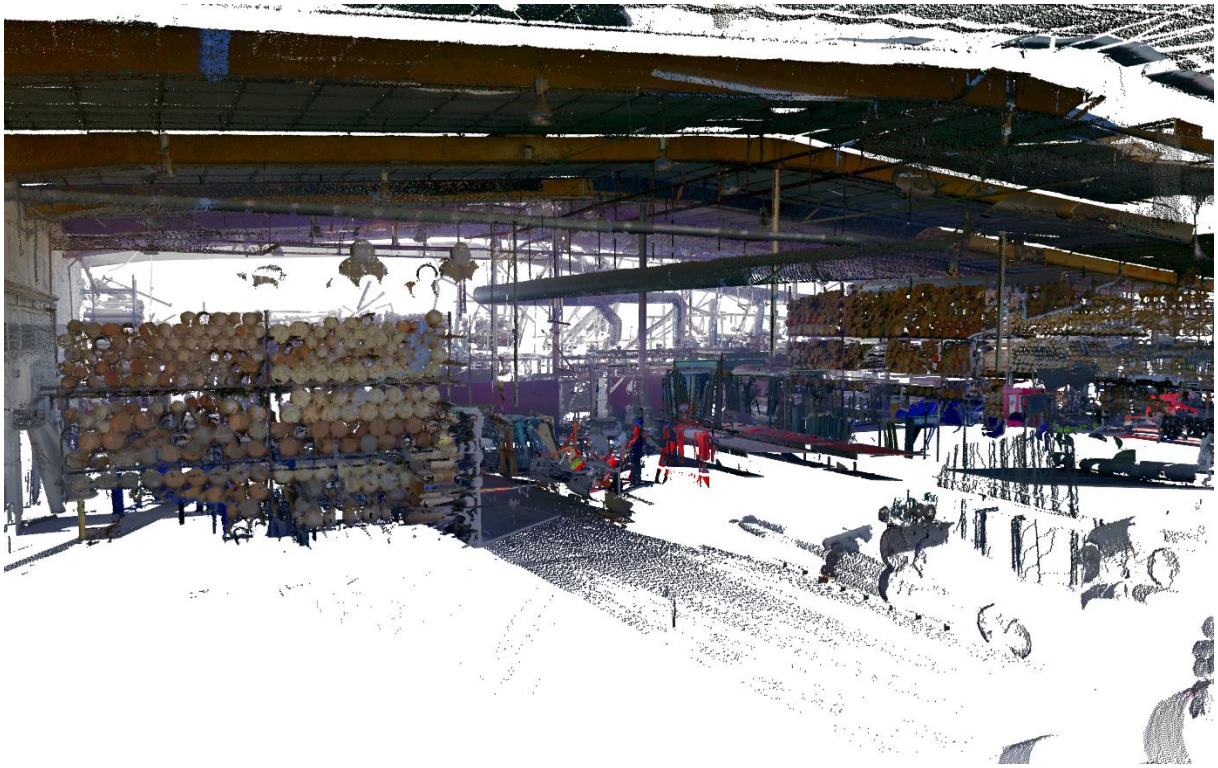

Figure 4.87. Inside view before cleaning showing only BLK360 data.

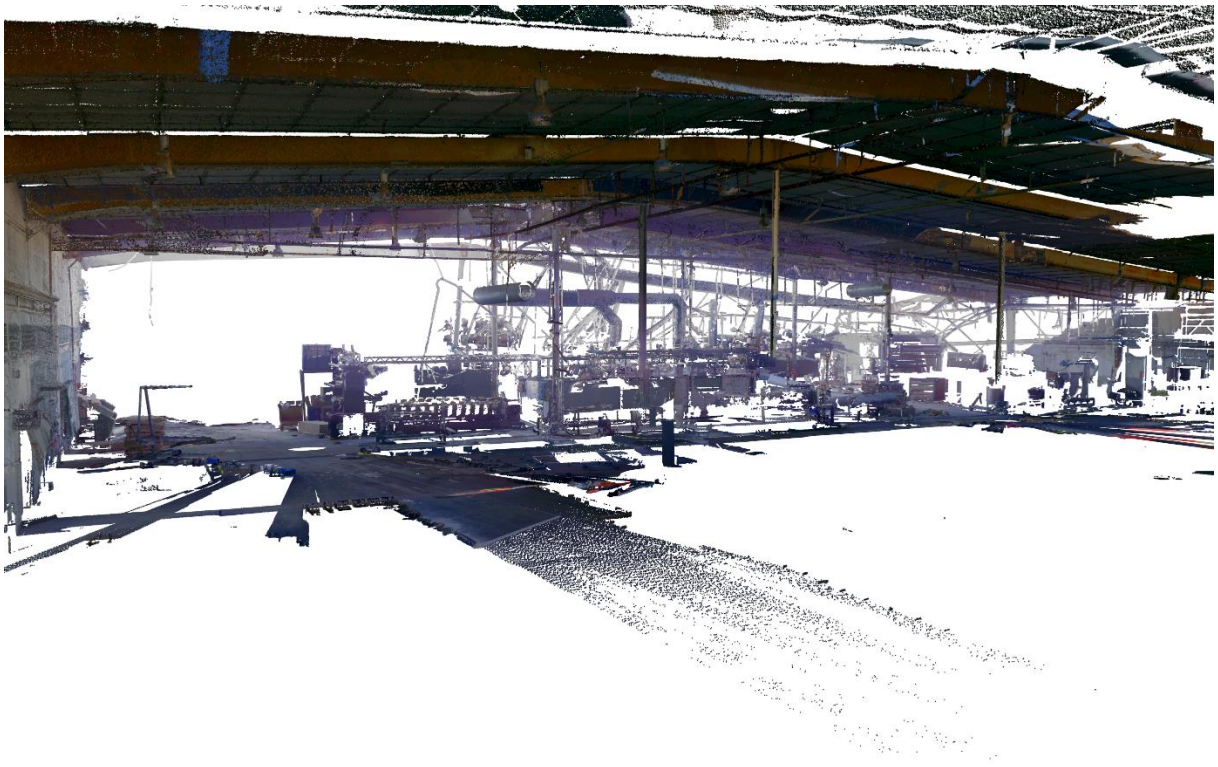

Figure 4.88. Inside view after cleaning showing only BLK360 data.

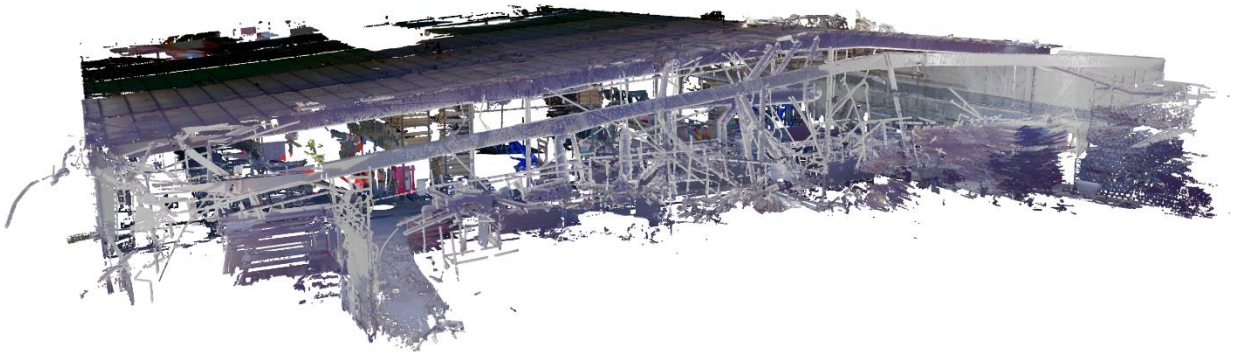

Figure 4.89. Outside view before cleaning showing BLK360 data.

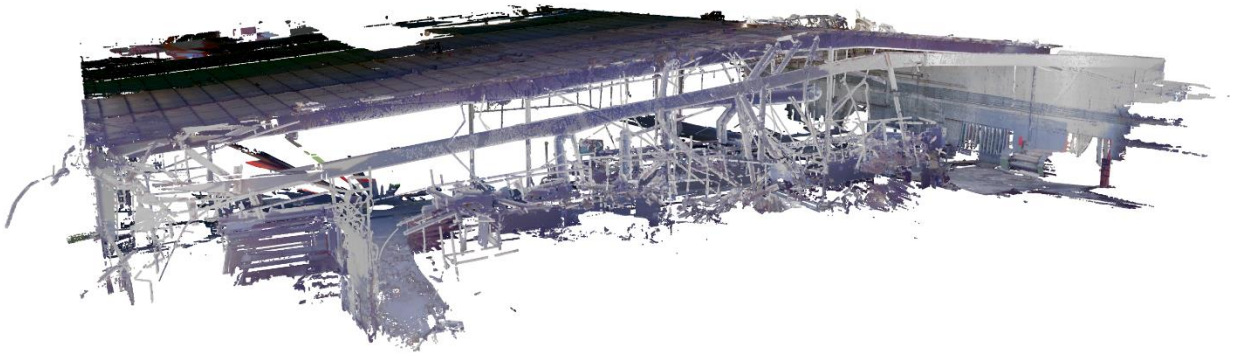

Figure 4.90. Outside view after cleaning showing BLK360 data.

Figure 4.91. A single frame from Parthenon.

Figure 4.92. A single bay from Parthenon.

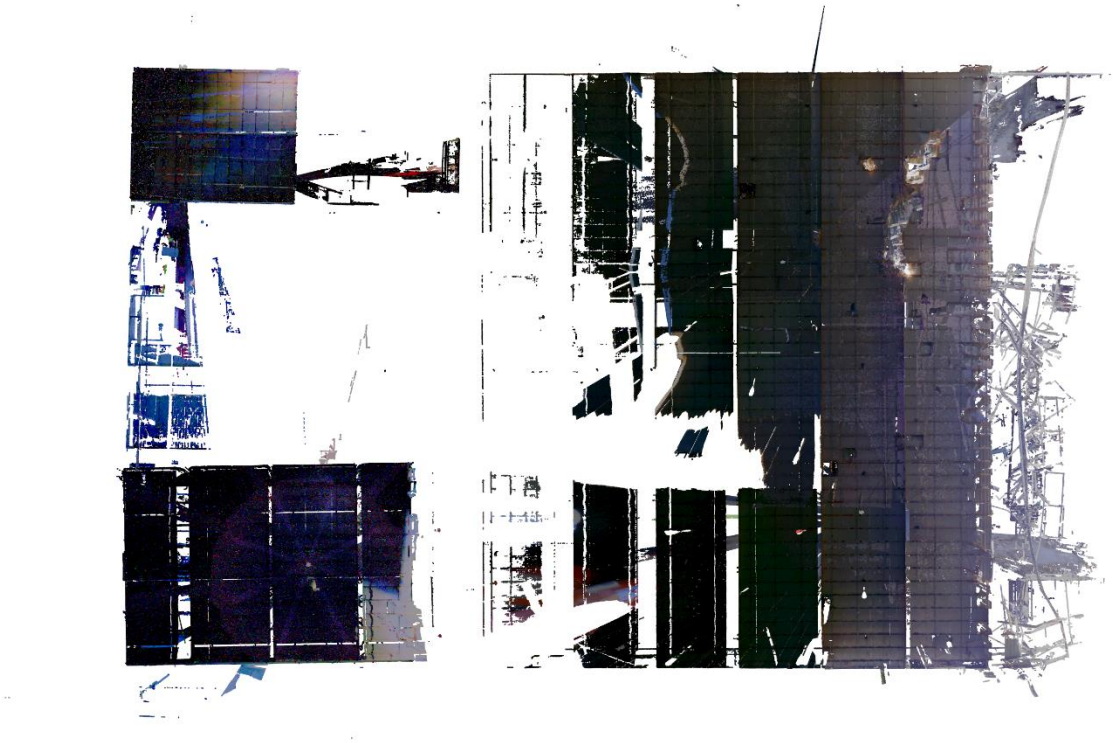

Figure 4.93. Approximate location of scans in rooms at the back of the building.

4.10.4 *Other observations*

No other observations were made.

4.11 MILLER DISTRIBUTION CENTER

4.11.1 *Review of available lidar data*

There were only XR3 scans available for Miller Distribution center and they were all taken from outside the damaged face of the building. Note that the reconnaissance team could not gain interior access to this structure as the damage was extensive. There were a total of six scans, of which two were single scan locations and two were double, i.e. there were two scans performed in the same location with different scan density settings. The scan locations can be seen in Figure 3.49.
The Maptek database containing all the scans is 5.04 GB.

4.11.2 *Data registration overview and challenges*

The final registration contained 99,348,716 points, all coming from the XR3 scans since there were no BLK360 scans. When compared to larger datasets in this study it is clear that no minimum separation filter is needed since the point cloud is already at a manageable size.
As can be seen in Figure 3.49, the scan locations are relatively far away from the building, which results in a sparse distribution of points in the area of interest.

4.11.3 *Point cloud cleaning*

Since there were only scans from the outside, the ratio of unnecessary points including vegetation and nearby structures is much higher than when scans are taken from the inside as well. This results in a rather small final point cloud of 13,411,895 points without having to apply any filters as the unchanged scans are rather sparse.

Figure 4.94 through 4Figure 4.97 show the cleaning process from various angles. Those figures come in pairs where the untouched model is showed first and the fully cleaned version follows.

Figure 4.98 shows a single frame from Miller Distribution Center and Figure 4.99 shows the following bay, demonstrating the slicing abilities of PointStudio to get a clearer view of elements of interest.

Figure 4.94. Aerial view before any modifications were done to the point cloud.

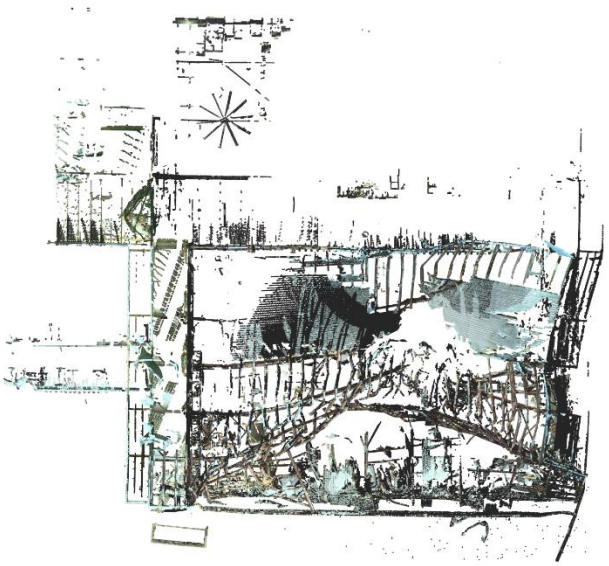

Figure 4.95. Aerial view after cleaning.

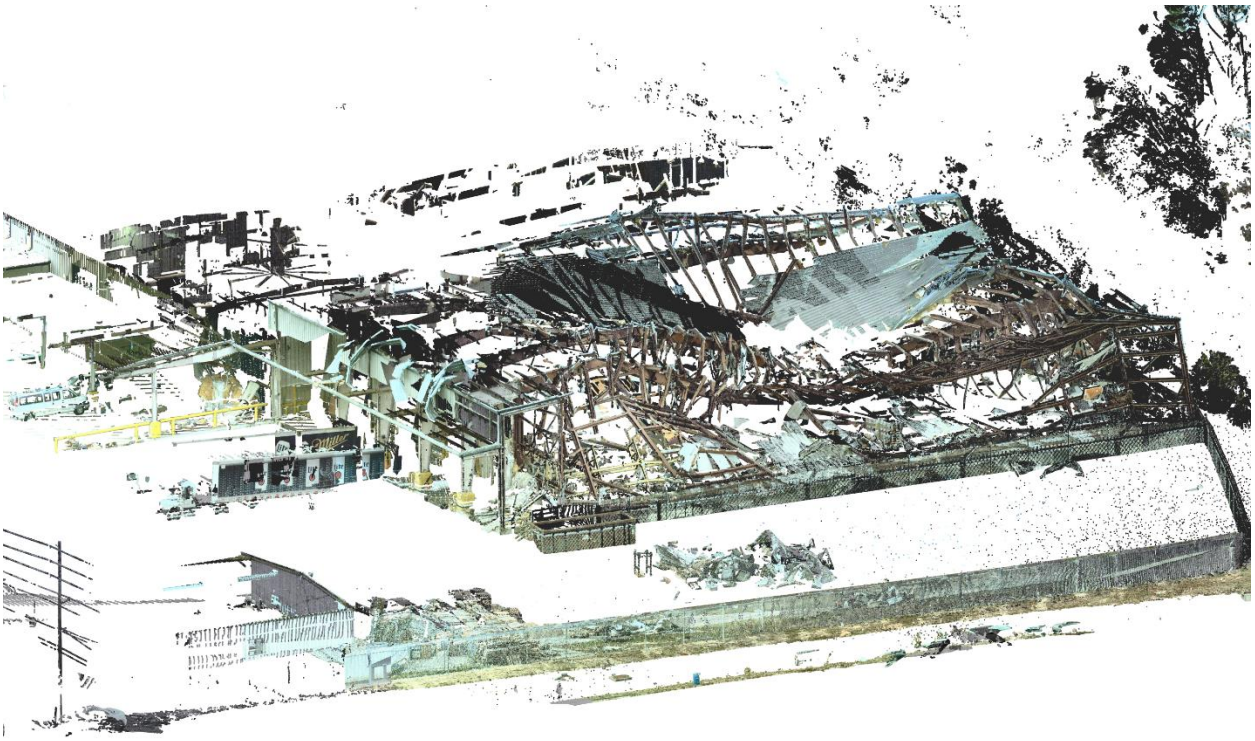

Figure 4.96. Outside view before cleaning showing XR3 data.

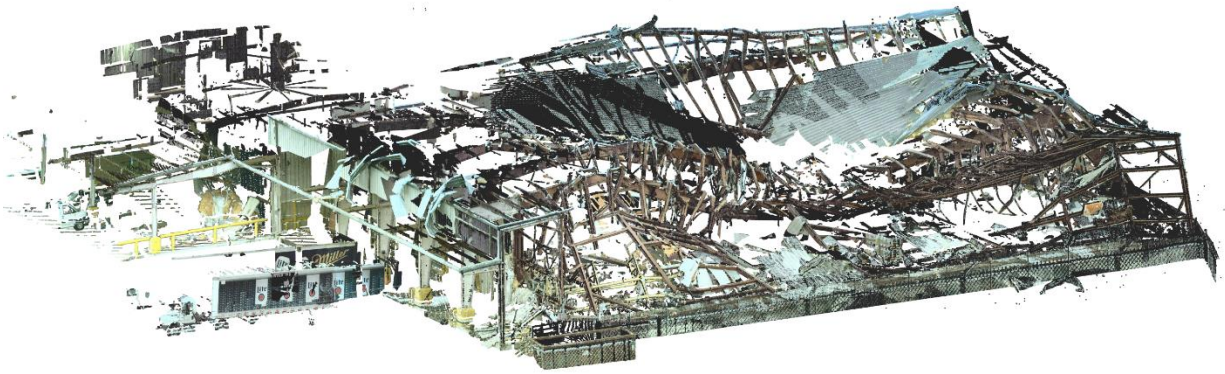

Figure 4.97. Outside view after cleaning showing XR3 data.

Figure 4.98. A single frame from Miller Distribution Center using XR3 data only.

Figure 4.99. A single frame from Miller Distribution Center using XR3 data only.

4.11.4 *Other observations*

The scans for Miller Distribution center were done in a low-light setting (night from 7:44-10:47 pm on November 6, 2018), as can be seen in the drone shot in chapter 3, and that could affect the efficiency of the scans. Slight modifications were done to the color representation in the model, such as increasing contrast and brightness, which makes it easier to distinguish between building parts.

4.12 PIRATES COVE MARINA

4.12.1 *Review of available lidar data*

Pirates Cove Marina was scanned much less extensively than all the other buildings as it contained only 1 XR3 scan from around 400 m away. The scan location can be seen in Figure 3.50.
The Maptek database containing that scan is 383 MB.

4.12.2 *Data registration overview and challenges*

No registration was done since there is only one scan containing 8,025,638 points. Not much can be done with this type of scan, other than extracting approximate envelope data and failure modes.

4.12.3 *Point cloud cleaning*

Due to the distance of the scan from the building the cleaning removed most of the points, leaving 239,963 points.

Figure 4.100 through Figure 4.103 show the cleaning process from an aerial view and from a closer outside view in pairs where the untouched model is showed first and the fully cleaned version follows.

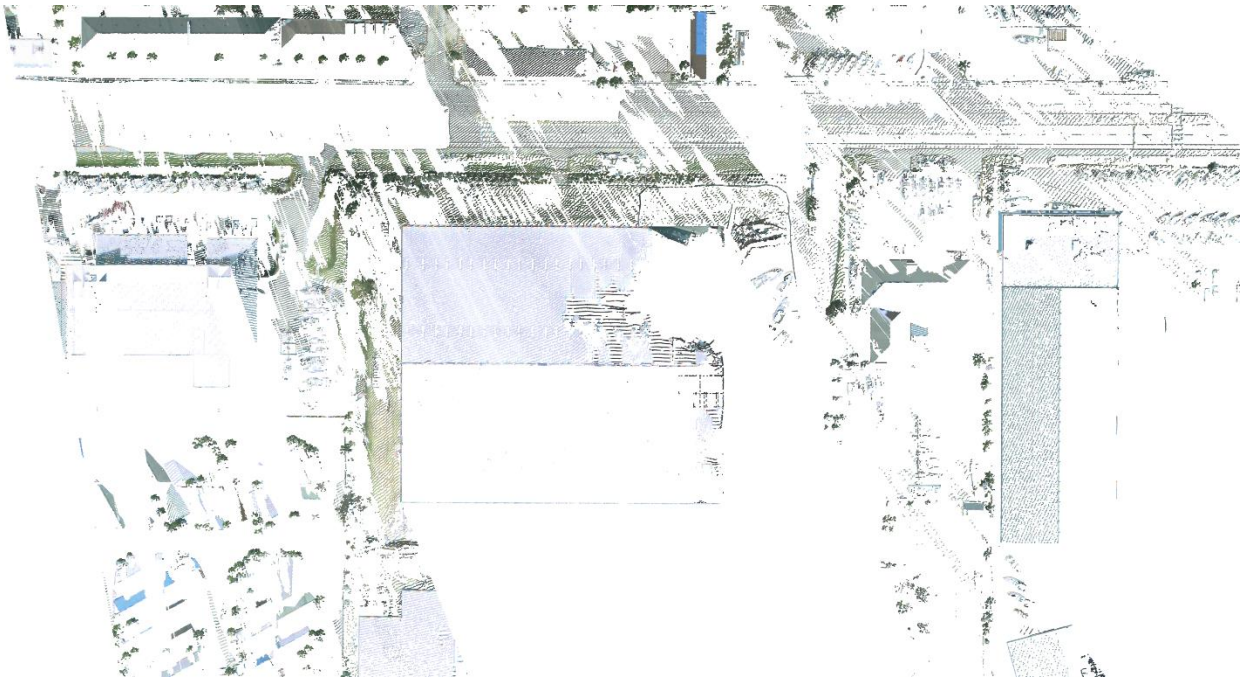

Figure 4.100. Aerial view before any modifications were done to the point cloud.

Figure 4.101. Aerial view after cleaning.

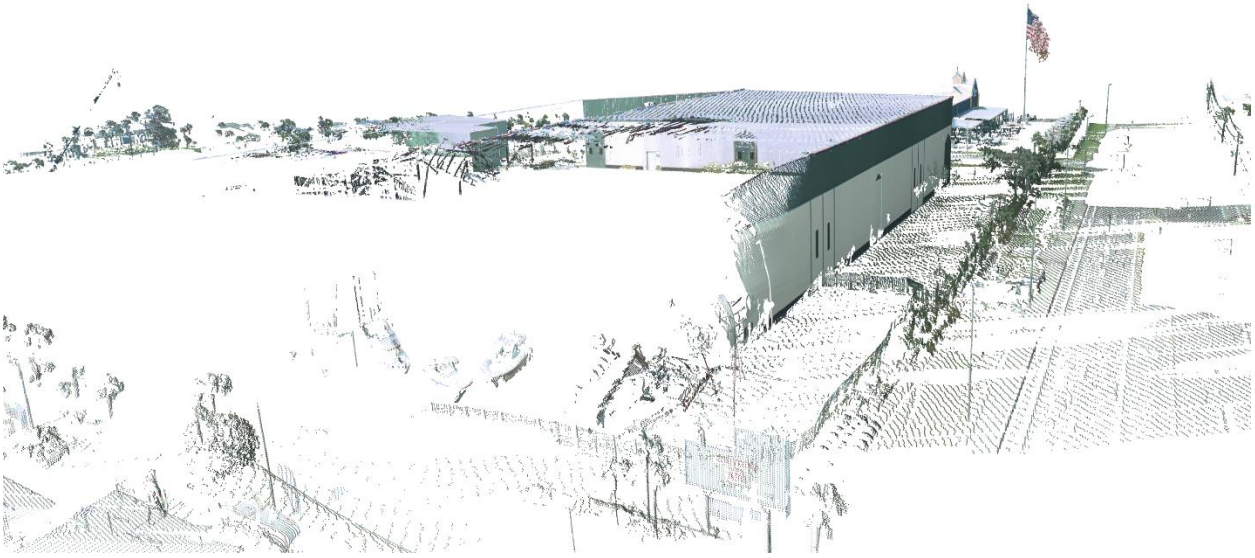

Figure 4.102. Outside view before cleaning showing XR3 data.

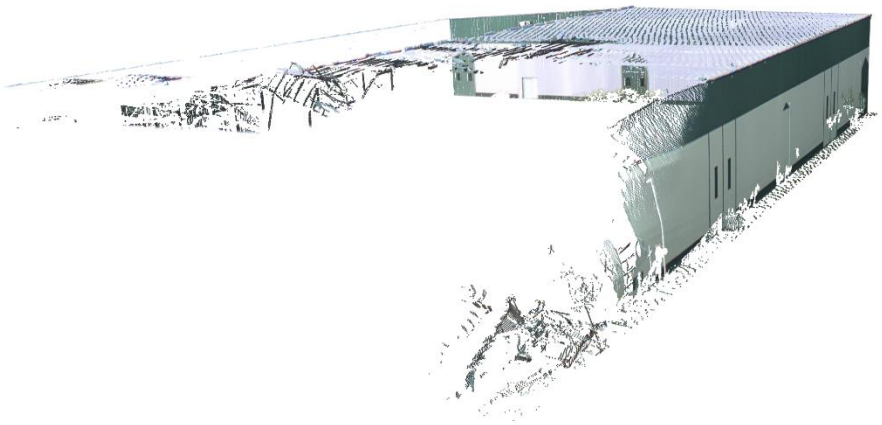

Figure 4.103. Outside view after cleaning showing XR3 data.

4.12.4 *Other observations*

No other observations were made.

Chapter 5. DATA INTERPRETATION

5.1 INTRODUCTION

The purpose of registering point clouds for collapsed buildings is to be able to continue analyzing them after the clean-up process has concluded. Certain information about buildings, e.g. envelope and various section data, might not be available for the reconnaissance crew and therefore it is essential to be able to extract that data from the point clouds to conduct the analysis. This data can then be compared to available drawings and the accuracy of the measurements estimated from those comparisons. In this case, drawings are available for Westrock East Terminal, Watson Landings Marina, and the Panama Distribution Center although the sections in the boat racks at Watson Landings Marina are proprietary, owned by Roof & Rack Products, Inc.

Some guesswork has to be done for the buildings without drawings as the scans are mostly placed inside the buildings and therefore the envelope data cannot account for inaccuracies resulting from unknown items on the outside. This can be unknown beam depth on the edges, unknown thickness of boarding or paneling on the outside etc. but a subjective estimation of the extension beyond the inner side of the building can be made by comparing the point cloud models to available photos from the sites.

Comparison to available drawings is not the only error estimator that is valid. The software used to register the point clouds calculates a cloud-to-cloud error, which is the error factor resulting from inaccuracies between different scans in the point cloud. That can serve as baseline but because not all regions of the point cloud carry the same importance to the researcher e.g. buckled purlins versus boats sitting on racks. The software does not distinguish between those two when calculating the registration error and therefore a more subjective analysis needs to be performed, where observations are made of critical areas. This includes looking at the density of the cloud, identifying stray points and disregarding along with comparisons to known shapes, such as wide flange beams.

5.2 PRELIMINARY TESTING

Preliminary testing was conducted to determine the necessary point density for the large-scale measurements done here. This was done by extracting a single HSS8x8x5/16 (Hollow Square Section that is 8 by 8 inches and wall thickness of 5/16 in) from the Intermodal Distribution Center, measuring the width, and seeing what effect the change in point density had on the measurements. The change in point density is implemented by using the minimum separation filter of Maptek's PointStudio, ranging from no filter to 50 mm with 5, 10 and 20 mm in between. This was done to examine the possibility of making the point clouds smaller so that less powerful computers can comfortably work with them along with reducing the storage space needed.

Along with the testing of the effect of point cloud density on the plane approximation measurements, the individual plane size was tested. The HSS8x8x5/16 section from the Intermodal Distribution Center was sliced to 7, 3 and 1 m lengths to determine if a larger surface would improve the plane approximation measurement method. The results can be seen in Figure 5.1 where the measurement error is shown against the number of points in the model. There is not a considerable difference between the different point densities, whereas the slice length seems to have an impact on the accuracy. The 3 m slice shows higher accuracy than the 7 m slice which seems counter intuitive, but it is worth noting that the ASTM tolerance of outside dimensions of HSS8x8x5/16 is 1% and both fall well within that. In addition to examining the effect of point density and plane size, Figure 5.1 compares the results for both plane-to-plane (p2p) and cloud-to-cloud (c2c) measurements, with the plane-to-plane measurements demonstrating greater accuracy in all categories.

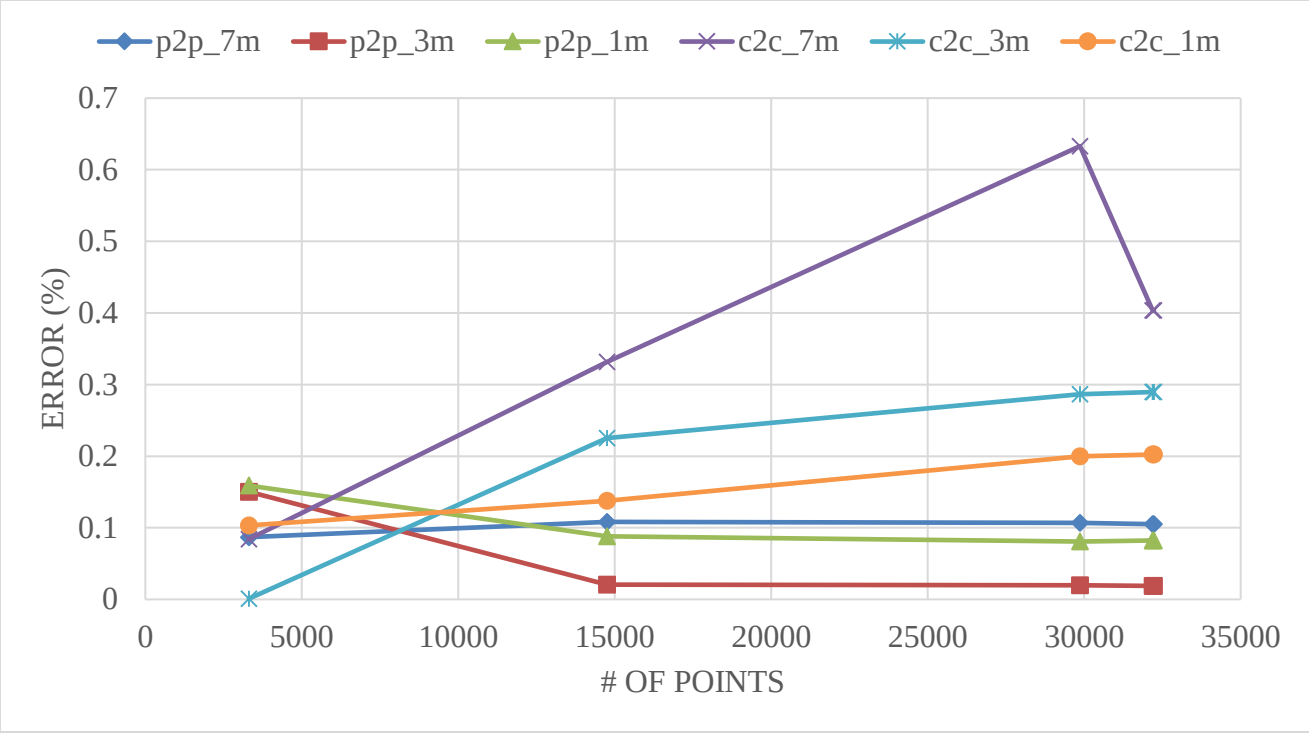

Figure 5.1. Graph showing the relationship between point density and measurement accuracy.

Therefore, it was determined that 50 mm minimum separation provided adequate results for envelope information and plane sizes were maximized for every dimension measured. For cross-sectional information, the full resolution was determined to be necessary since the scale of the dimensions are comparatively much smaller than what is seen in envelope information and the accuracy must be maximized at the cost of processing speed.

5.3 Envelope/Frame Data from Models

Using CloudCompare and its built-in plane fitting tool, the large-scale measurements were extracted from the point clouds by fitting planes to the edges of objects that were of interest and measure the distance between the centers of those planes. This is a quick method that requires little knowledge of point clouds or their manipulations and therefore can easily be replicated by other interested parties.

Maps showing the scan locations are vital in this process, as dimensions extracted from a single scan has no registration error and therefore is only affected by the error of the scanning device itself. Because of this, it is vital to choose a scan based on its location within the building so that it captures the dimension of interest e.g. a scan capturing the web of two columns in a row to measure the spacing. Care must be taken to determine which side of the web it captures, otherwise the thickness of the web will skew the results.

The process of extracting dimensions with the plane fitting method can be broken down into four steps:

1. Choose scans from map
2. Slice a section of equal dimensions in both places
3. Fit planes to the surfaces
4. Measure the distance between them

5.3.1 *Buildings with Known Dimensions*

Three buildings in the dataset analyzed here had structural drawings available to compare measured dimensions to. Those were Westrock East Terminal, Watson Landings Marina and the Intermodal Distribution Center. Large-scale, or envelope information, was gathered with the plane approximation method and they are summarized in the following tables. All the locations referenced in the tables correspond to column lines in the drawings found in Appendix A, the number of scans refers to how many scan locations were utilized in the extraction of that particular dimension, and the scan type can be XR3, BLK360 or both. The other columns are self-explanatory. For the sake of comparing collected measurements to drawings, a subjective analysis was done to determine whether other factors than scanning and registration accuracy could affect the results. Measurements determined to be affected by these outside factors were then grouped separately to avoid skewing the results.

Westrock East Terminal has a centrally offset pitch on the roof and as a result there are three different roof heights needed to establish the outline of the building. Height 1 corresponds to the northernmost side, height 2 is on the top of the pitch and height 3 on the southernmost side. Four

different column spacings are found in Westrock East Terminal and one of each length was measured. The purlin spacing is uniform over the whole roof, but two measurements were taken as a precaution.

The findings from Westrock East Terminal are summarized in Table 5.1 and it is apparent that dimensions affected by outside factors demonstrate a much larger error compared to those dimensions deemed to not suffer from such discrepancies. The factors affecting each measurement vary, with the length being possibly inaccurate due to sway on the front wall, the heights could not be accurately determined from drawings due to the scans not containing the outside of the roof and the dimensions of cladding etc. being unknown, and the purlin spacing possibly being inaccurate due to the fact their spacing is not mentioned in the available drawings so the length of a frame span was divided by the number of purlins.

Table 5.1. Envelope data from Westrock East Terminal

Dimension	Location	# of scans	Scan type	Measured (m)	Drawing (m)	Error (%)	Error (mm)	Outside factors
Length	E1-E21	1	XR3	182.532	182.880	0.19%	348.4	Y
Width	C3-R3	1	XR3	79.731	79.731	0.00%	0.4	N
Height 1	C 10-11	1	XR3	11.210	11.074	1.22%	135.7	Y
Height 2	P 2-3	1	XR3	13.854	13.741	0.82%	113.1	Y
Height 3	R 6-7	1	XR3	13.156	13.086	0.53%	69.7	Y
Roof slope 1	Height 1-2	2	XR3	1/24.207	1/24	0.86%	207.4	Y
Roof slope 2	Height 3-2	1	XR3	1/22.521	1/24	6.16%	1479.3	Y
Column spacing 1	C1-2	1	XR3	8.691	8.687	0.05%	4.4	N
Column spacing 2	C2-3	1	XR3	9.138	9.144	0.06%	5.6	N
Column spacing 3	1E-F	1	XR3	7.006	7.010	0.05%	3.7	N
Column spacing 4	L3-5	1	XR3	18.274	18.288	0.08%	13.7	N
Purlin spacing 1	R-Q 7-8	1	XR3	1.231	1.168	5.43%	63.5	Y
Purlin spacing 2	R-Q 7-8	1	XR3	1.147	1.168	1.76%	20.6	Y

Outside factors	Average error (%)	Average error (mm)
Both	1.33%	189.6
N	0.05%	5.6
Y	2.12%	304.7

Watson Landings Marina is almost completely symmetric around the long axis and therefore there are only two height measurements, one on western side and one 10 inches from the center to avoid the air duct running along the roof ridge. There are three different column spacings but five were extracted due to spans of the same length having varying column sections on either side. Two different purlin spacings are marked in the drawings so a span of each type was extracted.

The findings from Watson Landings Marina are summarized in Table 5.2. and, like Westrock East Terminal, the dimension affected by outside factors demonstrate a much larger error. The heights suffer from the same problem as Westrock East Terminal's since no scans from the top are available and various dimensions such as the cladding being unknown, and the length could also be affected by possible sway on the collapsed front side.

Table 5.2. Envelope data from Watson Landings Marina

Dimension	Location	# of Scans	Scan Type	Measured (m)	Drawing (m)	Error (%)	Error (mm)	Outside factors
Length	F1-F13	2	Both	97.722	97.739	0.02%	17.0	Y
Width	A11-H11	1	XR3	38.502	38.557	0.14%	55.3	N
Height 1	H3-2	1	XR3	17.443	17.069	2.19%	374.1	Y
Height 2	D-E13	1	XR3	17.854	17.874	0.11%	19.7	Y
Roof slope	Height 1-2	1	XR3	1/46.250	1/24	92.71%	22,249.8	Y
Column spacing 1	F13-12	1	XR3	6.902	6.909	0.09%	6.6	N
Column spacing 2	F12-11	1	XR3	6.710	6.706	0.05%	3.6	N
Column spacing 3	F11-10	2	XR3	6.711	6.706	0.07%	4.9	N
Column spacing 4	F10-9	1	XR3	9.150	9.144	0.07%	6.3	N
Column spacing 5	G2-3	2	BLK360	6.708	6.706	0.04%	2.4	N
Purlin spacing 1	A-B 9-10	1	XR3	0.910	0.914	0.45%	4.1	N
Purlin spacing 2	C-D 9-10	1	XR3	1.216	1.219	0.28%	3.4	N

Outside factors	Average error (%)	Average error (mm)
Both	8.02%	1895.6
N	0.15%	10.8
Y	23.76%	5665.2

Unlike most of the buildings examined here, the Intermodal Distribution Center has a flat roof so there was no pitch to examine here. Four different column spacings are found in the Intermodal Distribution center and one of each type was extracted along with the two different purlin spacings found, one of each type. All the purlins of the second type were completely collapsed, except for

one span which was heavily deformed as can be seen in Figure 5.2, so the distance between the two purlins was measured by fitting a mesh to each of them and measuring the average distance between them.

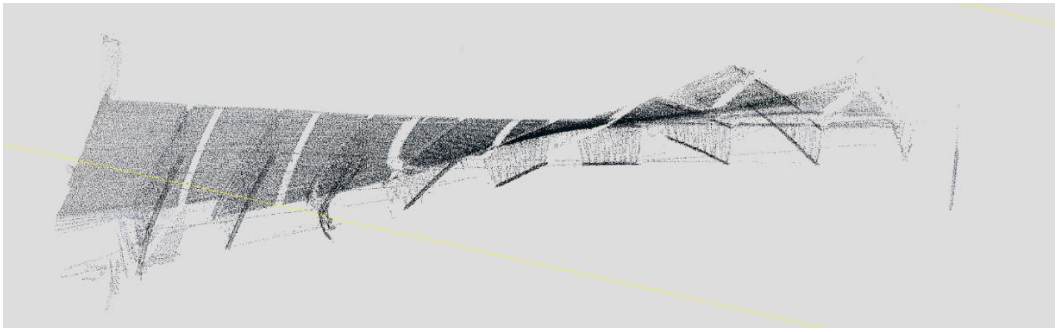

Figure 5.2. Deformed purlins (Purlin Spacing 2*) in Intermodal Distribution Center

The findings from Intermodal Distribution Center are summarized in Table 5.3. and the same trend continues, where there is a noticeably larger error where outside factors are determined to affect the results. Height continues to be an uncertainty due to unspecified thicknesses in the roof and no data being available from the top down. The length could not be accurately determined due to the whole front tilt-up wall being collapsed and the second type of purlins were heavily damaged, as stated before.

Table 5.3. Envelope data from Intermodal Distribution Center

Dimension	Location	# of Scans	Scan Type	Measured (m)	Drawing (m)	Error (%)	Error (mm)	Outside factors
Length	A11-A18	2	Both	100.264	100.076	0.19%	188.3	Y
Width	A12-G12	2	Both	97.085	97.130	0.05%	45.3	N
Height	A-B 12-13	1	BLK360	10.507	10.249	2.52%	258.2	Y
Column Spacing 1	B11.1-12	1	BLK360	13.694	13.716	0.16%	21.8	N
Column Spacing 2	B12-13	2	BLK360	14.321	14.326	0.03%	4.6	N
Column Spacing 3	12A-B	2	Both	18.165	18.186	0.11%	20.6	N
Column Spacing 4	12B-C	1	XR3	15.237	15.240	0.02%	2.9	N
Purlin Spacing 1	F-G 13-14	1	XR3	1.795	1.791	0.24%	4.4	N
Purlin Spacing 2*	A-B 17-18	1	BLK360	1.770	1.562	13.31%	207.9	Y

Outside factors	Average error (%)	Average error (mm)
Both	1.85%	83.77
N	0.10%	16.58
Y	5.34%	218.13

The dimensions that have unknown outside factors affecting them cannot be analyzed to any extent as all the data that is available comes from either point clouds or the structural drawings. For that reason, none of them could be verified in any way so the conclusions here were based solely on the measurements with known dimensions. Although the measurements are split into groups based on whether they have potential unknown error factors does not mean that the dimensions deemed to not suffer from these unknown outside factors are completely without error. As mentioned before, there is error stemming from the hardware of the scanners and in cases where more than one scan location is used there is a registration error. On top of this, there are physical factors to consider such as the previously mentioned allowable manufacturing error and when measuring spans across various distances the allowable erection tolerance has to be considered as well.

Figure 5.3 shows the relationship between measured error and the scale of the dimension extracted, using only the scans without unknown outside errors. There does not seem to be a noticeable difference between the types of scans used for measurements, but it is worth noting that the range of the BLK360 scanner is considerably lower than XR3 so measurements can generally not be taken from BLK360 data at all when the distance exceeds approximately 20m due to fall-off in point density and increase in scanning error.

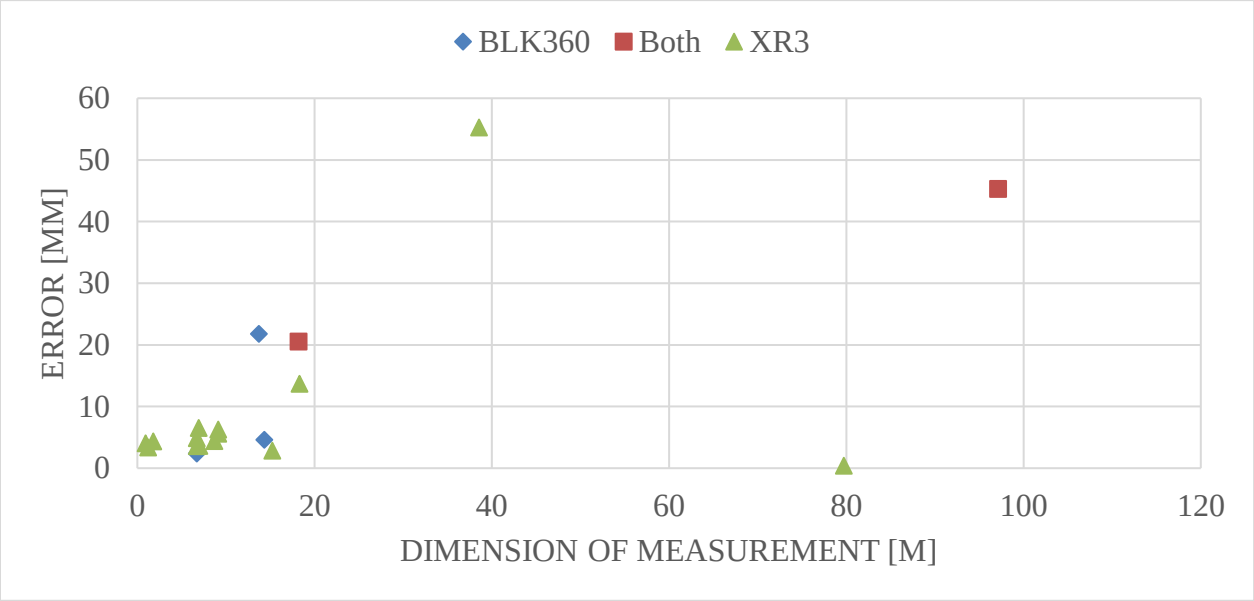

Figure 5.3. The relationship between the scale of measurements and error, separated based on the scan types used.

5.3.2 *Other Buildings*

Cargill Distribution Center: Scanned in a very similar fashion to Westrock East Terminal and Watson Landings Marina so it is expected to deliver similar results. The difference is mostly seen in the BLK360 scan locations as they are clustered at the back of the building instead of the front where most of the damage occurred.

Hangar 5: The centrality of the long-range XR3 scans should provide adequate points to measure basic envelope information.

Building 316: Small building that was thoroughly scanned so envelope information is extractable.

Building 333: Envelope information difficult to get due to the obstruction of view. With assumed repetition, everything but the full length is extractable.

Building 375: Very similar to Building 316 in size, shape and scan density, so it should provide very similar results.

Parthenon: Some missing data due to accessibility issues and very low scan density. In addition, there are only BLK360 scans and they are very central so range issues would be prevalent here.

Miller Distribution Center: Only scanned from the outside so there are quite a few gaps in the data. This results in most of the building being unscanned so aerial photographs would provide more information than the point cloud.

Pirates Cove Marina: One scan approximately 400m away provides little detail, but aerial photographs could provide some information.

5.4 Cross Section Data from Models

The approach to extracting cross-sectional data from the point clouds was virtually identical to the method used in the extraction of envelope data, apart from the fact that widths were measured by fitting meshes onto edges and measuring the width of that mesh, instead of using planes on either side. This is due to the fact that the planes that section off widths are often the thickness dimension of sections and they are too small to be captured in a reliable manner by the scanners. Additionally, cross-sectional data differs from envelope data due to the vast amounts of missing information in each section. Therefore, the assumption of symmetry has to be made on multiple occasions and some dimensions have to calculated from measurements of other parts.

An example of this is column 1C in Westrock East Terminal that is located in the westernmost corner of the building and therefore only has one scannable angle towards it. This is demonstrated in Figure 5.4 where the whole outwards facing side of the outer flange is recorded (Flange 1), the left facing side of the web is partially captured (Web), and half of the inwards facing side of the inner flange (Flange 2). This results in the width of the column being determined from the length of the mesh fitted to Flange 1, and the web thickness approximated by assuming symmetry and mirroring the section and positioning the mirrored Flange 2 in line with Flange 1. This can also be described as subtracting twice the length of Flange 2 from Flange 1. All other information is still unknown, and the best course of action is assuming a typical flange thickness based on the other dimensions, location of the column, and its assumed function in the structural system.

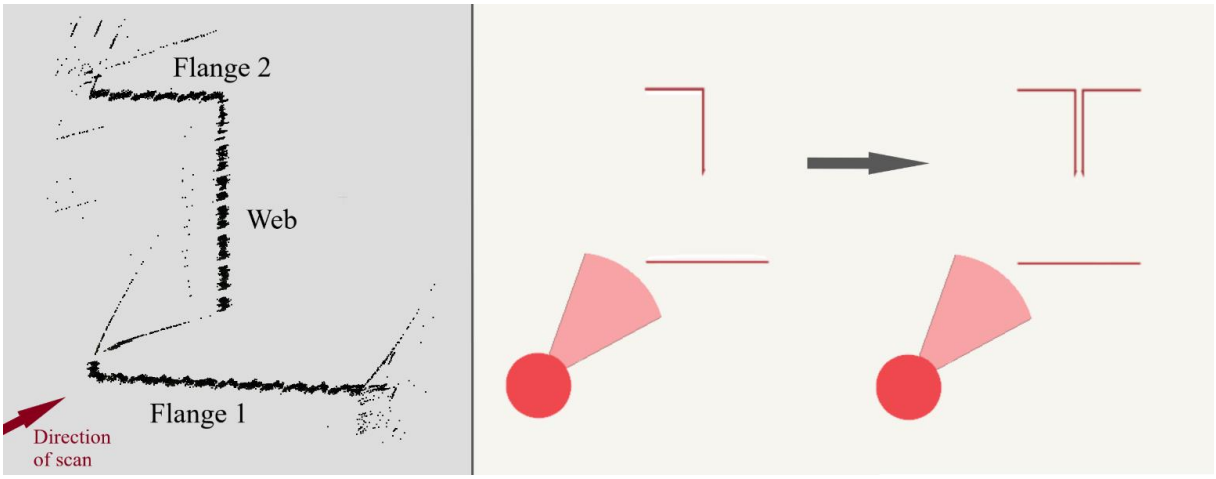

Figure 5.4. Example of an incomplete cross-sectional scan.

5.4.1 *Buildings with Known Dimensions*

The buildings for which drawings were made available to researchers remain the same; being Westrock East Terminal, Watson Landings Marina and the Intermodal Distribution Center. Available data in Watson Landings Marina was limited, due to the previously mentioned proprietary design of the boat racks, but the depths of all beams and columns are listed in the drawings while the thicknesses are not.

Westrock East Terminal's structural framing system is comprised mostly of wide flange beams and columns, with cross-bracing, joists and purlins of varying cross sections. For the results to be intercomparable, a decision was made to focus on those wide flange beams and to further enhance the comparability, only fully prismatic sections of the roof beam were chosen for measurements. The columns that were chosen were dispersed around the building to avoid the bias that results from choosing elements more favorably positioned with regards to scan locations.

The results of the measurements were divided into two categories based on the scale of measurements. Those categories were firstly the thickness of the flange and web, and secondly the depth along with the width. This is demonstrated in Figure 5.5 where the thickness looks to be much more prone to large percentage errors, most probably due to the similar ratio between scanner error and the measured dimension.

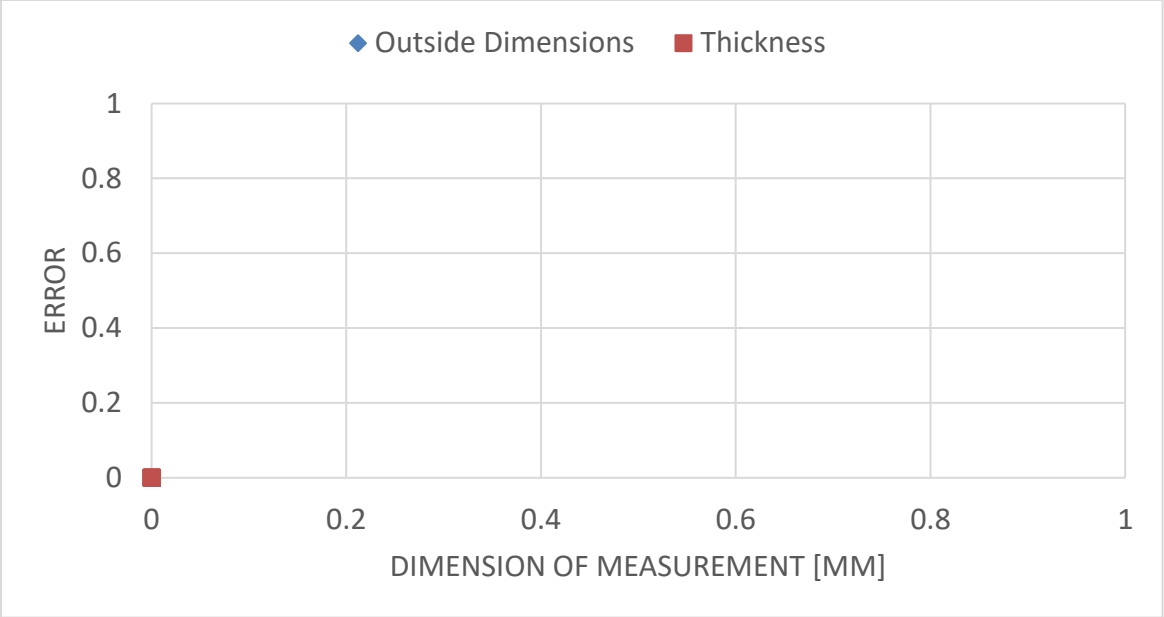

Figure 5.5. Percentage error vs the dimension of the measurement in question for Westrock East Terminal. Note that the three-point cluster of points at 30% is 180%, 225% and 768%.

Watson Landings Marina did not have a great number of known dimensions, and those that were known were depths of beams and columns. A random selection of elements was chosen, and they all turned out to be eight inch (203.2 mm) wide flange sections, so the only number to compare measurements with was the depth. This resulted in the analysis related to the sensitivity to different lengths being useless, but the results can be seen in Figure 5.6. The pattern for outside measurements continues from Westrock East Terminal, with Watson Landings Marina showing a slightly smaller error for unknown reasons.

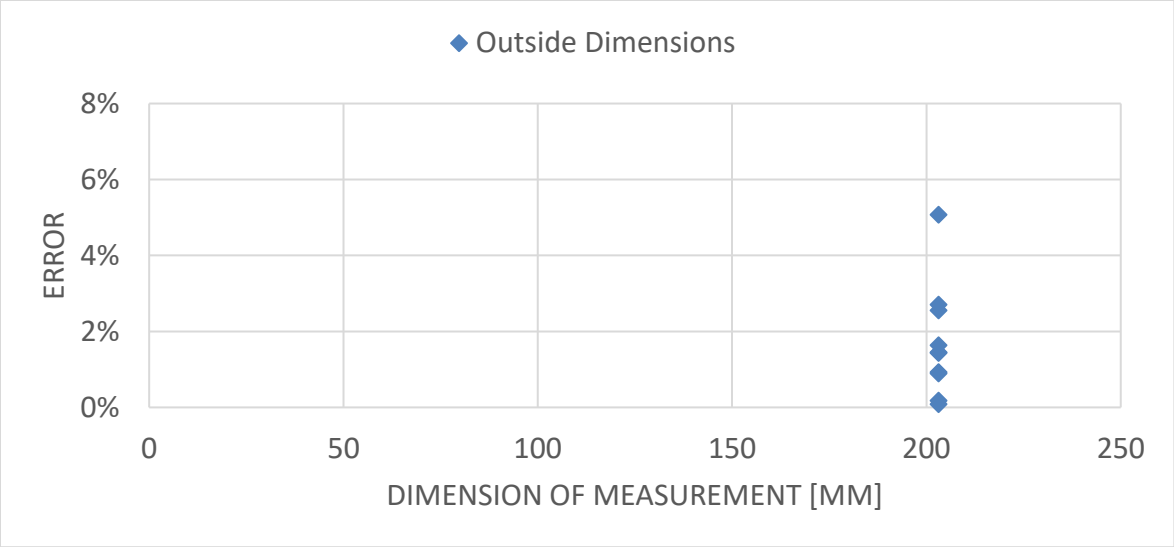

Figure 5.6. Percentage error vs the dimension of the measurement in question for Watson Landings Marina.

The dimensions extracted from the Intermodal Distribution Center turned out to be eight inches, much like Watson Landings Marina. This is because all the columns found in IDC are 8-by-8 inch square hollow sections, and the thickness dimension can not be extracted from hollow sections in general. The results from IDC can be seen in Figure 5.7 and are in line with that seen in the previous two buildings.

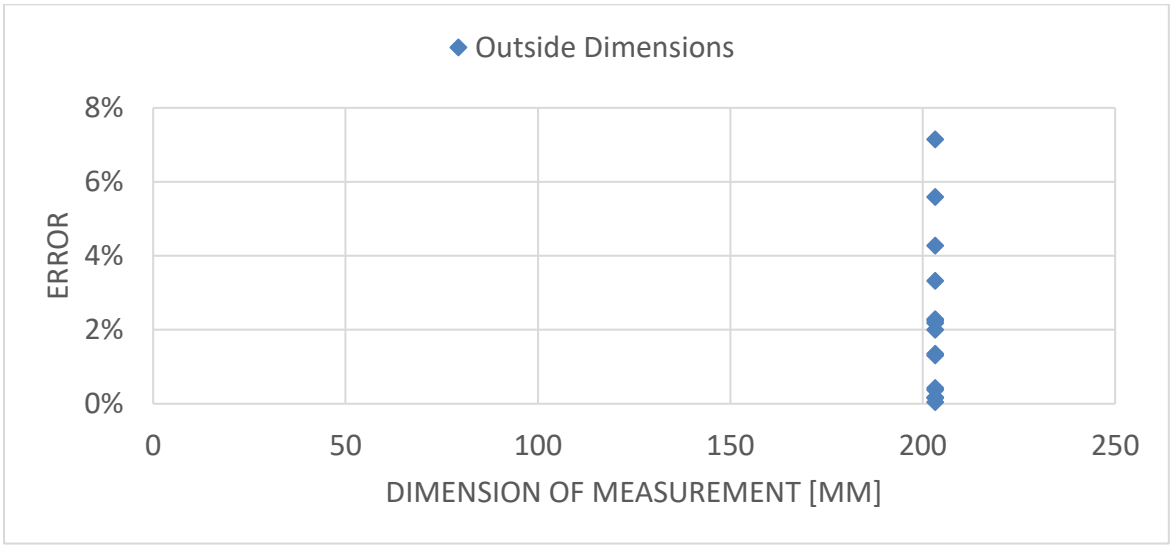

Figure 5.7. Percentage error vs the dimension of the measurement in question for Intermodal Distribution Center.

5.4.2 *Other Buildings*

Cargill Distribution Center: Scanned in a very similar fashion to Westrock East Terminal and Watson Landings Marina so it is expected to deliver similar results. The difference is mostly seen in the BLK360 scan locations as they are clustered at the back of the building instead of the front where most of the damage occurred.

Hangar 5: Not scanned as extensively as the three buildings with available drawings and half of the scans are in a corner with an obstructed view of the building. The arches are quite high up along the center so the point density is lower than one would prefer, but it should provide some information.

Building 316: Scanned very thoroughly due to its relatively small size and as a result it should provide as good, or better, section information than the three buildings with known dimensions. The fact that only BLK360 scans were used here should not be considered a downside since it is a small building where longer range scanners are unnecessary.

Building 333: Scanned thoroughly in one end, but very limited information available beyond that. This means that the data collected at the scanned end should provide adequate result, but the assumption of continuity is needed if more information is required.

Building 375: Very similar to Building 316 in size, shape and scan density, so it should provide very similar results.

Parthenon: Some missing data due to accessibility issues and very low scan density. In addition, there are only BLK360 scans and they are very central so range issues would be prevalent here.

Miller Distribution Center: Only scanned from the outside so there are quite a few gaps in the data. The scans are relatively close to the building and since they are long range XR3 scans, there should be data extractable from the front side of the building.

Pirates Cove Marina: One scan approximately 400m away so no details are visible.

5.5 Error Factors and Tolerances

Dimensional tolerances specified in Chapter 6 of the AISC *Code of Standard Practice for Steel Buildings and Bridges* for the elements measured here vary, with the outside dimensions of the cross sections ranging from 2.032 mm to 6.35 mm, but there are no allowable tolerances in the thickness of walls. The results from the cross-sectional measurements with the allowable tolerance included can be seen in Figure 5.8, where a large portion of the outside dimensions fall within the allowable error, and those who do not do not demonstrate a significant error.

The envelope data extracted is subject to the same dimensional tolerances specified here, in addition to erection tolerances and temperature related changes in the dimensions. All extracted measurements are well within these tolerances, since they scale with longer spans, and the largest errors were observed in the longest spans.

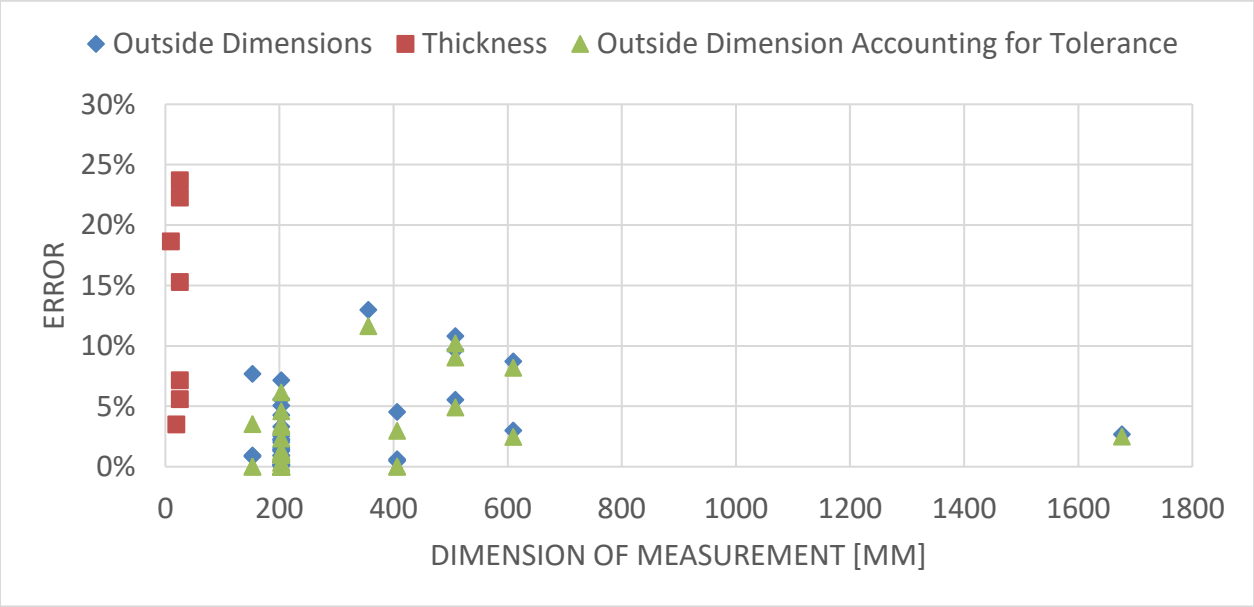

Figure 5.8. Section measurements accounting for fabrication tolerances.

Chapter 6. CONCLUSION

6.1 INTRODUCTION

Section 6.2 will summarize the results of the tests performed here. Section 6.3 discusses the conclusions drawn based on those results. Section 6.4 will provide recommendations for future work in the field of structural engineering reconnaissance, followed by the implications the results might have on work relating to automated extraction methods.

6.2 SUMMARY

The extraction of structural information from point clouds must be divided into at least two separate categories, depending on the scale of measurements performed. The two categories discussed here are large scale envelope data such as width, height and spacing of elements; and the smaller scale cross-sectional data of individual elements. Cross-sectional data must be divided even further into two separate categories; outside dimensions of elements and the wall thicknesses.

Envelope data analyzed here fell within the allowable margin of error expected from the fabrication of the steel members, in addition to the allowable error during the erection process as is demonstrated in Table 6.4.

Section extracted here suffered from problems with missing data due to the geometry and alignment of the elements in question. The larger scale outside dimensions that were captured of the elements were quite accurate and fell within the allowable margin of error as is shown in Table 6.4.

The smaller scale section data, i.e. the wall thickness of the elements demonstrated a proportionally larger error. This is due to the fact that wall thickness can only be extracted directly when it is thick enough for the lidar to detect it, and indirectly when two separate scans capture either side of the wall, but that adds a registration error. Additionally, the wall thickness of hollow structural sections (HSS) cannot be determined at all due to the hollow nature of it, as the name implies. A possible approximation for the square sections examined here would be measuring the radius of

the corner and assuming it follows the specifications of the Steel Construction Manual of the radius being three times the wall thickness, but no such approximations were attempted here. The summary of those results can be seen in Table 6.4. The high average error for thickness measurements is a direct result of three large outliers, but due to the fact that confirming their status as outliers is not possible, they are included in the calculations.

Table 6.4. Ratio of measurements within tolerance and the exceedance of those not within.

	Cross section data		Envelope data
	Wall thickness	Outside dim.	
Dim. within tol. (%)	0%	39.5%	100%
Avg. error past tol. (%)	126.9%	3.6%	0%
Avg. error past tol. (mm)	7.62	14.96	0%

6.3 CONCLUSION

Lidar data collection as a reconnaissance engineering tool shows great promise and substantial information was uncovered here. In particular, the problems unplanned reconnaissance missions face due to the uncontrollable and unpredictable nature of them. Therefore, researchers must come up with, and follow, general principles rather than a concrete set of rules when field work is done to ensure the post-processing will be as effective as possible.

Principles observed here are as follows:

Scan locations: The data collected for this study featured a high density of scans around the damaged area, but only a few are needed to observe the failure modes in a larger scheme. Instead, the focus should be on identifying repeating patterns within the buildings and scan the repeated versions of the failure areas, if any are found, more extensively. This is because deformed members are much harder to measure, so the general shape and size of the deformed members can be compared to the identified repetitions to confirm their similarity.

Scan type: The difference in measurements between XR3 and BLK360 data was minor, with XR3 performing better in general, even when areas closer to the scanners were examined where the BLK360 should not have compromised accuracy.

Geometry of elements: Field crews should be mindful of the geometric constraints of various structural elements and do what they can to mitigate them. This requires the field crew to have a general idea of what elements are of interest, which cannot always be the case when time sensitive reconnaissance work is conducted.

6.4 Recommendations for Future Work

Further research on the matter of extracting structural elements from point clouds must be done, particularly regarding the problem of inaccessible geometry. As of now, the technology to extract measurements from locations not within the line of sight of the scanners is non-existent, but perhaps there will be commercially available sensors that can detect light transmitted back to the scanner that has been cast off one or more surfaces on its way back.

The automation of the processes described here could be implemented by discretizing the different structural sections and develop an algorithm that detects those different shapes. As an example, a wide flange beam has discrete zones where a scanner might be located, based solely off whether that scan location has the ability to capture a side fully, or partially. This is demonstrated in Figure 6.1. Figure 6.1where these zones are shown for a symmetric wide flange beam. Furthermore, a rudimentary program was written to analyze every possible combination of scan locations and whether those can produce a full cross section. This does not account for obstructions of view within the building or the angle at which the scanner captures the section in 3D space. Implementation of this spatial analyzes will be left for other researchers in the future.

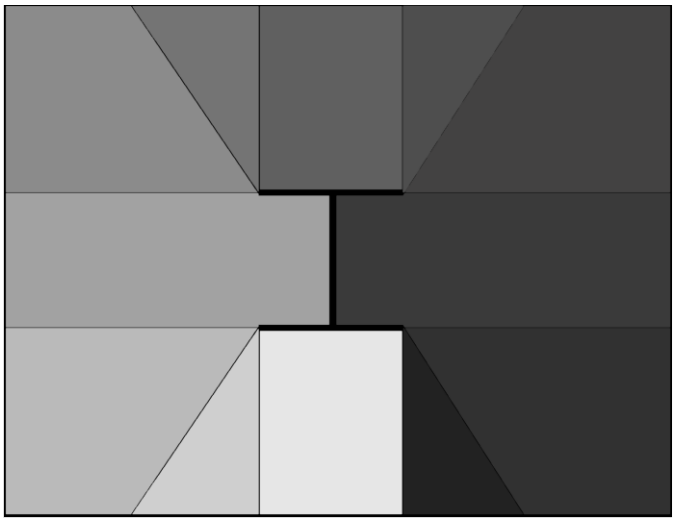

Figure 6.1. All possible scan locations in 2D space for a symmetric wide flange section.

Another suggestion for future researchers in the field of reconnaissance structural engineering is to take aerial photographs like the ones shown in Figure 6.2. This might seem unnecessary since the point clouds provide a much more thorough overview of buildings, but these types of photographs are invaluable in the registration process to orient the scans and get a spatial overview in the initial phases.

Figure 6.2. Aerial photographs of Pirates Cove Marina

REFERENCES

American Institute of Steel Construction (AISC). (2016). *Code of Standard Practice for Steel Buildings and Bridges* (ANSI/AISC 303-16). Retrieved from https://www.aisc.org/globalassets/aisc/publications/standards/code-of-standard-p

Berman, J. Marshall, J. Roueche, D. Dafni, J. (2020) "Low-Rise Large Volume Building Reconnaissance after Hurricane Michael using RAPID Facility Technologies (lidar, UAVs, GPS, photos)", in *Hurricane Michael Reconn-Large Volume Buildings*. DesignSafe-CI. https://doi.org/10.17603/ds2-3jpz-sk97.

Beven, J.L. II, Berg, R., Hagen, H. (2019). National Hurricane Center Tropical Cyclone Report: Hurricane Michael. Retrieved from the National Oceanic and Atmospheric Administration, National Hurricane Center website: https://www.nhc.noaa.gov/data/tcr/AL142018_Michael.pdf.

Cabaleiro, M., Riveiro, B., Caamano, J.C. (2015). Algorithm for beam deformation modeling from LiDAR data. *Measurement*, 76, 20-31.

Cabaleiro, M., Riveiro, B., Arias P., Caamano, J.C., Vilan, J.A. (2014). Automatic 3D modelling of metal frame connections from LiDAR data for structural engineering purposes. *ISPRS Journal of Photogrammetry and Remote Sensing*, 96, 47-56.

Erkal, B., Hajjar, J. (2017). Laser-based surface damage detection and quantification using predicted surface properties. *Automation in Construction*, 83, 285-302.

Hou, T. S., Liu, J.W., Liu, Y.W. (2017). Algorithmic Clustering of LiDAR Point Cloud Data for Textural Damage Identifications of Structural Elements. *Measurement*, 108.

Maptek releases PointStudio 8 spatial data application. (2018, November 8). *Mining Magazine*. Retrieved from https://www.miningmagazine.com/simulation-optimisation/news/1350670/maptek-releases-pointstudio-8-spatial-data-application.

Mohammadi, M.E. & Wood, R.L. (2018). Post-Earthquake Structural Damage Assessment Through Point Cloud Data. *University of Nebraska Civil Engineering Faculty Publications*, 161.

National Centers for Environmental Information (NCEI). (2019, February 6) *the U.S. Climate in 2018.* National Oceanic and Atmospheric Administration. https://www.ncei.noaa.gov/news/national-climate-201812.

New Radar System. (1961, February 28). *Odessa American.*

Olsen, M. (2013). In Situ Change Analysis and Monitoring through Terrestrial Laser Scanning. *Journal of Computing in Civil Engineering*, 29(2).

Olsen, M., Kuester, F., Chang, B., Hutchinson, T. (2009). Terrestrial Laser Scanning-Based Structural Damage Assessment. *Journal of Computing in Civil Engineering*, 24(3).

Philipps, D. (2018a October 17). *Exposed by Michael: Climate Threat to Warplanes at Coastal Bases.* New York Times. https://www.nytimes.com/2018/10/17/us/tyndall-afb-damage-hurricane-michael.html?action=click&module=In%20Other%20News&pgtype=Homepage&action=click&module=News&pgtype=Homepage.

Philipps, D. (2018b October 26). *While Trump Calls Climate Change a Hoax, Hurricane Michael Damaged US Fighter Jets Worth $6 Billion*. Democracy Now! https://www.democracynow.org/2018/10/26/while_trump_calls_climate_change_a.

Synge, E.H. (1930). A method of investigating the higher atmosphere. *The London, Edinburgh, and Dublin Philosophical Magazine and Journal of Science*, 9, 1014-1020.

Valenca, J., Puente, I., Julio E., Gonzales-Jorge, H., Arias-Sanchez, P. (2017). Assessment of cracks on concrete bridges using image processing supported by laser scanning survey. *Construction and Building Materials*, 146.

Vosselman, G., Gorte, B., Sithole, G., Rabbani, T. (2003). Recognising Structure in Laser Scanner Point Clouds. *International Institute of Geo-Information Science and Earth Observation (ITC)*, 46.

Walsh, S., Borello, D., Guldur, D., Hajjar, J. (2013). Data Processing of Point Clouds for Object Detection for Structural Engineering Applications. *Computer-Aided Civil and Infrastructure Engineering*, 28(2), 495-508.

Watson, C., Chen, S., Bian, H., Hauser, E. (2011). LiDAR Scan for Blasting Impact Evaluation on a Culvert Structure. *Journal of Performance of Constructed Facilities*, 27(4).

Wilson, H. (2019 April 30.) *Congress must step up for Air Force bases devastated by natural disaster*. Miami Herald. https://www.miamiherald.com/article229848384.html.

Wood, R.L., Mohammadi, M.E. (2015). LiDAR Scanning with Supplementary UAV Captured Images for Structural Inspections. *International LiDAR Mapping Forum 2015*, Denver, CO, February 23-25, 2015, 10pp.

Xiong, X., Adan, A., Akinci, B., Huber, D. (2013). Automatic creation of semantically rich 3D building models from laser scanner data. *Automation in Construction*, 31, 325-337.

Zeng, Q., Lai, J., Li, X., Mao, J., Liu, X. (2008). Simple building reconstruction from LIDAR point cloud. 1040 - 1044. 10.1109/ICALIP.2008.4590062.

APPENDIX A

Drawings are attached to the end of this document.

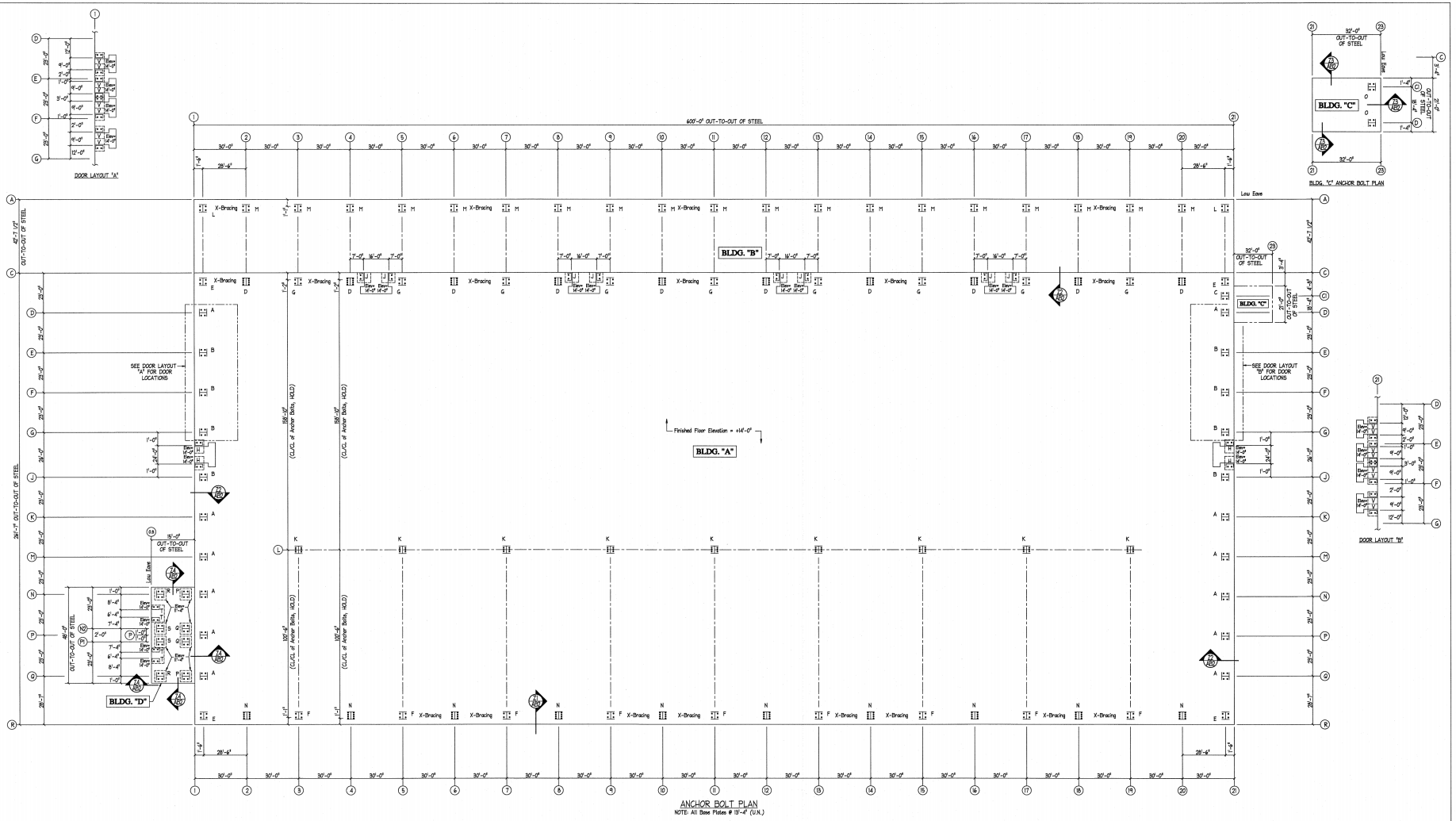

ANCHOR BOLT PLAN
NOTE: All Base Plates @ 13'-4" (U.N.)

ANCHOR BOLT SUMMARY - BLDG. A

Qty	Locate	Dia (in)	Type	Proj (in)
● 56	Jamb	5/8"	F1554-GR36	2.50
● 4	Endwall	1"	F1554-GR36	3.00
● 80	Endwall	3/4"	F1554-GR36	2.50
● 136	Frame	1 1/4"	F1554-GR36	3.00
● 36	Frame	1"	F1554-GR36	2.50
● 16	Frame	3/4"	F1554-GR36	2.50
● 54	Frame	1 1/2"	F1554-GR36	3.00
● 160	Soldier	3/4"	F1554-GR36	2.50

ANCHOR BOLT SUMMARY - BLDG. B

Qty	Locate	Dia (in)	Type	Proj (in)
● 84	Frame	3/4"	F1554-GR36	2.50

ANCHOR BOLT SUMMARY - BLDG. C

Qty	Locate	Dia (in)	Type	Proj (in)
● 8	Frame	3/4"	F1554-GR36	2.50

ANCHOR BOLT SUMMARY - BLDG. D

Qty	Locate	Dia (in)	Type	Proj (in)
● 8	Jamb	5/8"	F1554-GR36	2.50
● 32	Frame	3/4"	F1554-GR36	2.50

GENERAL NOTES

1. All baseplates @ same elevation unless noted otherwise.
2. Anchor bolt design for embedment is not by the manufacturer and must be determined by the foundation engineer.
3. The width of the sheet notch and/or brick ledge, though shown on these drawings, is not included in these dimensions.
4. See base plate details for correct placement of anchor bolts.

For Customer Service issues, please contact one of the following:
TODD FISCHER
JEFF RIPPEE
BILL BROOKS

ACI BUILDING SYSTEMS, LLC
10125 HWY. 6 WEST
BATESVILLE, MS. 38606
(662) 563-4574

ENGINEERING SEAL

This certification covers parts fabricated and delivered by the manufacturer only and excludes parts such as doors, windows, foundation design and erection of the building. Sealed drawings do not constitute an agreement that the signed engineer is acting as the engineer of record for the overall project.

KEITH P. SHEDD
LICENSE
No 48014
STATE OF FLORIDA
PROFESSIONAL ENGINEER
PROFESSIONAL ENGINEER

RELEASE HISTORY

BNG	COMMENTS	DATE	#
	MARK		
	REVISIONS		
	NOTES		
	Revised Per Returned Approvals	9/7/17	1
	Revised Per Returned Approvals	10/30/17	2
	CONST. PERMIT APPRVL.	12/27/17	3
	REV.	1/16/18	4
	CONST. PERMIT APPRVL.	2/19/18	5
	REV.		
	DWG/BOLTS		

CUSTOMER: Culpepper Construction
Tallahassee, FL 32304

JOB NAME: East Terminal Development
Panama City, FL 32401

ACI BUILDING SYSTEMS, LLC
P.O. BOX 1316 - BATESVILLE, MS - 38606
(662) 563-4574 - (662) 563-1142 (FAX)

ENG BY:	JJM
CAD BY:	REA
DET BY:	REA
CKD BY:	ALL

JOB NUMBER: B17-8460

DWG NUMBER: AB1 of 4

PLOT: D

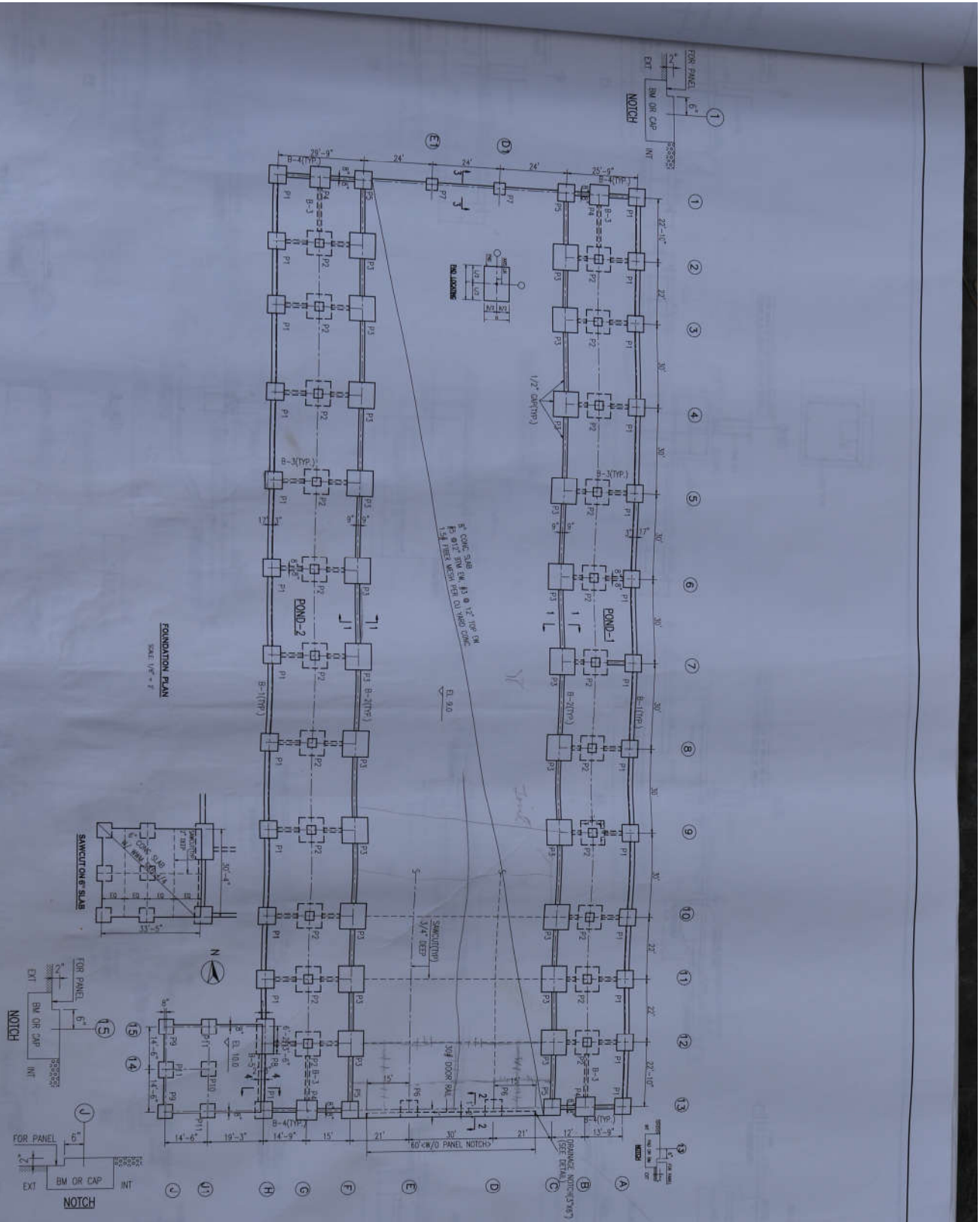

ROOF DESIGN GROUP, INC.
P.O. BOX 1330
BOCA RATON, FL 33429
(800) 555-4701 FAX (561) 393-4796
www.roofntrack.com

ROOF & RACK

WATSON LANDING MARINA
(ANCHOR BOLT LAYOUT PLAN)
SOUTH PORT, FLORIDA

DATE: 12/13/13
DRAWN BY: RON
JOB NO.:

REVISIONS		
DATE:	BY:	DESCRIPTION:
7-8-14	RON	FOR CITY COMMENTS(6-11-14)
7-28-14	RON	ADDED SMOKE VENT STRUCTURE
8-13-14	RON	ADDED 2 STORIES OFFICE
8-28-14	RON	REMOVED 3' OVERHANG

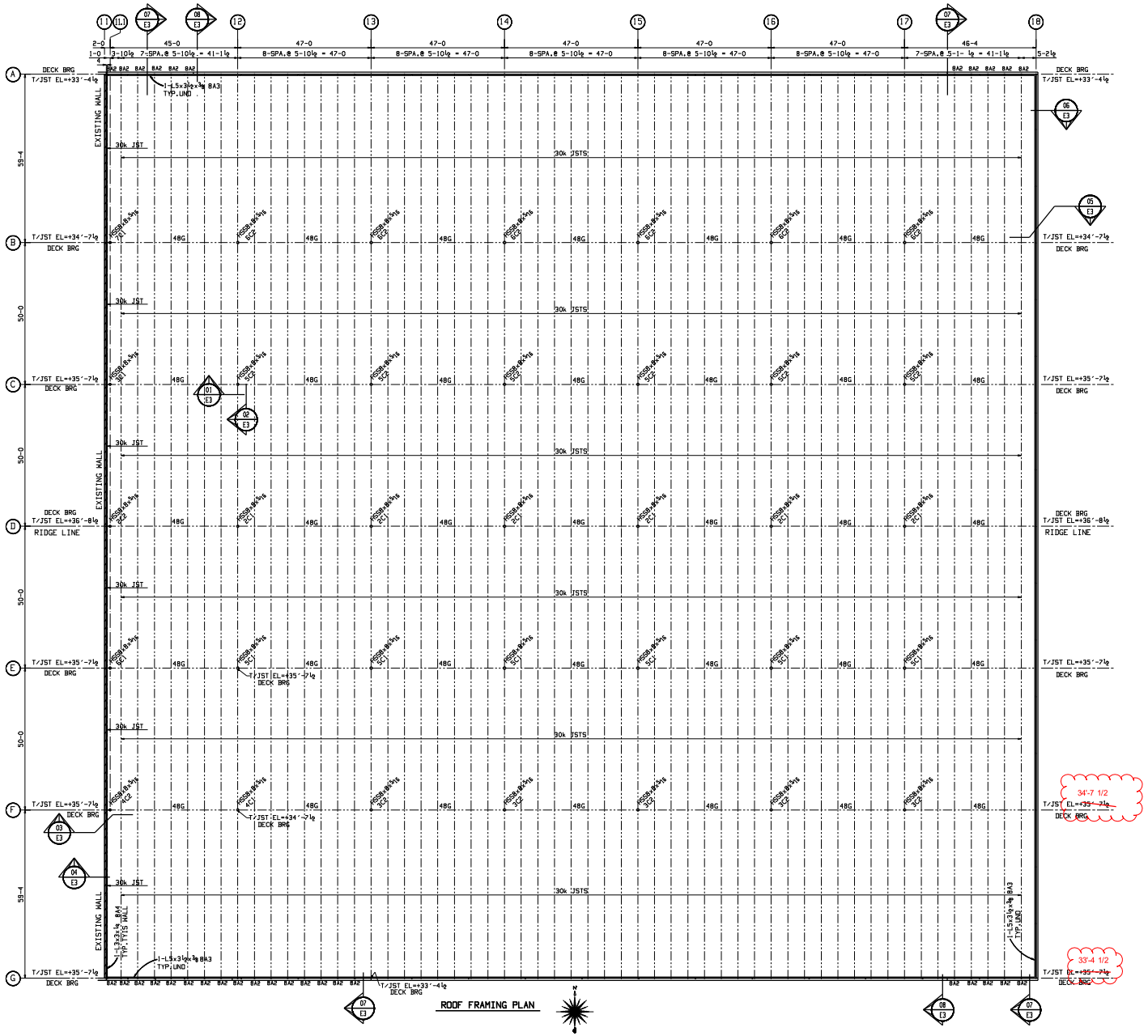

NO.	REVISION	DR.	DATE
0	ISSUED FOR CONSTRUCTION	MM	
A	ISSUED FOR APPROVAL	MM	04-22-16

WILLIAMS STEEL
315 LAKE STREET
JACKSON, TENNESSEE
PHONE (731)423-4900

JOB: PC PORT AUTHORITY

LOCATION: PANAMA CITY, FL.

CONTRACTOR: ALSTON CONSTRUCTION

ARCHITECT: WAKEFIELD BEASLEY & ASSOCIATES

MODEL NAME: 12275 PC PORT AUTHORITY

DRAWN BY	CHECKED BY	CONTRACT	SHEET NO.
MM	JC	12275	E2